Ph.D. thesis

Effect of actin-binding proteins on the structure and conformational dynamics of the actin monomer

Roland Kardos

Supervisor:
Dr. Gábor Hild

University of Pécs
Medical School
Department of Biophysics

Pécs, 2014

Interdisciplinary Medical Science Doctoral School D93

Head of Doctoral School: Prof. Dr. Balázs Sümegi

Program (B-130): Investigating functional protein dynamics using biophysical methods

Program leader: Prof. Dr. Miklós Nyitrai

Supervisor: Dr. Gábor Hild

“The first principle is that you must not fool yourself and you are the easiest person to fool.”

Richard Feynman

Acknowledgements

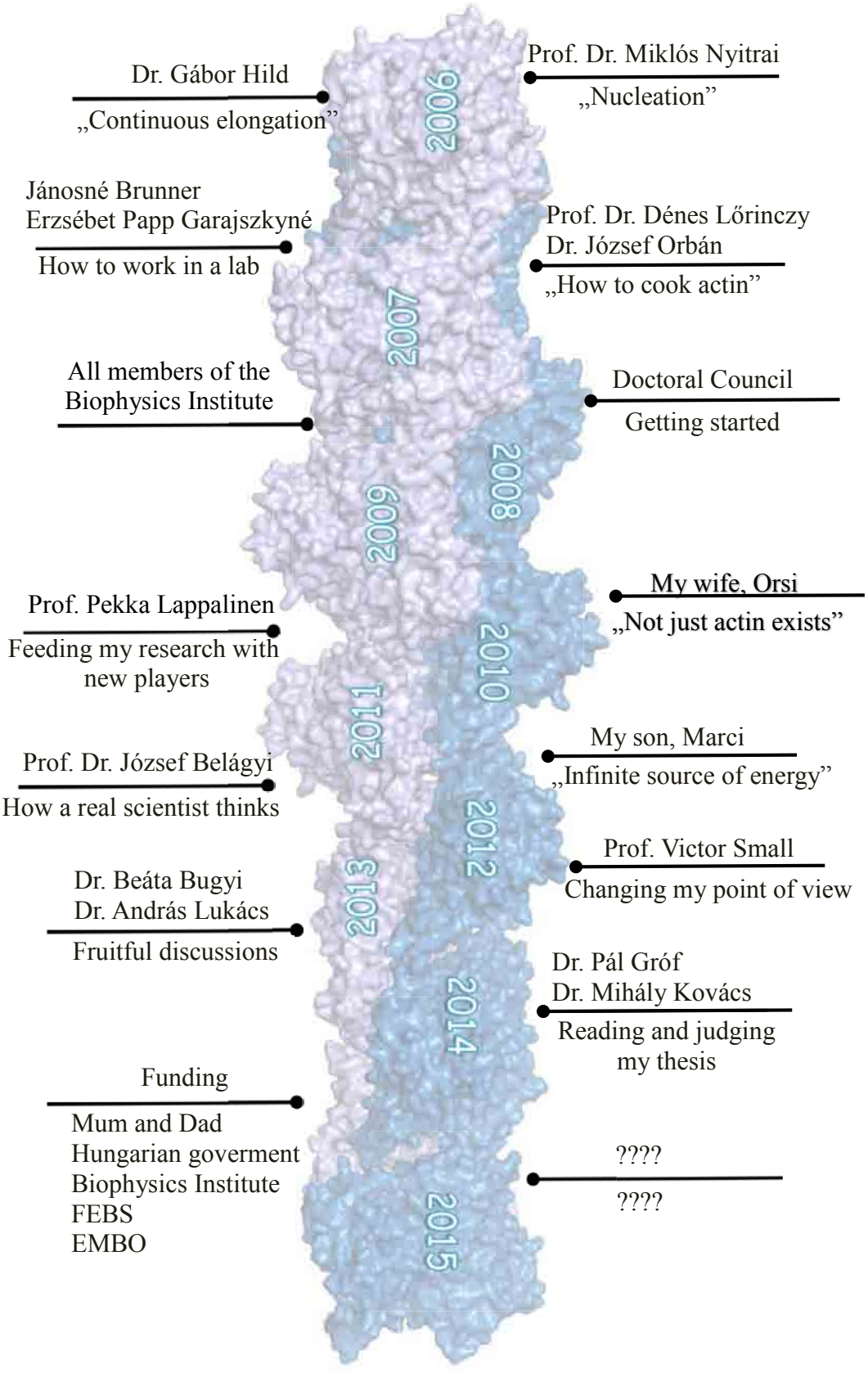

Table of contents

I. Introduction

Actin is the most abundant protein found in all eukaryotic organism from plants to animals. The property of the actin molecule to assemble into filament in a reversible way make it suitable for playing an indispensable role in different cellular processes such as cell locomotion, morphogenesis, membrane trafficking, and cell division. To precisely fulfil its versatile function, the spatiotemporal organisations of diverse actin filament networks are controlled by a large number of actin-binding proteins. These effectors can disrupt unnecessary "old" actin structures and assist in the assembly of new actin networks with diverse architecture depending on the cellular process in which they are involved. To understand the actin-based cellular processes in details it is necessary to explore the conformational and dynamic changes occur within the actin molecule due to the action of actin-binding proteins.

I.1 Properties of the actin molecule

Actin is an ATPase protein sharing similar three-dimensional structure with hexokinases, glycerokinases, Hsp70 proteins [1-4]. Based on the first atomic structure of actin monomer resolved at an effectively high resolution the actin molecule consists of two main domains termed as large and small domain [5]. The main domains can be further divided into subdomains; the large domain is composed of subdomains 3 and 4, while the small domain is built up from subdomains 1 and 2 (Figure 1/B). The contact between the two main domains is restricted to the loop centred at Lys336 and a linker helix Gln137-Ser145 resulting in a formation of two clefts on the opposite sites of the actin molecule. The cleft open toward the pointed end of the monomer is called the nucleotide-binding cleft because it binds the nucleotide (ATP or ADP) and the associated divalent cation (Mg^{2+} in cells). The other cleft located on the barbed end of the actin monomer consists of hydrophobic residues and considered as the primary binding site for the actin monomer binding proteins [6].

The actin monomers under appropriate conditions can bind to each other in a head to tail manner forming a double-stranded helix that is termed F-actin (Figure 1/A) [7]. The F-actin has structural polarity due to the asymmetric nature of the actin

monomers.Based on the electron micrograph of actin filaments decorated with myosin one of the ends of the filament is called barbed and the other is termed pointed end [8].

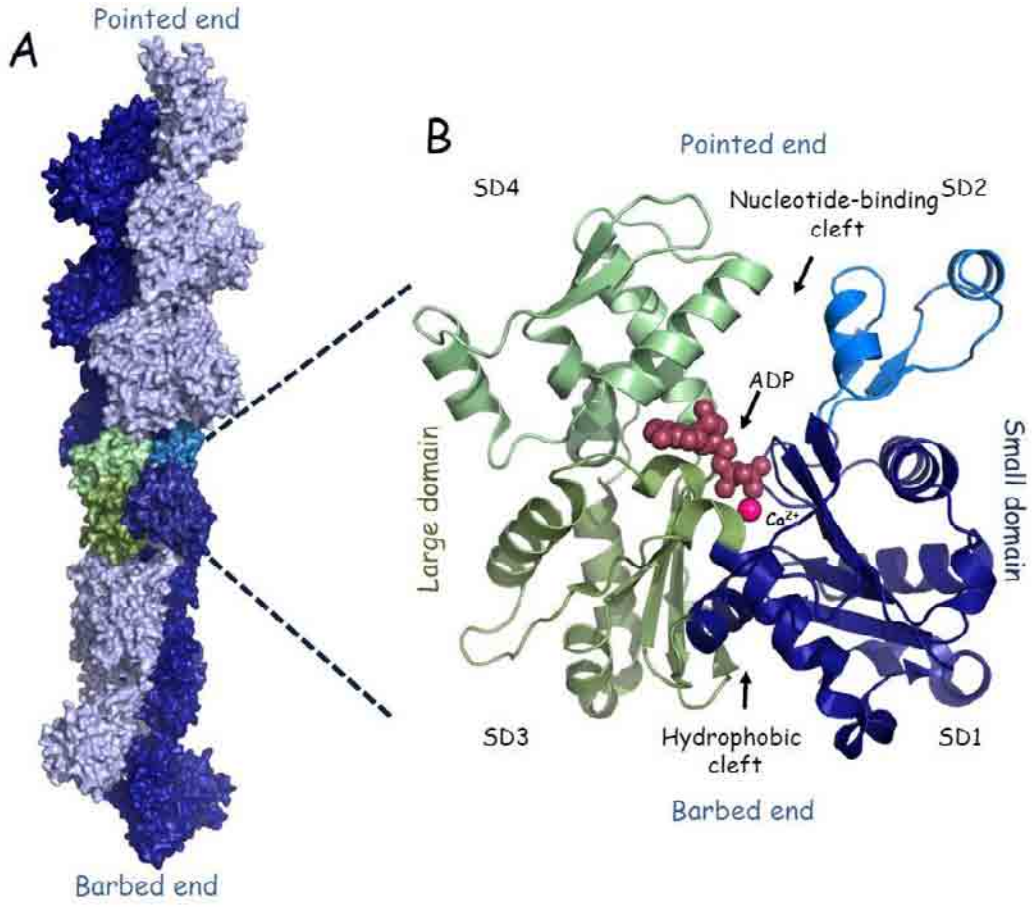

Figure 1.) A.) Double-stranded helix of actin filament. The two strands of the actin filament are distinguished with different blue colours. B.) Crystal structure of the actin monomer in cartoon representation (PDB code: 1J6Z). The large and the small domain of actin are represented in green and blue, respectively. The subdomains are numbered and distinguished by different colours. Based on the orientation of the actin monomer within the actin filament the subdomain 1 and 3 end is called the barbed end, while the subdomain 2 and 4 end is termed the pointed end of the actin monomer ADP and Ca^{2+} are shown as red and pink spheres, respectively.

I.1.1. Actin polymerisation

I.1.1.1 Steps of actin polymerisation

The transformation of the globular form of actin (G-actin or actin monomer) into filamentous (F-actin or actin filament) form is a spontaneous process that can occur without the assistance of any actin-binding effectors. The polymerisation of actin *in vitro* can be initiated by elevating the salt concentration of the solution to the physiological level (2 mM $MgCl_2$ and 100 mM KCl) [9]. The polymerisation process

starts with the formation of actin nuclei consisting of 2-4 actin monomers. The nucleation step of the actin polymerisation is an unfavourable process from a thermodynamic point of view due to the unstable nature of the actin dimers and trimers [10]. However when the actin seeds are formed, the actin nuclei start to elongate with different kinetics at the two ends of the filament. The barbed end of the filament grows fast (fast-growing end or + end), while the pointed end elongates slowly (slow-growing end or - end). The rate of the elongation of each end of the filament depends on the concentration of actin monomers (C_{free}) available in the solution and the rate constants for the association (k_{on}) and dissociation (k_{off}) of the actin subunits at the filament ends. It was measured by using electron microscopy that the association and dissociation rate constants of ATP-loaded actin monomers at the barbed end are 11.6 $\mu M^{-1}s^{-1}$ and 1.4 s^{-1}, respectively resulting in a dissociation equilibrium constant (K_d) of 0.12 μM for the actin monomer at the barbed end [11]. The elongation of the barbed end of the filament can progress until the concentration of free ATP-loaded actin monomers above this dissociation equilibrium constant, therefore this concentration of free actin monomers is termed the critical concentration of the barbed end (C_{cB}) elongation.

The dissociation rate constant of the ATP-loaded actin subunits from the pointed end is 0.8 s^{-1} similar to the value observed at the barbed end (1.4 s^{-1}), whereas the association rate constant is 1.3 $\mu M^{-1}s^{-1}$ around 10 times lower than at the barbed end (11.6 $\mu M^{-1}s^{-1}$) [11]. These rate constants give a K_d of 0.62 μM between the ATP-loaded actin monomer and the pointed end of the filament. Similar to the barbed end this equilibrium dissociation constant determines the critical concentration of free actin monomers (C_{cP}) above the growing of the pointed end of actin filament can take place. Considering the rate constants obtained for each end of the actin filament the elongation rate is around one order of magnitude higher at the barbed end (fast-growing) than at the pointed end (slow-growing) of the filament. This difference in the rate of elongation between the barbed end and pointed end was demonstrated by direct visualisation of growing actin filaments in TIRF microscopy assays [12].

The elongations of actin filaments proceed until a dynamic equilibrium is established between the actin monomers and filaments. The dynamic equilibrium between monomers and filaments maintains a continuous presence of around 0.14 μM free actin monomer in the solution. This steady-state concentration (C_{SS}) of free actin monomers is slightly above the critical concentration of the barbed end (C_{cB}=0.12 μM) and well below the critical concentration of the pointed end (C_{cB}=0.62 μM), therefore

the actin monomers predominantly incorporate at the barbed end and dissociate at pointed end of the filament in steady-state. This continuous flux of actin subunits from the pointed end to the barbed end is called the treadmilling (or turnover) of the actin filaments [13-15].

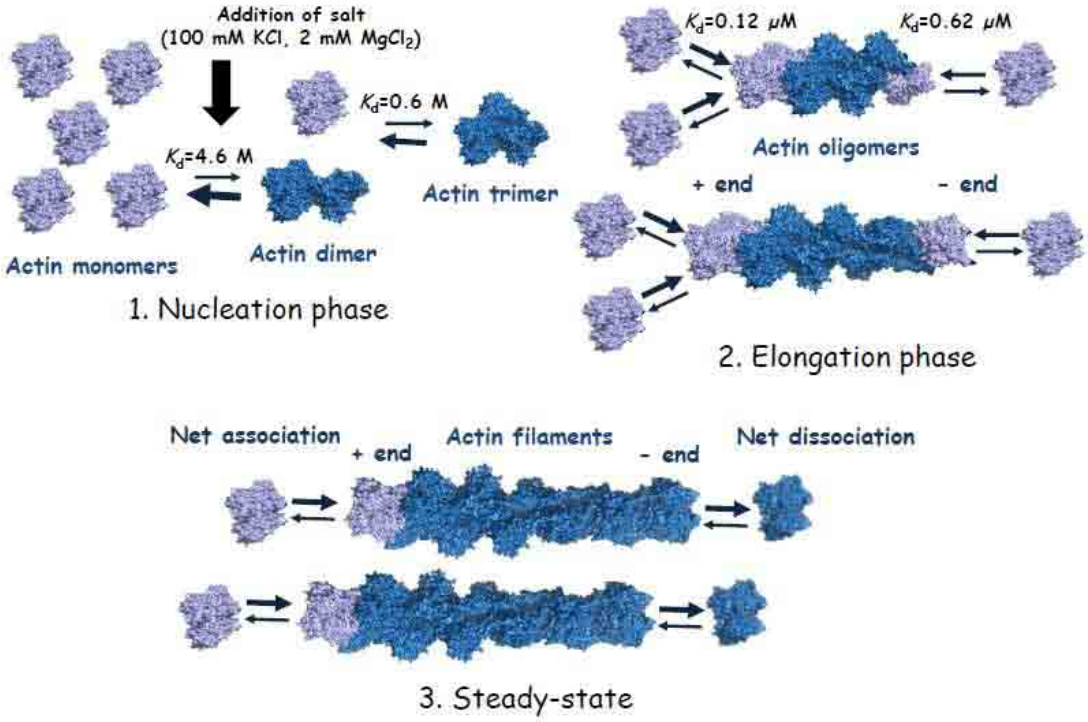

Figure 2.) Steps of the actin polymerisation in the presence of ATP including the nucleation, elongation and steady-state phases. Polymerisation starts with the formation of actin dimers (sky blue) and trimmers (sky blue) from G-actin (light blue). In the elongation phase both ends of the actin filament grow but the + end elongates with a higher rate than the pointed end of the filament. In steady-state the + end grows with the same rate as the – end shrinks in the presence of ATP.

I.1.1.2 Treadmilling of actin filaments

In spite of in steady-state continuous association and dissociation of actin monomers take place at both ends of the actin filaments the average length of the filaments do not change. It was demonstrated by using evanescent microscopy that in steady-state the rate of elongation of the barbed end of actin filaments was compensated with the rate of shrinking of the pointed end of the filaments in the presence of ATP [16]. The nature of this unidirectional growing and shrinking of the actin filaments

arises from the structural and biochemical dissimilarity of the two ends of the filament [17].

During the assembly of actin filaments, the actin monomers bind to each other in a head to tail manner resulting in a structural polarity of the two ends of the actin filament [7]. Using a single particle analysis of cryo-electron micrographs of actin filaments it was revealed that at the pointed end of the actin filament there was an extra loop-loop contact between the terminate end penultimate subunits which was missing at the barbed end. This extra interaction makes the pointed end of the filament less dynamic than the barbed end explaining well the observed differences in the k_{on} and k_{off} of ATP-loaded actin monomers at the two ends of the filament (see previous paragraphs).

In addition to the structural difference, the hydrolysis of actin-bound ATP upon incorporation into the filament is also necessary to maintain the treadmilling of actin filaments [18]. The actin monomer has weak ATPase activity (0.6 h^{-1}) but when its associate to the filament the bound ATP is hydrolysed rapidly with a half time of around 2 s. The ATP hydrolysis is irreversible process and the product of that is ADP+P_i containing actin subunits within the filament. The release of inorganic phosphate is delayed it occurs with a half time of around 6 minutes therefore the ADP+P_i containing subunits are relatively long-lived intermediates within the filament. The consequences of the ATP hydrolysis and phosphate release are the presence of freshly incorporated ATP-actin subunits at the barbed end of the filament followed by an already hydrolysed ADP+P_i containing segment and the formation of ADP-actin regions after phosphate release toward the pointed end of the filament (Figure 3.). The ADP-actin subunits have a dissociation equilibrium constant of 1.8 μM to the pointed end of the filament that is much higher than the steady-state concentration of actin monomers (0.14 μM) therefore finally the ATP hydrolysis enhances the dissociation of actin subunits at the pointed end of the filament [19]. It is worth to mention that the treadmilling can occur until free ATP is available in the solution because the ADP-loaded actin monomer has the same affinity to both ends of the filament.

The bound ADP in the dissociating actin subunit has to be replaced with ATP before the next round of incorporation at the barbed end of the filament [20]. The rate-limiting step of the nucleotide exchange process is the dissociation of ADP from the actin monomer that has a dissociation rate constant of around 0.02 s^{-1} in vitro. In the

cells this process can be influenced by different actin-binding proteins such as cofilin, thymosin β4 and profilin.

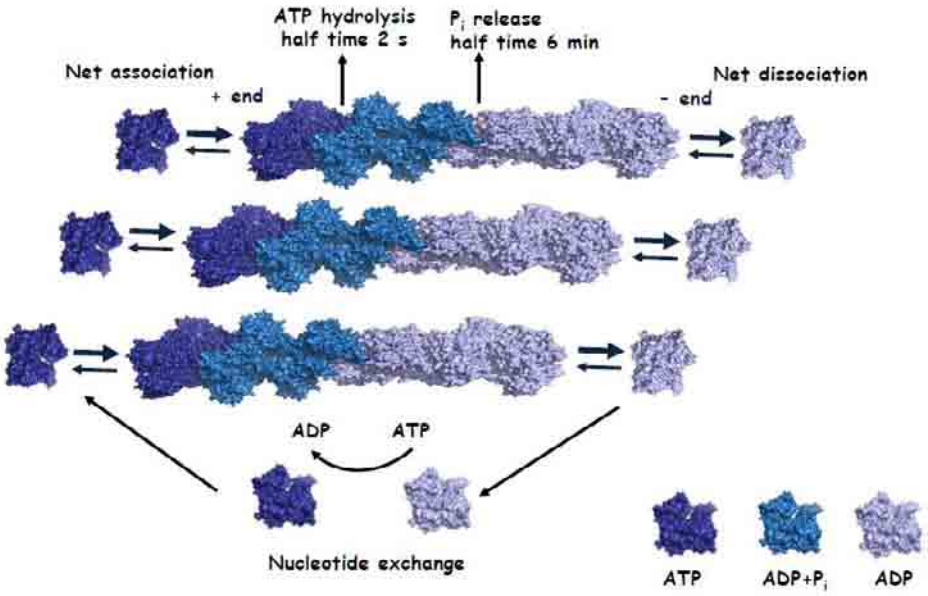

Figure 3.) Treadmilling of an actin filament in the presence of ATP [7, 19, 21]. In steady-state the actin filament grows with the same rate at the barbed end as it shrinks at the pointed end. The incorporation of ATP-loaded actin monomer at the barbed end followed by the hydrolysis of ATP and a delayed phosphate release resulting in an ATP and ADP containing regime at the barbed end and the pointed end of the filament, respectively. The interior of the actin filament is mainly composed of ADP+P_i actin subunits. The dissociating ADP-loaded actin subunit undergoes nucleotide exchange before the next round of incorporation.

The rate-limiting step of the actin filament treadmilling is the dissociation rate of ADP-actin subunits (0.2 s^{-1}) at the pointed end of the filaments [11, 22]. Interestingly this rate is around two orders of magnitude higher e.g. in lamellipodia of migrating cells than the observed rate of treadmilling in vitro in the absence of any auxiliary factors [23, 24]. The explanation behind the faster turnover rate of actin filaments in cells is the presence of actin-binding proteins, which can modify the kinetics of each step of the actin filament polymerisation and treadmilling.

I.1.2. Conformation, flexibility, and allostery of the actin molecule

The number of resolved actin structures under different conditions and/or in complex with actin-binding proteins and drugs increases exponentially providing a valuable source for revealing the conformational variability of the actin molecule. Comparison of these structures showed that the secondary structure of actin is invariable in all cases but the topology of the actin molecule shows global and/or local differences depending on the circumstances or the binding partner of the actin molecule present in the crystallisation process.

Based on the orientation of the main domains of actin with respect to each other the atomic structures can be classified into three different conformational groups [25]. The majority of the resolved atomic structures of actin monomers belong to the twisted and closed conformational group except the structure of the profilin-β-actin complex that has an open and twisted conformation (Figure 4/A and B).

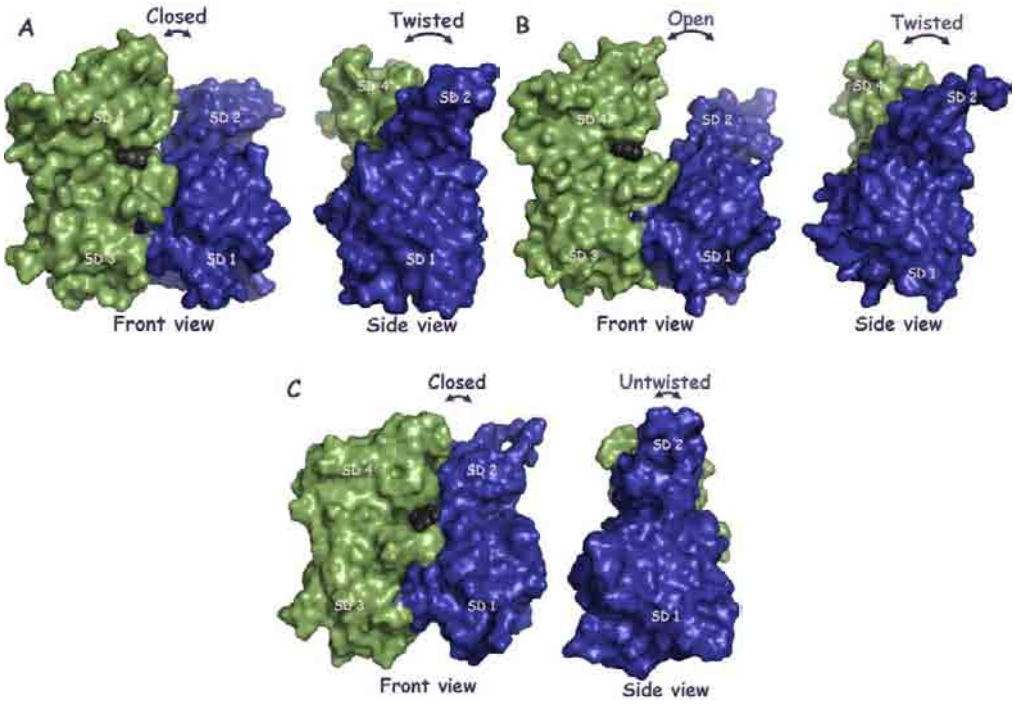

Figure 4.) Groups of actin monomer structures based on the orientation of their domains. A.) Twisted and closed conformational group. In the front view the large (green) and small (blue) domains close the nucleotide binding cleft. Side view shows that the actin molecule is in a twisted conformation (PDB code: 1J6Z). B.) Twisted and open conformational group. In the front view the large (green) and small (blue) domains open the nucleotide-binding cleft. In the side view it can be seen that the actin molecule is in a twisted conformation (PDB code: 1HLU). C.) Untwisted and closed conformational group. In the front view the large (green) and small (blue) domains close the nucleotide-binding cleft. In the side view it can be seen that the actin molecule is flat and exhibits an untwisted conformation (actin subunit extracted from the actin filament structure PDB code: 2Y83).

The third group includes a unique structure of the actin molecule that is closed and untwisted (Figure 4/C) and can be observed only in the filamentous form of actin [26]. The transition of the actin molecule from one conformational state to the other occurs through a scissor- and propeller-like motion of the main domains of actin with respect to each other. These domain rearrangements have important physiological relevance. The scissor-like motion results in the closing and opening of the nucleotide binding cleft that is attributed to the nucleotide exchange ability of the actin monomer, while the propeller-like motion can twist or flatten the actin molecule that is linked to the G- to F-actin transition [27-29].

Comparing 88 atomic structures of the actin monomer revealed that beside the global conformational changes related to the motion of the main domains of actin, local conformational variability also occurred in several regions of the actin molecule [17]. These regions include the major part of subdomain 2, especially the DNase I binding loop, the N- and C-terminus of actin, and three loops located on the surface of subdomain 4 (Figure 5.).

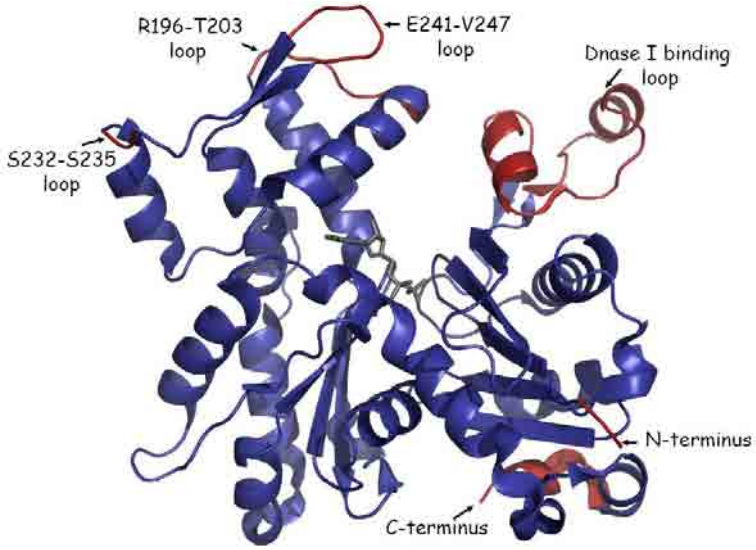

Figure 5.) Actin monomer in cartoon representation (PDB code: 1J6Z). The rigid and flexible regions are represented in blue and red, respectively. The flexible regions include the C- and N-terminus of actin, the DNase I binding loop, and three loops on the surface of subdomain 4.

The conformational heterogeneity of the aforementioned regions of the actin molecule is attributed to the inherent flexibility of these segments. Wealth body of evidence suggest that these flexible parts of the actin molecule play an important role in the formation of contacts between the actin subunits within the actin filament and the interaction of the actin molecule with actin-binding proteins. By using elastic neutron

scattering method it was demonstrated that the global dynamic heterogeneity is higher in G-actin than in F-actin. The authors concluded that the observed difference in the internal dynamics of the two states of actin is the consequence of the limited motion of the flexible regions involved in the interaction of actin protomers in the filamentous form of actin. Moreover it was suggested that the flexibility of these parts of the actin molecule was important in the recognition mechanism of the contact surfaces between actin monomers in the nucleation phase of the actin polymerisation [30].

In addition to the characteristic domain motions and conformational heterogeneity of the flexible regions another important feature of the actin molecule is the allosteric coupling between the subdomains and/or the nucleotide binding cleft. One of the most impressive proofs for the allosteric communication between the subdomains of actin was demonstrated by the Rubenstein group. They constructed a hybrid yeast actin that contained muscle specific residues in subdomain 1. It turned out that the presence of the muscle specific residues in subdomain 1 resulted in a muscle-like behaviour in subdomain 2 of yeast actin [31]. It was also pointed out that the replacement of yeast residues for muscle-specific ones in subdomain 1 slowed down the nucleotide exchange process on this muscle-yeast hybrid actin close to the value characteristic for the muscle G-actin [32]. Taking into account that the most actin monomer associating proteins (e.g. cofilin, profilin) form a contact with the subdomain 1 it seems reasonable that they have the potential to modify the behaviour of actin (e.g. nucleotide exchange, polymerisation ability) through a long-range allosteric effect that propagates from the binding site to another part of the actin molecule.

I.2. Actin-binding proteins

I.2.1. ADF/cofilin family

I.2.1.1 The history of ADF/cofilin family

Members of the ADF/cofilin protein family are small (13-19 kDa) actin-binding proteins containing one (coactosin, cofilin, GMF) or two copies (e.g. twinfilin) of the characteristic ADF/cofilin (AC) domain. They are present in all eukaryotic organisms from plants to mammals suggesting their indispensable role in the regulation of the actin cytoskeleton system of the living cells [33-36]. The first member of the ADF/cofilin family was isolated from embryonic chick brain extract and was named actin depolymerising factor (ADF) based on the observation of actin filament disassembly in the presence of this protein [33]. The second member of the ADF/cofilin family was discovered 4 years later, and appeared in the literature as cofilin according to its ability to cosediment with the actin filament [37]. These pioneer observations proposed that the members of the ADF/cofilin family can bind to the actin cytoskeleton system and can cause its partial depolymerisation of that.

I.2.1.2 Biochemical function of ADF/cofilin

All studies agree that the main function of cofilin in the living cells is to enhance the actin filament treadmilling in the highly dynamic regions of the actin cytoskeleton system (e.g. at the leading edge of the moving cells), but the underlying mechanisms are still controversial. Several in vitro studies pointed out that ADF/cofilin can facilitate the dissociation of ADP-actin monomers at the pointed end of the filament resulting in an increased flux of actin subunits from the pointed to the barbed end [38, 39]. Taking into account that the rate limiting step of the actin filament treadmilling is the off-rate of ADP-actin monomers at the shrinking end, the ADF/cofilin stimulated disassembly at the minus end can be a good interpretation for the faster actin filament turnover rate observed in the presence of ADF/cofilin. Another possible mechanism has been revealed by direct observation of actin filament fragmentation in the presence of ADF/cofilin by light and electron microscopy techniques [40-44]. This severing activity

of ADF/cofilin generates free barbed ends therefore increases the probability of actin subunits to collide with the fast growing filament ends. The third mechanism that can contribute to the enhanced actin filament treadmilling is the ability of ADF/cofilin to stimulate the release of inorganic phosphate (P_i) from the filament that leads to the faster "aging" of the ADF/cofilin decorated actin structures [45]. All the above mechanisms enhance the actin filament treadmilling by accelerating the aging of the actin filaments or the disassembly of the already aged actin filament meshwork. Beside these functions ADF/cofilin has a stimulating effect on the kinetics of actin filament assembly presumably via stabilising the actin dimers formed in the nucleation step of the actin polymerisation [43, 46, 47].

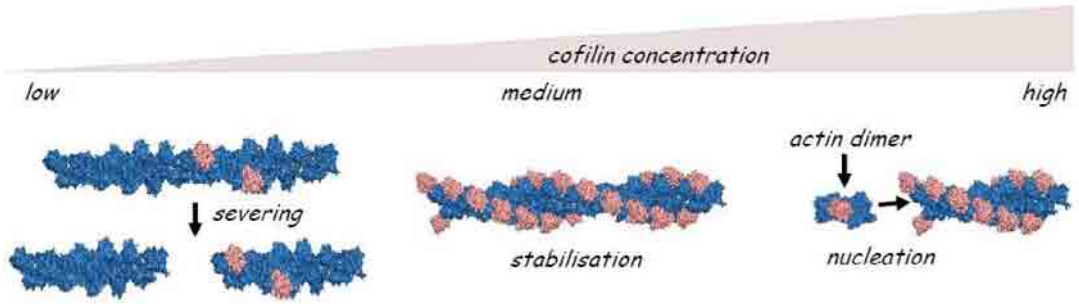

Figure 6.) Newest model proposed for the versatile function of ADF/cofilin in a concentration-dependent manner. At low cofilin-actin ratio the ADF/cofilin (salmon) effectively severs the actin filaments (blue), but at higher ratio this effect is abolished and the severing function of ADF/cofilin turns into an actin filament stabilizing function. At high ADF/cofilin concentration the ADF/cofilin can promote the de novo polymerization of actin filaments by stabilising the actin dimers in the nucleation step.

I.2.1.3 Binding of ADF/cofilin to actin

The members of the ADF/cofilin family can form 1:1 stoichiometric complex with both the G- and F-form of actin. ADF/cofilin prefers to associate with the ADP-loaded form of the actin monomer and filament which suggests that the ADF/cofilin prominently interacts with the "aged" regions of the actin cytoskeleton network [38, 48-51]. Recently the atomic structure of the actin filament decorated with human cofilin 2 was reconstructed based on cryoelectron microscopy images [52]. This three-dimensional reconstruction revealed that the cofilin could form contact with two adjacent actin monomers along the long axis of the filament by simultaneously interacting with the hydrophobic groove between the subdomains 1 and 3 of the "upper" actin subunit and to the subdomain 2 of the "lower" actin subunit (Figure 7/A).

This binding mode induces a substantial twist in the turn of the actin filament helix, a structural change that is thought to be responsible for the observed severing activity of ADF/cofilin [53]. In the lack of the atomic structure of the actin monomer in complex with ADF/cofilin the precise binding fashion to actin monomer is still elusive. It is noteworthy that the studies investigating the binding of cofilin to the actin monomer propose both binding fashions mentioned above regarding to the interaction between cofilin and actin filament [48, 54-57]. Recently the atomic structure of the C-terminal ADF-H domain of twinfilin in complex with actin monomer was resolved [58]. This structure favours the interaction of ADF/cofilin with the groove located between the subdomains 1 and 3 of the actin monomer (Figure 7/B). This binding fashion resembles the interaction of cofilin 2 with the upper actin subunit within the actin filament.

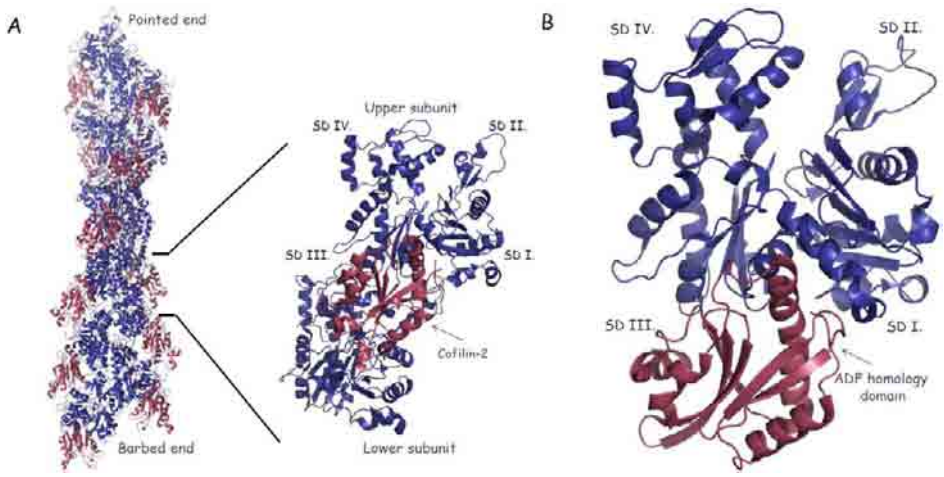

Figure 7.) Atomic structure of ADF/cofilin with actin. A.) Atomic structure of α-skeletal actin filament (blue) decorated with cofilin 2 (red) (PDB code: 3J0S). The right side of panel A illustrates the binding arrangement of cofilin to two adjacent actin monomers. B.) Atomic structure of ADF homology domain of twinfilin (red) with α-skeletal actin monomer (blue) (PDB code: 3DAW). The binding resembles to the interaction of cofilin 2 with the upper actin subunit in the actin filament.

I.2.1.4 Regulation of ADF/cofilin

ADF/cofilin can be regulated by the phosphorylation of the serine 3 residue located in the N-terminus of the protein. The phosphorylation of ADF/cofilin impairs

its binding ability to both the G- and F-actin resulting in a loss of function related to the actin cytoskeleton system. LIM kinases (LIMK) and testicular kinases (TESK) catalyse the phosphorylation of ADF/cofilin leading to the deactivation of ADF/cofilin in the living cells [59-61]. Deactivated ADF/cofilin molecules can be reactivated through the cleavage of the attached phosphate by Slingshot and chronophin phosphatases [62]. The activity of ADF/cofilin can also be controlled by phosphatidylinositol phosphates such as PIP_2 and PIP_3 which can prevent the association of ADF/cofilin to actin filaments [63-65].

I.2.2 Profilin family

I.2.2.1 History of the profilin family

The profilin is a small (19 kDa) actin-binding protein widely distributed in eukaryotic organisms from plants to mammals. The profilin was discovered in 1976 as a factor which can prevent the polymerisation of actin [66]. The name of profilin originates from the observation that it keeps the actin in the pro-filamentous form (actin monomer). It has a remarkably high expression level in the cytoplasm (20-100 μM) suggesting an important role of the molecule in maintaining a large reservoir of unassembled actin in the cells [67].

I.2.2.2 Biochemical function of profilin

The main function of profilin is to maintain a large pool of polymerisation competent actin in the cell cytoplasm. This function can be fulfilled by different actions of profilin. Dissociation of ADP-loaded actin monomers at the shrinking end of the filament is followed by a subsequent exchange of ADP for ATP before the next cycle of incorporation into the growing end of the filament. Profilin can facilitate this nucleotide exchange process on ADP-loaded actin resulting in the accumulation of a large polymerisation competent actin monomer pool [68, 69]. Profilin impairs the formation of the actin nuclei resulting in a slower kinetics for the nucleation step of actin filaments [70]. It prevents the addition of actin subunits to the pointed end of the filament, while the profilin-actin complex is able to participate in barbed end assembly but with a slightly lower rate than actin alone [70, 71]. These effects of profilin drive

the ATP-recharged actin subunits toward the fast growing end of the filament. In this sense profilin does not behave like a typical actin sequestering protein such as thymosin β4, because in the presence of free barbed ends the profilin-actin complex can effectively incorporate into the filaments [72].

I.2.2.3 Binding of profilin to actin

Profilin can form a 1:1 stoichiometric complex with the actin monomer. The profilin prefers to bind to the ATP-loaded actin monomer with a remarkably high affinity [69, 73-75]. This strong binding of profilin to the ATP actin monomer enables profilin to compete with thymosin β4 for actin monomer binding [76, 77]. This ability of profilin is important in actin-based motility processes, because in the cells large portion of actin monomer is in complex with thymosin β4 being unable to participate in filament elongation, while the profilin-actin complex can productively incorporate into actin filaments.

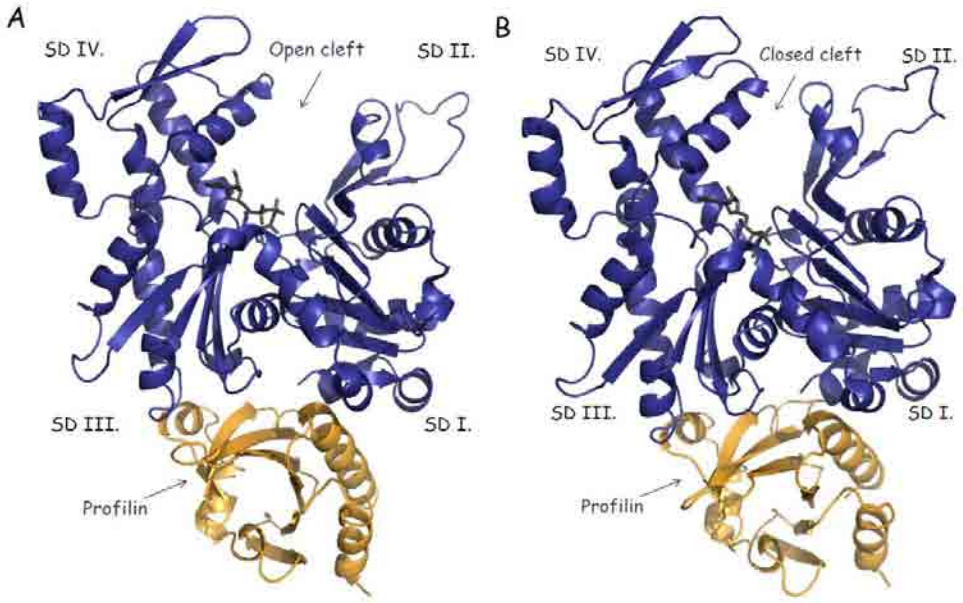

Figure 8.) Atomic structure of bovine profilin in complex with β-actin monomer. A.) Profilin- β-actin complex in open conformation. Blue and yellow cartoons represent actin and profilin, respectively. Subdomains are numbered and ATP is shown as sticks in the centre of the actin molecule (PDB code: 1HLU). B.) Profilin- β-actin complex in closed conformation. Actin (blue) and profilin (yellow) are in cartoon representation. Subdomains are numbered and ATP is in the centre of the actin molecule in sticks representation (PDB code: 2BTF).

So far several structures of the profilin-actin complex have been determined under different circumstances by using different isoforms of actin and profilin [78-82].

All these structures are similar in that profilin binds to the hydrophobic groove located between subdomains 1 and 3 of actin monomer. In two of these structures the actin monomer adopts an open conformation that can be linked to the enhanced nucleotide exchange process on actin monomer in the presence of profilin (Figure 8/A). In the rest of the structures the nucleotide-binding cleft of actin is in a closed conformation when it is in complex with profilin (Figure 8/B). Contrary to the strong interaction with the actin monomer, profilin has a weak binding ability to the actin filament [71].

I.2.2.4 Regulation of profilin

Profilin can bind phosphatidylinositol phosphates such as PIP_2 and PIP_3 which can prevent its binding to the actin molecule [83, 84]. Profilin has two PIP_2 interacting surfaces one of that overlaps with the actin binding sites whereas the other one is close to the poly-(L-proline) binding surface [85, 86]. The latter PIP_2 binding region can play a role in the control of the interaction of profilin with actin filament elongation factors such as the members of the formin and Ena/VASP families [81, 87-89].

II. Aims of the thesis

The main goal of the work presented in this thesis was to explore the effect of actin monomer binding proteins on the conformational state and intrinsic dynamics of the actin molecule in the context of actin function. The work was mainly focused on the conformation of the nucleotide-binding cleft of actin in the presence of cofilin or profilin. Most of these two actin monomer binding proteins have opposite effect on the nucleotide exchange process on actin and presumably on the conformation of the nucleotide-binding cleft as well. In addition to get information about the conformation of nucleotide-binding cleft we attempted to elucidate the contribution of the conformational dynamics of the small domain of actin to the nucleotide exchange process.

The following questions were addressed:

1.) How does yeast cofilin or profilin affect the nucleotide exchange on the α-skeletal actin monomer?

2.) What type of conformational change is induced in the nucleotide binding cleft of ATP-loaded actin monomers due to the binding of yeast cofilin or profilin?

3.) How does yeast cofilin or profilin change the structure and conformational dynamics of the small domain of the actin monomer?

4.) What relationship exists between the conformational state of the nucleotide binding cleft of actin and the heat stability of the actin monomer?

III. Preparative and experimental procedures

III.1 Protein preparation

III.1.1 Preparation of α-skeletal actin

Acetone-dried muscle powder was obtained from rabbit skeletal muscle as was described earlier by Feuer et al. [90]. First, ~360-370 g of psoas major muscle and the longissimus dorsi muscle of the euthanised rabbit were placed in ~350 ml cold distilled water and then the meat was ground two times. The ground flesh was placed in 1 litre of buffer-1 (0.15 M KH_2PO_4, 0.15 M K_2HPO_4, 0.1 M KCl – pH 6.5) and stirred with a glass stick for 15 minutes. After the stirring the fluid phase was filtered through 4 layers of gauze and the muscle mince was placed in 2 litres of buffer-2 (0.05 M $NaHCO_3$ – pH 6.5) and stirred with a glass stick for 10 minutes. This step was followed by another filtering with 4 layers of gauze. The residue was then placed in 1 litre of buffer-3 (1 mM EDTA, pH 7.0), stirred for 10 minutes and then filtered through 4 layers of gauze. 2 litres of distilled water was poured on the residue and after 5 minutes of stirring it was filtered through 4 layers of gauze. The last step with the distilled water wash was repeated. Then, in a ventilated laboratory hood there were overall 5 acetone-washing steps were carried out, each was taking for 5-10 minutes in 1 litre clean acetone by gently stirring the sample at room temperature. Each step was followed by filtration through 4 layers of gauze. The muscle powder was then left in the lab-hood overnight to dry. Next day the mass of the acetone-dried muscle powder was weighted and then was kept at -20 °C. The calcium bound G-actin was prepared from acetone powder according to the method of Spudich and Watt with a slight modification introduced by Mossakowska et al. [91, 92]. Each gram of acetone-dried muscle powder was extracted by stirring in 20 ml G-buffer containing 4 mM Tris-HCl (pH 8.0), 0.2 mM ATP, 0.1 mM $CaCl_2$, 0.5 mM DTT and 0.005 % NaN_3 at 4 °C temperature. After 30 minutes of gentle stirring the liquor was filtered through 4 layers of gauze and then the extraction step was repeated with the same volume of fresh G-buffer. After the second filtration the filtered liquid was collected in measuring cylinder and was

polymerized at room temperature by the addition of 100 mM KCl and 2 mM $MgCl_2$ After 2 hours of polymerisation 0.6 M solid KCl was measured in the sample which was gently stirred and kept at 4 °C for 30 minutes. When the KCl was completely dissolved the sample was sedimented at 328.000x*g* for 40 minutes at 4 °C and the pellets were swollen on ice for at least 2 hours in few ml of G-buffer. The swollen pellets were gently homogenised and then were dialysed against G-buffer overnight. On the following day the actin sample was centrifuged at 328.000x*g* for 40 minutes at 4 °C in order to separate the G-actin from the remaining filamentous actin. The supernatant was considered to be solely G-actin. The absorption of G-actin was measured by a Shimadzu UV-2100 spectrophotometer and the concentration of G-actin was calculated by using an absorption coefficient of 1.11 mg^{-1} ml cm^{-1} and 0.63 mg^{-1} ml cm^{-1} at 280 nm and 290 nm, respectively [93]. A relative molecular mass of 42,300 Da was used for G-actin [94].

III.1.2 Preparation of yeast cofilin

The plasmid construction (pGAT2 – GST-fusion expression vector) containing the nucleotide sequence of yeast cofilin (generous gift from Prof. Pekka Lappalainen) was transformed into BL21 (DE3) *Escherichia coli* strain. Next day a single colony of bacteria was used for inoculation of 300 ml of Luria Broth medium and kept in a shaker on 37 °C overnight. On the following day this *small culture* of cells was used to make 6 litre of *large culture* expressing the GST-fusion yeast cofilin. The cells were grown on 37 °C until the optical density reached 0.6 at 600 nm and the expression was induced by adding 0.2 mM isopropyl-β-D-1-thiogalactopyranoside (IPTG). The course of the induction was 16 hours, at 20 °C with continuous shaking of the culture. After the induction the cells were centrifuged for 25 minutes at 4.000 × *g* at 4 °C and washed with 100 ml of 20 mM Tris-HCl buffer (pH 7.5). The washed cells were dissolved in 60 ml of phosphate buffer saline (PBS) containing 1 % Triton X-100, 0.2 mM phenylmethylsulfonyl-fluoride (PMSF) and lysed by sonication and pelleted for 15 minutes at 15.000 × *g*. Glutathione-agarose beads were added to the supernatant in order to selectively bind the GST-fusion proteins. The beads were incubated with the supernatant for 4 hours at 4 °C and shaked gently continuously. After the incubation the beads were pelleted and the supernatant was removed. Then the beads were washed 5

times with PBS and incubated (at 4 °C, overnight) with thrombin (5units/ml) to cleave the yeast cofilin from the beads. On the following day the elution was loaded on a Superdex-75 HiLoad gel filtration column equilibrated with 20 mM Tris-HCl (pH 7.5) and 50 mM NaCl. The peak fractions were pooled and dialysed against 20 mM Tris-HCl buffer containing 50 mM NaCl at 4 °C overnight. The dialysed sample was concentrated to ~ 250 μM by using 10-kDa cut off filter tube. The absorption of the yeast cofilin was measured by a Shimadzu UV-2100 spectrophotometer and the concentration was calculated at 280 nm by using an absorption coefficient of 1.002 mg^{-1} ml cm^{-1}. The purified yeast cofilin sample was divided into small aliquots, frozen in liquid nitrogen, and kept at -80 °C. The frozen yeast cofilin was used within few months and centrifuged prior to all measurements.

III.1.3 Preparation of yeast profilin

The plasmid construction (pHAT2 – His-tagged expression vector) containing the sequence of yeast profilin (generous gift from Prof. Pekka Lappalainen) was transformed into BL21 (DE3) *Escherichia coli* strain and plated on Luria Broth medium containing 100μg/ml ampicillin on the same day. Next day a single colony of bacteria was used for inoculating of 300 ml of Luria Broth medium and kept in a shaker on 37 °C overnight. On the following day this *small culture* of cells was used to make 6 litre of *large culture* expressing the 6 x His-tagged fusion yeast profilin. The cells were grown on 37 °C until the optical density reached 0.5 at 600 nm and then the expression was induced by adding 0.2 mM isopropyl-β-D-1-thiogalactopyranoside (IPTG). The time course of the induction was 16 hours, at 20 ºC by shaking the culture continuously. After the induction the cells were centrifuged for 25 minutes at 4.000 × *g* at 4 ºC and washed with 100 ml of 20 mM Tris-HCl buffer (pH 7.5). The cells containing the His-tagged fusion proteins were resuspended in a buffer containing 50 mM Tris-HCl (pH 8), 250 mM NaCl, 10 mM imidazole, 1 % Triton X-100 and 0.2 mM PMSF. The cells were sonicated and centrifuged for 25 minutes at 10.000×g, at 4 ºC. After the centrifugation the supernatant was mixed with Nickel-NTA beads and incubated for 4 hours in a cold room, with continuous shaking. After the incubation the beads were washed five times with buffer containing 50 mM Tris-HCl (pH 8.0), 250 mM NaCl, and 20 mM Imidasole to remove the contaminating proteins from the suspension. The

elution of the recombinant protein was initiated by adding a buffer containing 50 mM Tris-HCl (pH 8.0), 50 mM NaCl, and 250 mM imidasole. The elution was loaded on a Superdex-75 HiLoad gel filtration column equilibrated with 20 mM Tris-HCl (pH=7.5) and 50 mM NaCl. The peak fractions corresponding to the yeast profilin were collected and concentrated in 10-kDa cut-off filter tube to a final concentration of ~400 μM. The absorption of the yeast profilin was measured by a Shimadzu UV-2100 spectrophotometer and the concentration of that was calculated at 280 nm by using an absorption coefficient of 1.458 mg^{-1} ml cm^{-1}. The sample was divided into small aliquots, frozen in liquid nitrogen, and kept at -80 °C. The frozen yeast profilin was used within few months and prior to all measurements it was centrifuged in a Beckman ultracentrifuge.

III.2 Protein labelling

III.2.1 Labelling of cysteine 374 of actin with IAEDANS

The labelling of actin monomer with IAEDANS at Cys374 was performed as described earlier [95]. The labelling started with the transformation of G-actin into filamentous form by supplementing the G-actin solution (50 μM) with $MgCl_2$ and KCl in a final concentration of 2 mM and 100 mM, respectively. F-actin (2 mg/ml) was incubated with 10-fold molar excess of IAEDANS for 1 h at room temperature. The labelling process was terminated by adding MEA to the solution in a final concentration of 2 mM. The labelled F-actin was centrifuged at 328.000 x *g* for 40 min at 4 °C. After the centrifugation the supernatant containing the unbound fluorescent dyes was discarded, and the pellet was dissolved, homogenised, and dialysed in G-buffer overnight. On the following day the labelled-actin was centrifuged and the concentration of the supernatant was determined with a Shimadzu UV-2100 spectrophotometer. The extinction coefficient of 0.63 mg^{-1} ml cm^{-1} at 290 nm was used for calculating the concentration of actin [93]. The contribution of the light absorption of IAEDANS to the absorption of actin at 290 nm was taken into account in the calculation. The concentration of IAEDANS was calculated at 336 nm using the extinction coefficient of 6.100 M^{-1} cm^{-1} [96]. The labelling ratio of five independent preparations was between 0.86 and 0.92.

III.2.2 Labelling of lysine 61 of actin with FITC

FITC was attached to unlabelled (for fluorescence quenching experiments) or IAEDANS-labelled (for FRET experiments) G-actin at the position of Lys-61 according to Miki et al. [95]. Before the labelling, G-actin was dialysed against a buffer containing 4 mM borate (pH 8.5), 0.5 mM ATP, 0.1 mM $CaCl_2$, and 1 mM MEA overnight. FITC dissolved in 0.1 M NaOH was added to the G-actin solution in 10-fold molar excess. The reaction mixture was stirred gently at room temperature for 3 hours, maintaining the pH at 8.5 by the addition of an appropriate volume of 0.1 M NaOH. To eliminate the unlabelled actin (FITC-labelled actin monomers have impaired polymerisation ability), the solution was polymerized by adding KCl and $MgCl_2$ in a final concentration of 100 mM and 2 mM, respectively. After 2 hours incubation at room temperature the sample was centrifuged at 328.000 x *g* for 40 minutes at 4 °C. The supernatant was loaded on a Sephadex G-25 gel filtration column in order to remove the unbound fluorescent dyes. The labelled-actin was eluted with a buffer containing 100 mM KCl, 0.2 mM ATP and 20 mM Tris/HCl (pH 7.6). Front peaks were collected and dialysed against a buffer containing 4 mM Tris/HCl (pH 8.0), 100 mM KCl, 0.2 mM ATP, 0.1 mM $CaCl_2$, 0.5 mM MEA, and 0.005% NaN_3 overnight. The protein solution was further dialysed against G-buffer overnight. The concentration of FITC-labelled actin was calculated from the absorption spectrum of the labelled-actin by using the extinction coefficient of 0.63 mg^{-1} ml cm^{-1} at 290. The contribution of light absorption of FITC to the absorption of actin at 290 nm was taken into account in the calculation. The concentration of double-labelled (IAEDANS and FITC) actin was determined by Bradford protein assay using G-actin as a standard [97]. The concentration of FITC was calculated from the absorption spectrum of labelled-actin species by using the extinction coefficient of 74.500 M^{-1} cm^{-1} at 493 nm [98]. The ratio of labelling was between 0.95 and 0.99 in five independent preparations.

III.2.3 Labelling of the nucleotide binding cleft of actin with etheno-ATP

G-actin binding the fluorescent ATP analogue (ε-ATP) was prepared according to Carlier et al. [75]. The concentration of G-actin was adjusted to 50 μM in 1.2 ml of

ATP-free G-buffer. This actin solution was supplemented with 180 µl ion exchanger resin (50 % DOWEX 1x2-400) to remove the unbound ATP present in the sample. The mixture of the G-actin and ion exchanger resin was immediately centrifuged (13.200 x *g* at 4˚C for 3 minutes) to avoid the dissociation of the bound ATP. The supernatant was mixed again with the same amount of DOWEX-1 to ensure that only a negligible fraction of free ATP remains in the solution. The centrifugation step was repeated to clarify the G-actin solution from the ion exchanger resin completely. The supernatant contained 1:1 molar ratio of Ca-ATP-G-actin complex (50 µM) which was mixed with 5-fold molar excess of ε-ATP (final concentration 250 µM) and was kept on ice overnight. Next day the ε-ATP-labelled actin sample was treated for a short time with DOWEX-1 to decrease the amount of free ε-ATP in the solution. The absorption spectrum of ε-ATP-labelled actin was recorded with a Shimadzu UV-2100 spectrophotometer and the concentration of that was calculated by using the extinction coefficient of 1.1 ml^{-1} mg cm^{-1} and 0.63 ml^{-1} mg cm^{-1} at 280 nm and 290 nm, respectively. The contribution of ε-ATP to the absorption spectrum of actin was taken into account in the calculation.

III.3 Fluorescence spectroscopy assays

III.3.1 Nucleotide exchange experiments on ε-ATP labelled actin

The dissociation rate of the etheno-ATP was investigated by using an Applied Photophysics SX.18MV-R Stopped-Flow instrument. Syringe-A contained 2 µM Ca-G-actin labelled with etheno-ATP and varying concentration of yeast cofilin and profilin. Syringe B was filled up with 1 mM ATP dissolved in buffer containing 4mM TRIS (pH 8.0), 0.2 mM $CaCl_2$, 0.5 mM MEA, 0.005 % NaN_3. The nucleotide exchange rate is monitored by following the drop of fluorescence intensity of ε-ATP dissociating from the actin monomers. The etheno-ATP bound to actin was excited at 320 nm and the fluorescence emission was filtered by an FG 385 cut-off filter. The change of the fluorescence intensity was recorded for 500 s and the observed rate constant (k_{obs}) was determined by fitting a single or double exponential function to each trace.

III.3.2 Fluorescence quenching

III.3.2.1 Steady-state fluorescence quenching of etheno-ATP

Steady-state fluorescence quenching measurements were carried out on a Perkin-Elmer LS50B spectrofluorometer equipped with a thermostated cuvette holder. The ε-ATP was dissolved in G-buffer not containing any ATP. The concentration of ε-ATP was set to 5 μM in all measurements. The fluorescence signal of ε-ATP was quenched by adding acrylamide in a final concentration of 0.3 M in 22 steps. The excitation wavelength was set at 320 nm and the emission spectra were recorded between 320 nm and 600 nm at 20 °C. The ratio of the fluorescence intensity of ε-ATP in the absence and presence of the quencher was plotted against the quencher concentration (so called Stern-Volmer plot). The Stern-Volmer constant (K_{SV}) characterising the accessibility of the fluorophore was derived from the slope of the straight line fitted on the experimental data according to the classical Stern-Volmer equation:

$$\frac{F_o}{F} = 1 + K_{SV}[Q] \qquad (1)$$

where F_0 is the fluorescence intensity of the fluorophore in the absence of the quencher, and F is the fluorescence intensity of the fluorescent dye at different quencher concentration [Q].

III.3.2.2 Time-resolved fluorescence quenching of etheno-ATP

Time-resolved fluorescence measurements were performed on an ISS K2 Multifrequency Cross-Correlation Phase and Modulation spectrofluorometer equipped with a thermostated cuvette holder. The fluorescence lifetime of 50 μM ε-ATP dissolved in G-buffer lacking of ATP was measured upon quenching with acrylamide. The concentration of the quencher was raised from 0 to 0.3 M in 6 concentration steps. Freshly prepared glycogen solution was used as reference (lifetime=0 ns). The excitation wavelength was set to 320 nm and the intensity of the light source (300 W Xe arc lamp) was modulated sinusoidally with a double-crystal Pockels cell. The fluorescence emission of the sample was filtered with an FG 320 high-pass filter. The

phase delay and demodulation ratio of the fluorescence signal coming from the sample was measured with respect to the phase delay and demodulation ratio of the glycogen solution. The modulation frequency was changed from 2 to 64 MHz in 10 steps. The data were analysed by the Vinci (version BETA.1.6) instrument software. The fluorescence lifetime of ε-ATP was determined by using nonlinear least-square analysis. The goodness of fit was estimated from the value of the reduced χ^2. This factor was below 2.5 in all data processing. The ratio of the fluorescence lifetime of ε-ATP in the absence (τ_0) and presence (τ) of the quencher molecule was plotted against the concentration of the quencher. The Stern-Volmer constant (K_{SV}) was calculated from the slope of the straight line fitted to the plotted data:

$$\frac{\tau_o}{\tau} = 1 + K_{SV}[Q] \qquad (2)$$

III.3.2.3 Time-resolved fluorescence quenching of etheno-ATP labelled actin

The fluorescence lifetime of 20 μM ε-ATP labelled G-actin was quenched with acrylamide in the presence and absence of 20 μM cofilin and profilin. The instrumentation and the parameters of the experiments were the same as described at the time-resolved fluorescence quenching of pure ε-ATP solution. During the data analysis the best fit was achieved assuming two discrete lifetime components.

III.3.2.4 Steady-state fluorescence quenching of etheno-ATP-labelled actin

The fluorescence emission of 5 μM ε-ATP-labelled actin was quenched with acrylamide in the absence and presence of 15 μM or 20 μM cofilin or profilin, respectively. The instrumentation and the parameters of the experiments were the same as described at the steady-state fluorescence quenching of pure ε-ATP solution. The data analysis required special considerations, because the Stern-Volmer plot deviated from the straight line. It was supposed that both static and dynamic quenching processes contribute to the decrease of the fluorescence signal. In this special case the following equation can be used to fit to the result of the Stern-Volmer plot:

$$\frac{F_o}{F} = (1 + K_{SV\_S}[Q])(1 + K_{SV\_D}[Q]) \quad (3)$$

where K_{SV_S} and K_{SV_D} are the static and dynamic Stern-Volmer constant of the fluorophore, respectively. In a more complicated situation when both quenching processes are responsible for the decrease of the fluorescence signal and there are more than one fluorophore population with different accessibility for the quencher the modified form of the Stern-Volmer equation is necessary to be applied:

$$\frac{F_o}{F} = \left(\sum_{i=1}^{n} \frac{\alpha_i}{\left(1+K_{SV\_S_i}[Q]\right)\left(1+K_{SV\_D_i}[Q]\right)} \right)^{-1} \quad (4)$$

where K_{SV_Si} and K_{SV_Di} are the static and dynamic Stern-Volmer constant of the i^{th} fluorophore population represented with the fraction of α_i, respectively. The estimation of the accessibility of ε-ATP bound to the nucleotide binding cleft of actin was approached by using the latter form of the Stern-Volmer equation.

III.3.2.5 Fluorescence quenching of IAEDANS-labelled actin

The local environment of the C-terminus of actin was investigated by quenching the fluorescence intensity of IAEDANS attached to cysteine 374 with acrylamide in the presence and absence of cofilin and profilin. Fluorescence quenching measurements were carried out at a constant temperature of 20 °C. In all experiments the concentration of the labelled actin was set to 2 μM in G-buffer and the final concentration of cofilin and profilin were adjusted to 10 and 25 μM, respectively. The emission spectrum of IAEDANS-labelled actin was recorded in the range of 365 and 600 nm with an excitation wavelength of 360 nm. The concentration of the acrylamide (Q) was increased from 0 to 0.5 M and the integral of the emission spectrum was considered as an appropriate value to characterise the fluorescence intensity. The ratio of the fluorescence intensity in the absence (F_0) and presence (F) of the quencher molecule is plotted against the concentration of the quencher. The Stern-Volmer constant (K_{SV}) is derived from the slope of the straight line fitted to the experimental data according to the Stern-Volmer equation (Equation 1.).

III.3.2.6 Fluorescence quenching of FITC-labelled actin

Local environment of lysine 61 (located in subdomain 2) of actin was investigated by applying steady-state fluorescence quenching method. The fluorescence intensity of FITC attached to lysine 61 was quenched with acrylamide in the presence and absence of either cofilin or profilin separately. The measurements were carried out at a constant temperature of 20 °C. In all experiments the concentration of the labelled actin was set to 2 μM in G-buffer and the final concentration of cofilin and profilin were adjusted to 10 and 25 μM, respectively. The emission spectrum of FITC-labelled actin was recorded in the range of 500 and 600 nm with an excitation wavelength of 495 nm. The concentration of the acrylamide (Q) was increased from 0 to 0.5 M. The area under the emission spectrum was considered as a measure of the fluorescence intensity of the reporter molecule. The ratio of the fluorescence intensity in the absence and presence (F) of the quencher molecule was plotted against the concentration of the quencher. The Stern-Volmer constant (K_{SV}) was obtained from the slope of the straight line fitted to the experimental data according to the Stern-Volmer equation (Equation 1.).

III.3.3 Fluorescence Anisotropy

III.3.3.1 Steady-state fluorescence anisotropy measurements

Steady-state fluorescence anisotropy was applied to determine the affinity of cofilin and profilin to IAEDANS-labelled actin. Fluorescence anisotropy experiments were performed on a Perkin-Elmer LS50B spectrofluorometer equipped with a thermostated cuvette holder at a constant temperature of 20 °C. The excitation and emission wavelength were set at 336 nm and 475 nm, respectively. The setting of excitation and emission polarisers in vertical (V) and horizontal (H) positions were executed automatically by the instrument software. Both the excitation and emission slits were adjusted to 5 nm. The concentration of G-actin was 2 μM in all measurements and the concentration of cofilin and profilin was increased until the

saturation level. Fluorescence anisotropy was calculated by using the following equation:

$$r = (F_{VV} - GF_{VH})/(F_{VV} + 2GF_{VH}) \quad (5)$$

where F_{VV}, F_{VH}, F_{HV}, and F_{HH} are the polarised fluorescence components (the first and second subscripts refers to the orientation of the excitation and emission polarisers, respectively) and G is the instrument correction factor (also known as geometry factor) which can be calculated as follows:

$$G = F_{HV}/F_{HH} \quad (6)$$

The steady-state anisotropy values were plotted against the concentration of cofilin and profilin in order to determine the dissociation constant (K_D) of the cofilin- and profilin-actin complex. Based on the work of Pollard et al [48] the following equation was applied to calculate the equilibrium dissociation constant of the cofilin- and profilin-actin complex:

$$\frac{r-r_{min}}{\Delta r_{max}} = ((B_{tot} + A_{tot} + K_D) - \sqrt{(B_{tot} + A_{tot} + K_D)^2 - 4A_{tot}B_{tot}})/2P_{tot} \quad \ldots.(7)$$

where r_{min} and r is the measured anisotropy value in the absence and presence of actin binding proteins. Δr_{max} is the difference between the anisotropy value measured at the saturation level and the anisotropy value obtained for the IAEDANS-labelled actin in the absence of actin binding proteins (r_{min}). A_{tot} and B_{tot} correspond to the concentration of actin and either of the actin binding protein (cofilin or profilin), respectively.

III.3.3.2 Time-resolved fluorescence anisotropy measurements

Time resolved fluorescence anisotropy measurements were carried out by using a Horiba Jobin-Yvon Nanolog spectrofluorometer operating in time-resolved single photon counting mode. The temperature of the cuvette holder was controlled by a HAAKE A25 heated bath circulatory system. The temperature of the sample was increased from 5 to 35 °C in steps of 5 °C as like in the temperature-dependent FRET assays. The IAEDANS-labelled actin was excited at 321 nm using a solid-state NanoLED light source with a pulse width of 1.2 ns at a repetition rate of 1 MHz. The

emission wavelength was set to 465 nm and the fluorescence signal was filtered with a 16 nm width bandpass filter. The emitted photons were collected for 400 ns with 0.11 ns channel width. The fluorescence emission was collected in parallel (F_{VV}) and perpendicular (F_{VH}) polarization in respect to the vertically polarized excitation beam for 60 seconds until the peak difference reached at least 5.000 counts. The concentration of IAEDANS-labelled actin was 20 μM and theconcentration of cofilin and profilin was adjusted to 25 μM and 35 μM, respectively. The FITC-labelled actin sample was excited at 455 nm by using a solid-state NanoLED light source with a pulse width of 0.8 ns at a repetition rate of 1 MHz. The emission fluorescence was collected at the wavelength of 520 nm with 8 nm width of bandpass filter. The fluorescence emission was collected for 200 ns in channels with 0.055 ns width. The fluorescence emission was recorded in the vertical (F_{VV}) and horizontal (F_{VH}) polarisation plane with respect to the vertically polarised excitation beam for 60 seconds until the peak difference reached the 10.000 counts. The concentration of FITC-labelled actin was 2 μM and the concentration of cofilin and profilin was 10 μM and 25 μM, respectively. The instrument response function (IRF) in parallel (IRF_{VV}) and perpendicular (IRF_{VH}) polarisation setup was recorded by using freshly prepared glycogen solution.

Data analysis

The fitting process was applied separately on the parallel (I_{VV}) and perpendicular (I_{VH}) decay curves by using the following equations to recover the rotational correlation time of the jth component and the contribution of that (β_j) to the anisotropy decay process:

$$I_{VH}(t) = G\int_{-\infty}^{t} IRF_{VH}(t')\frac{1}{3}\sum_{i=1}^{n}\alpha_i\, e^{-\frac{t-t'}{\tau_i}}\left[1+2\left(R_{INF}+\sum_{j=1}^{m}\beta_j e^{-\frac{t-t'}{\theta_j}}\right)\right]dt' \qquad (8)$$

$$I_{VV}(t) = G\int_{-\infty}^{t} IRF_{VV}(t')\frac{1}{3}\sum_{i=1}^{n}\alpha_i\, e^{-\frac{t-t'}{\tau_i}}\left[1+2\left(R_{INF}+\sum_{j=1}^{m}\beta_j e^{-\frac{t-t'}{\theta_j}}\right)\right]dt' \qquad (9)$$

where G is the ratio of the sensitivity of the detection system for the vertically and horizontally polarised light (geometry factor), R_{INF} is the residual anisotropy, τ_i and α_i

are the lifetime and amplitude of the i^{th} fluorescence decay component, respectively. The decay curves were analysed by using the Fluofit software that uses nonlinear least square minimisation based on the Levenberg-Marquardt algorithm. In the case of the IAEDANS-labelled actin the best fit was obtained, when two lifetimes and two rotational correlation times were supposed to be present. The anisotropy decay curves of the FITC-labelled samples required three lifetime and two rotational correlation time components for retrieving acceptable goodness of the fitting.

Determining the half-cone angle of the fluorophore motion with respect to the protein surface

The local motion of the fluorophore can be modelled as the stochastic diffusion of the emission dipole vector of the fluorophore within a static cone defined by a semi-angle of θ_0 [99]. The semi-angle is related to the degree of spatial restriction of the fluorophore's wobbling due to the local environment. The semi-angle can be calculated according to the following equation:

$$\frac{r_G}{r_o} = \left[\frac{1}{2}cos\theta_0(1 + cos\theta_o)\right]^2 \qquad (10)$$

where r_G and r_o are the fractional amplitude of the global motion of the protein, and the time zero anisotropy, respectively.

III.3.4 Fluorescence resonance energy transfer (FRET) experiments

FRET experiments were carried out with a Perkin-Elmer LS50B spectrofluorometer equipped with a thermostated cuvette holder. Actin was labelled with IAEDANS (donor) in subdomain 1 at Cys374 and with FITC (acceptor) in subdomain 2 at Lys61 as described by Miki et al. [95]. The efficiency of the energy transfer between the two fluorophores was determined in a temperature dependent manner; increasing the temperature of the sample from 5 °C to 35 °C in steps of 5 °C in the presence and absence of cofilin or profilin. The excitation wavelength was set at 360 nm and the emission of the donor was monitored between 420 nm and 475 nm where the emission of the acceptor is negligible. Both the excitation and emission slits

were set to 5 nm. The obtained intensities of the donor were corrected for the inner filter effect by applying the next equation:

$$F_{corr} = F_{obs} antilog[(OD_{EX} + OD_{EM})/2] \quad (11)$$

where F_{corr} is the corrected fluorescence intensity, F_{obs} is the measured fluorescence intensity of donor fluorophore, and OD_{EX} and OD_{EM} are the optical densities of the sample at the excitation and emission wavelengths of the donor fluorophore, respectively. In order to calculate the fluorescence resonance energy transfer efficiency (E), the intensity of the donor was measured in the presence (F_{DA}) and absence (F_D) of the acceptor. The energy transfer efficiency was calculated according to the following equation:

$$E = \left[1 - \left(\frac{F_{DA}}{F_D} \cdot \frac{c_D}{c_{DA}}\right)\right] / \beta \quad (12)$$

where β is the labelling ratio of the acceptor, c_{DA} and c_D are the concentrations of the donor molecule in the presence and absence of the acceptor, respectively.

In order to know the precise concentration of the donor (c_{DA}) for the double labelled actin after the measurements the samples were incubated with 0.4 mg/ml trypsin overnight. Trypsin digests the double-labelled actin into a large fragment (69-372) and small peptides, which results in the separation of the donor and acceptor molecule and finally the abolishment of the energy transfer between the fluorophores. Considering that the intensity of the fluorophore is directly proportional to the concentration, the c_{DA} can be determined precisely in the double labelled actin by measuring the intensity of the donor after the digestion.

It was shown previously that the energy transfer efficiency (E) normalised by the fluorescence intensity (F_{DA}) of the donor in the presence of the acceptor can provide information about the flexibility of the protein matrix between the FRET fluorophore pair. This normalised energy transfer efficiency is called flexibility parameter (f') that was introduced in 1984 by Somogyi et al [100]. The flexibility parameter can be calculated by using the following equation:

$$f' = E/F_{DA} \quad (13)$$

The flexibility of the proteins is related to the thermal fluctuations of protein segments relative to each other. It is expected that the increase in temperature generates higher amplitude of motion of the protein domains relative to each other. Fluctuations with a greater amplitude refers to a more flexible protein structure and results in a higher value for the flexibility parameter [101]. In our experiments the flexibility parameter was determined from 5 °C to 35 °C at seven equidistant temperature levels (steps of 5 °C). Each flexibility parameter was normalised for the flexibility parameter obtained at the lowest temperature level (5 °C) and this relative flexibility parameter was plotted against the temperature. The slope of the curve corresponds to the flexibility of the protein structure between the donor and acceptor fluorophores.

III.4 Differential Scanning Calorimetry (DSC) measurements

DSC experiments were carried out with a Setaram Micro DSC III calorimeter. Before the measurements actin was dialysed in buffer containing 4 mM MOPS (pH=8), 0.2 mM ATP, 0.1 mM $CaCl_2$, and 0.5 mM MEA. The heatflow-temperature curve of the samples was recorded between 0 $^{\circ}$C and 100 $^{\circ}$C, under 0.7 atm pressure at a scanning rate of 0.3K/min. In all experiments the concentration of actin was set to 23 μM. The heat denaturation curve of monomeric actin was recorded in the absence and presence of 23 μM yeast cofilin or profilin. The reference vessel contained only buffer in which the proteins were dissolved and the weight of that was balanced with the sample vessel with the accuracy of 1 mg. The heating of the samples was repeated immediately after the first cooling phase in order to check the reversibility of the thermal denaturation of proteins. The data obtained from the first heating phase were corrected by subtracting the second calorimetric trace. The excess heat flow of the sample with respect to the reference vessel was plotted in the function of the temperature and was further analysed by using Microcal Origin 6.0 software. The melting temperature (T_m) of the proteins and the full width at half maximum (FWHM) were determined by fitting Gaussians on the heat transition curves. The enthalpy change (ΔH) was calculated by taking the integral of the area under the heatflow-time denaturation curve.

IV. Results and conclusions

IV.1 Conformation of the nucleotide binding cleft of actin

It is a long-standing question whether there is a link between the kinetics of the nucleotide exchange process and the conformation of the nucleotide binding cleft of actin. The most accepted evidence supporting this connection relies on the crystal structure of profilin-β-actin in a conformation that shows a wide-opening of the nucleotide-binding cleft. The function-conformation relationship seems to be obvious, because one would expect that the wider nucleotide-binding cleft allows a faster nucleotide exchange on actin as it occurs in the presence of most of the profilin orthologues. To clarify this interdependence transient kinetics and fluorescence quenching assays were employed.

IV.1.1 Nucleotide exchange on actin

The propensity of G-actin to polymerise into F-actin depends on the nucleotide state of the actin monomer. The assembly of actin filaments strongly favours ATP-loaded actin over the ADP-loaded form [102]. Therefore, dissociation of ADP-bound actin monomers at the pointed end of the filament must be followed by the replacement of ADP by ATP before the next round of incorporation at the barbed end of the filament. This step of the actin turnover can be influenced by different actin monomer binding proteins such as ADF/cofilin, profilin, twinfilin, and thymosin β4 [103-105]. Members of the profilin family can promote the nucleotide exchange on G-actin. This function seems to be conserved among profilin orthologues, except for plant profilin that has no significant effect on this step of the actin turnover [48, 75, 106]. In general ADF/cofilin from different species reduce the rate of nucleotide exchange on actin, except for the recently described *Plasmodium malariae* ADF2 and *Plasmodium falciparium* ADF1 which stimulate the nucleotide exchange on actin [36, 107-109].

The impact of yeast cofilin and profilin on the nucleotide exchange of α-skeletal actin monomers was investigated in fluorescence kinetics experiments. The nucleotide exchange experiments were carried out with a stopped-flow apparatus used to study fast

chemical reactions. Actin was labelled with a fluorescent ATP analogue (ε-ATP) and the replacement of that with non-fluorescent ATP was initiated by mixing the sample with a great excess of ATP (1 mM). The fluorescence intensity of the actin-bound form of ε-ATP is higher than that of the non-bound form, therefore the nucleotide exchange process can be followed by measuring the drop in the fluorescence signal of dissociating ε-ATP as a function of time [110].

Mixing 1 μM ε-ATP labelled actin with 1 mM ATP resulted in an exponential decrease in the fluorescence intensity of ε-ATP. The process of the exchange of ε-ATP with ATP terminated within 500 s and by fitting a single exponential on the curve 0.012 s^{-1} was obtained as an observed rate constant [111]. This value is in good agreement with previous results obtained for the kinetics of nucleotide exchange on actin under similar conditions [112].

When the concentration of yeast cofilin was increased in the solution the change in the fluorescence intensity slowed down (Figure 9/A). The observed rate constant decreased from 0.012 s^{-1} to 0.002 s^{-1} when 3 μM cofilin was applied (Appendix Table 1.). The observed rate constant was obtained by fitting a single exponential on each trace. The decrease in the observed rate constant implies that yeast cofilin can effectively slow down the nucleotide exchange on α-skeletal actin in line with the results of previous studies using different isoforms of actin and cofilin [48]. Besides the decrease in the observed rate constant the fluorescence intensity of the exchange curves reached the plateau at a higher intensity level indicating the complete blocking of nucleotide exchange process on a large portion of actin.

Contrary to cofilin, yeast profilin effectively stimulated the nucleotide exchange on actin (Figure 9/B) similarly to other members of the profilin family [75, 113-116]. The nucleotide exchange curves obtained in the presence of profilin could be analysed by fitting a double-exponential function. The double-exponential fitting yielded two rate constants; one is similar to the value obtained for actin alone and nearly independent from the concentration of profilin, while another one is strongly dependent on the amount of profilin used in the experiment (Appendix Table 1.). The latter component increased from 0.012 s^{-1} to 0.75 s^{-1} as the concentration of yeast profilin was elevated from 0 to 1 μM in the reaction mixture. The possible reason why in the case of yeast profilin the nucleotide exchange curves has to be fitted with a double-exponential

function is the slow dissociation rate of profilin from actin compared to the rate of nucleotide exchange.

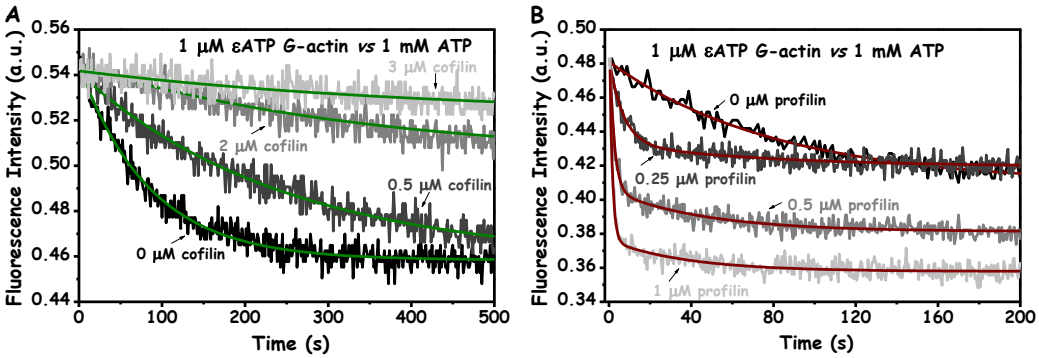

Figure 9.) Nucleotide exchange curves in the presence of cofilin or profilin. A.) Change in the fluorescence intensity of 1 µM ε-ATP-actin upon the mixing with 1 mM ATP in the absence (black line) and presence of 0.5 µM (dark grey line), 1 µM (grey line), and 3 µM (light grey line) yeast cofilin. The observed rate constant was obtained by fitting a single exponential function on each trace (green line). B.) Change in the fluorescence intensity of 1 µM ε-ATP-actin upon the mixing with 1 mM ATP in the absence (black line) and presence of 0.25 µM (dark grey line), 0.5 µM (grey line), and 1 µM (light grey line) yeast profilin. The observed rate constants were obtained by fitting a double exponential function on each curve (red line).

The slow dissociation rate results in a clearly distinguishable population of actin in the nucleotide exchange process (actin alone and profilin-actin complex). In an earlier study a similar observation was made with profilin purified from bovine spleen [75]. In the case of yeast cofilin the double-exponential nature of the nucleotide exchange curve does not appear because the condition for the rapid equilibrium between the actin monomers and cofilin is satisfied [49].

Conclusions:

The investigated proteins have opposite effect on the nucleotide exchange process. Cofilin slows down the kinetics of the nucleotide exchange on actin, while profilin facilitates it.

IV.1.2 Accessibility of ε-ATP located in the nucleotide-binding cleft

It has been demonstrated in this thesis and in many previous reports that the majority of actin monomer binding proteins can modify the rate of nucleotide exchange on G-actin [69, 75, 103, 113, 117, 118]. One possible explanation behind this effect is the rotation of the two main domains of actin relative to each other resulting in the closing or opening of the nucleotide-binding cleft. This concept was based on the comparison of the atomic structures of actin in complex with different actin-binding proteins. Aligning these atomic structures showed that the widening of the nucleotide binding cleft vary on a broad range. For instance in the structure of the profilin-β-actin complex (Figure 10/B) the actin molecule is in a twisted conformation resulting in a wide opening of the nucleotide binding cleft, while in the atomic structure of ADF-homology domain in complex with actin (Figure 10/A) the large domains partially close the nucleotide binding cleft [78] [58].

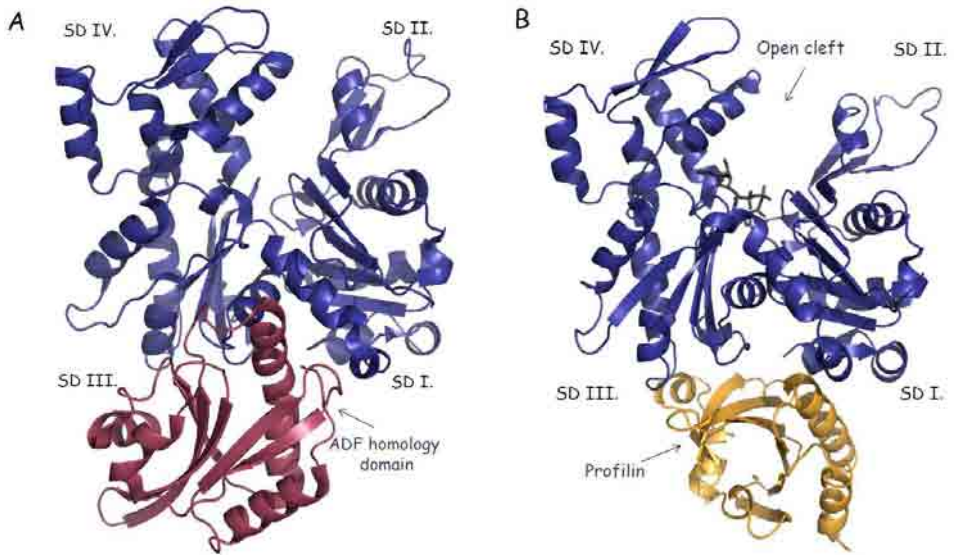

Figure 10.) A.) Atomic structure of twinfilin ADF-homolog domain with actin monomer (PDB code: 3DAW). The secondary structure elements of actin and the ADF homology domain of twinfilin are in a blue and purple cartoon representation, respectively. B.) Atomic structure of profilin with actin monomer (PDB code:1HLU)). The secondary structure elements of actin and profilin are in a blue and yellow cartoon representation, respectively.

Although these atomic structures are seemingly consistent with the results of the nucleotide exchange experiments (profilin enhances, cofilin impairs nucleotide exchange), the condition used in the crystallization process is different from the physiological environment of the proteins and in addition in crystalline form additional

forces appear in the crystal that can change the structure of the proteins [119]. In order to explore the conformational state of the nucleotide binding cleft of actin in the presence of actin-binding proteins, under physiological conditions, a series of fluorescence quenching assays were employed. Cofilin and profilin were good candidates to validate the assay, because they have opposite effects on the nucleotide exchange rate and presumably on the conformation of the nucleotide binding cleft as well. In the experiments actin was labelled with ε-ATP at the nucleotide binding site and the fluorescence signal of ε-ATP was quenched by acrylamide in the absence and presence of cofilin or profilin. The accessibility of the fluorescence ATP analogue to the quencher molecule was characterised by the Stern-Volmer constant.

IV.1.2.1 Steady-state fluorescence quenching of ε-ATP labelled actin

Steady-state fluorescence quenching experiments were carried out using 5 μM ε-ATP labelled actin. Before the measurements a short ion exchanger resin treatment was applied on the sample to remove the majority of the unbound fluorophore from the sample. This treatment leaves around 5-15 μM unbound ε-ATP in the sample, that is necessary to avoid the rapid denaturation of G-actin in the absence of free nucleotide [120]. The fluorescence signal of 5 μM ε-ATP labelled G-actin was quenched effectively by increasing the acrylamide concentration from 0 to 0.3 M (Figure 11/A).

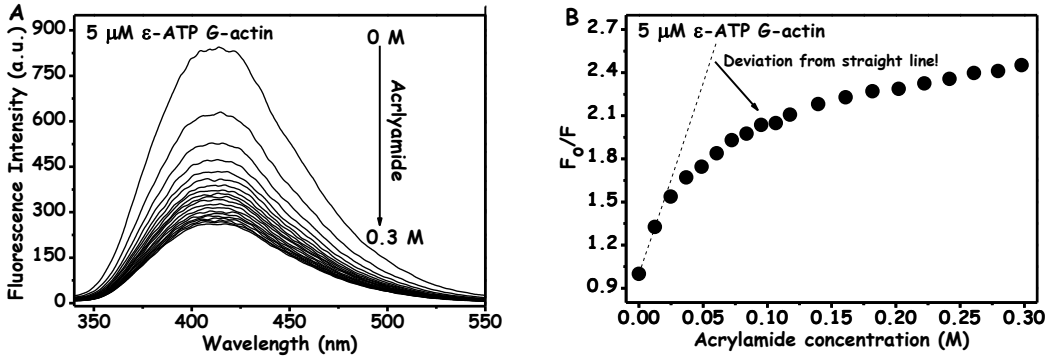

Figure 11.) Steady-state fluorescence quenching of 5 μM ε-ATP labelled G-actin. A.) Fluorescence emission spectra of 5 μM ε-ATP labelled G-actin at different concentrations of acrylamide. B.) Classical Stern-Volmer plot of the fluorescence intensity of 5 μM ε-ATP labelled G-actin as a function of quencher concentration. The dotted line represents a linear fit on the first three data points.

The classical Stern-Volmer plot resulted in a downward curvature that can indicate the coexistence of different fluorophore populations with respect to the accessibility for the quencher and/or different quenching processes (dynamic or static)

present in the sample (Figure 11/B). In this type of complex quenching process a modified form of the Stern-Volmer equation is necessary to be applied in order to derive the Stern-Volmer constants (Equation 4.). This equation includes the dynamic (K_{SV_D}) and static components (K_{SV_S}) of different fluorophore populations and their fractional contribution (α) to the quenching process. It was assumed that at least two different fluorophore populations existed with respect to the accessibility for the quencher; one that is the free and another one is the ε-ATP located in the nucleotide binding cleft of actin. In the preliminary experiments the free ε-ATP was characterised in parallel steady-state and time-resolved measurements, and the values obtained from these assays were considered as fixed components in the modified Stern-Volmer equation (Equation 4.) applied on the complex situation.

IV.1.2.2 Steady-state fluorescence quenching of free ε-ATP

In steady-state fluorescence quenching assays, the fluorescence emission of 5 μM ε-ATP was quenched by titrating the solution with a neutral quencher (acrylamide) up to a final concentration of 0.3 M (Figure 12/A). The ratio of the fluorescence emission of ε-ATP in the absence and presence of the quencher was plotted against the concentration of the quencher molecule (Figure 12/B).

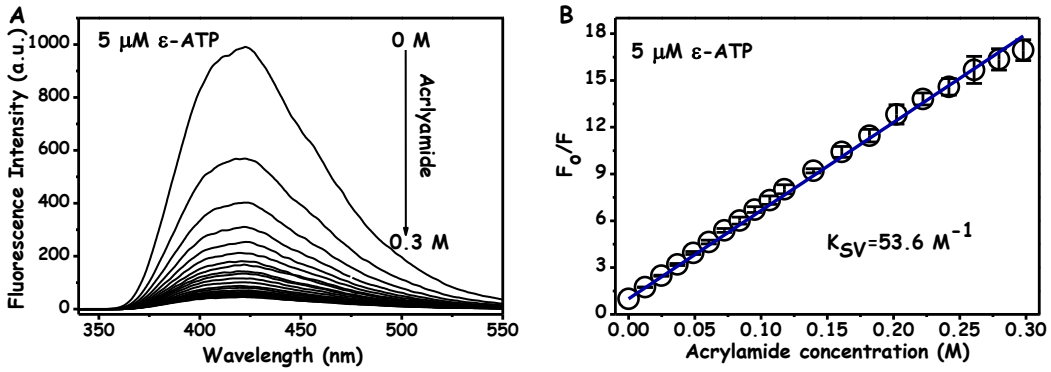

Figure 12.) Steady-state fluorescence quenching of 5 μM ε-ATP solution. A.) Fluorescence emission spectra of ε-ATP at different concentrations of acrylamide. B.) Classical Stern-Volmer plot of the fluorescence intensity of ε-ATP as a function of the quencher concentration. Error bars represent standard deviation (n=3). Straight line (blue) is obtained by fitting Equation 1. to the plotted values.

The Stern-Volmer constant (K_{SV}) was derived from the slope of the straight line obtained by the classical Stern-Volmer plot (Equation 1.). This value was 53.6 ± 3.19 M^{-1} that significantly does not differ from the value (57.81 M^{-1}) reported in an earlier study [121].

IV.1.2.3 Time-resolved fluorescence quenching of free ε-ATP

The accessibility of the free fluorophore was also tested by applying time-resolved fluorescence quenching measurements. The fluorescence lifetime of 50 μM ε-ATP was measured at 6 different acrylamide concentrations. In the absence of the quencher the lifetime of the ε-ATP was 24.52 ± 0.01 ns and declined to 1.41 ± 0.03 ns by adding acrylamide in a final concentration of 0.3 M (Figure 13/A). The ratio of the lifetime of ε-ATP in the absence and presence of the quencher was plotted against the concentration of the acrylamide (Figure 13/B). The Stern-Volmer constant was determined from the slope of the fitted line (Equation 2.). The K_{SV} value was 54.05 ± 1.2 M^{-1} that is in good agreement with the value (53.6 M^{-1}) obtained from the steady-state measurements. Comparing the results of the steady-state and time-resolved quenching of free ε-ATP it can be concluded that the free ε-ATP is solely quenched through a dynamic quenching process (the fluorescence intensity and lifetime of ε-ATP decreased by the same extent). In the light of this result, the static ($K_{SV\_S\_free\ \varepsilon\text{-}ATP}$) and dynamic ($K_{SV\_D\_free\ \varepsilon\text{-}ATP}$) quenching components of the free ε-ATP were considered to be 0 M^{-1} and 54.05 M^{-1}, respectively.

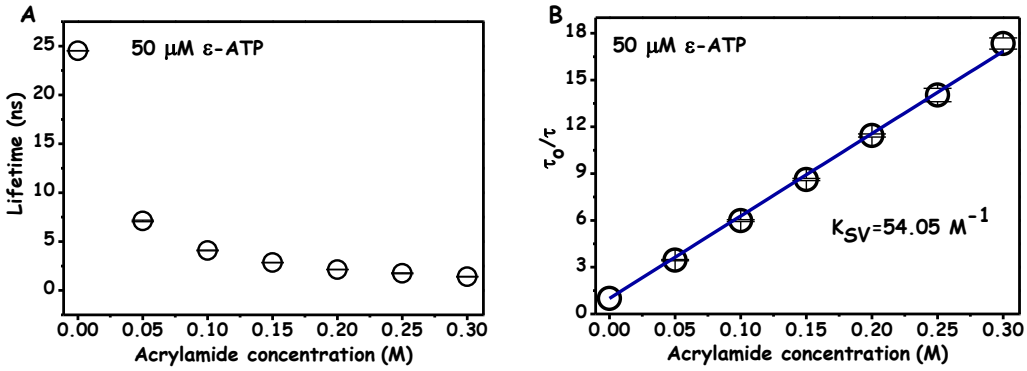

Figure 13.) Time-resolved fluorescence quenching of 50 μM ε-ATP. A.) Lifetime of 50 μM ε-ATP at different concentrations of acrylamide. B.) Classical Stern-Volmer plot of the fluorescence lifetime of 50 μM ε-ATP as a function of the quencher concentration. The black open circles show the values obtained from the experimental data. Error bars represent standard deviation (n=3). Straight line (blue) is obtained by fitting Equation 2. to the plotted values.

IV.1.2.4 Time-resolved fluorescence quenching of ε-ATP labelled actin

Time-resolved fluorescence quenching experiments were performed on 20-30 μM ε-ATP-labelled G-actin in order to clarify the quenching mechanism (static or dynamic) responsible for the quenching of actin bound ε-ATP can be quenched. In the

absence of the quencher molecule two distinct lifetime components were identified with a lifetime of 34.1 ± 4.5 ns and 25.4 ± 0.1 ns. The shorter lifetime was attributed to the unbound fluorophore, because the shorter component was almost identical with the lifetime of the free ε-ATP (24.52 ns) measured in the absence of actin-binding protein. The difference between the lifetime of the free and bound ε-ATP is probably the result of the shielding of the bound fluorophore by the nucleotide-binding cleft that can reduce the contribution of the non-radiating processes to the deexcitation of fluorophores and therefore increase the lifetime of the fluorescent dye. As the concentration of the quencher was increased from 0 to 0.3 M in the solution the value of the shorter lifetime component dropped to 1.55 ± 0.05 ns (Figure 14/A). The slope of the straight line of the classical Stern-Volmer plot (Figure 14/B) revealed a value of 49.2 ± 4.28 M^{-1} for the Stern-Volmer constant that is very close to the value obtained for the free ε-ATP in separate time-resolved experiments (54.05 M^{-1}). This result further confirms that the fluorescence component with a short lifetime belongs to the unbound fluorophore. The longer component was assumed to be the lifetime of the bound ε-ATP.

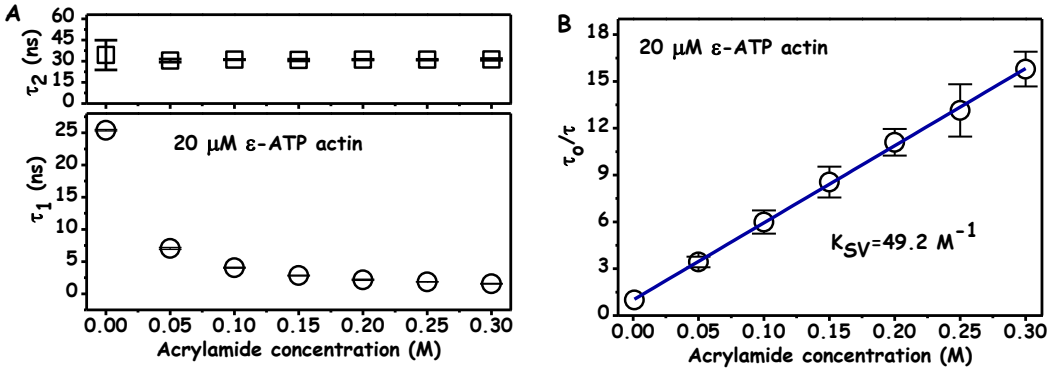

Figure 14.) Time-resolved fluorescence quenching of 20 μM ε-ATP labelled G-actin. A.) The upper and the lower panel show the change in the lifetime of the longer (τ_2) and shorter (τ_1) lifetime components as, respectively as a function of the quencher concentration. B.) Classical Stern-Volmer plot of the fluorescence lifetime of the shorter lifetime component (τ_1). The black open circles show the values obtained from the experimental data. Error bars represent standard deviation (n=3). Straight line (blue) was obtained by fitting Equation 2. to the plotted values.

In contrast to the shorter lifetime, the value of the longer component did not change significantly as the quencher concentration was raised from 0 to 0.3 M. This finding is in a good agreement with an earlier observation that the ε-ATP bound to actin is insensitive for collisional quenching [122]. Based on this result the fluorescence intensity of bound ε-ATP can be quenched solely in a static quenching process, thus the

dynamic quenching component ($K_{SV\_D\_bound\ \varepsilon\text{-}ATP}$) of the actin-bound fluorophore is considered to be 0 M^{-1}.

IV.1.2.5 Time-resolved fluorescence quenching of ε-ATP labelled actin in the presence of actin-binding proteins

Time-resolved fluorescence quenching assays were employed in order to test whether the binding of cofilin or profilin to the actin monomer can change the static nature of the quenching process observed in the case of the actin-bound ε-ATP. In the case of cofilin the measurements were carried out on 20 μM ε-ATP labelled G-actin in the presence of 20 μM yeast cofilin. Taking into account that the dissociation constant of yeast cofilin from α-skeletal G-actin is 0.59 μM at this stoichiometry around 98 % of the actin monomers were in complex with cofilin. The two lifetime components observed in the absence of the quencher molecule were similar to the pure ε-ATP labelled G-actin solution.

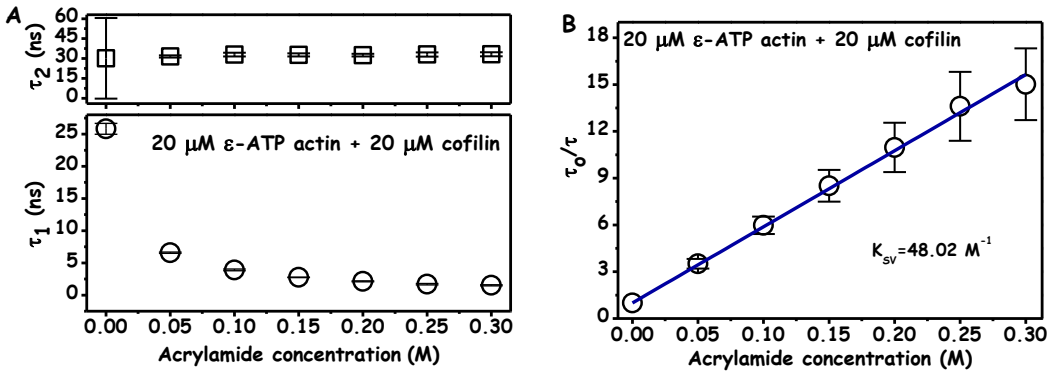

Figure 15.) Time-resolved fluorescence quenching of 20 μM ε-ATP labelled G-actin in the presence of 20 μM yeast cofilin. A.) The upper and the lower panel show the change in the lifetime of the longer (τ_2) and shorter (τ_1) lifetime components as a function of the quencher concentration, respectively. B.) Classical Stern-Volmer plot of the fluorescence lifetime of the shorter component as a function of the quencher concentration. The black open circles show the values obtained from the experimental data. Error bars represent the standard deviation (n=3). Straight line (blue) is obtained by fitting Equation 2. to the plotted values.

The shorter lifetime component was 25.82 ± 0.85 ns that almost identical with the lifetime of free ε-ATP (24.52 ± 0.01 ns). Upon increasing the quencher concentration to 0.3 M the shorter component decreased to 1.52 ± 0.85 ns (Figure 15/A). The Stern-Volmer plot of the shorter lifetime component resulted in a straight line (Figure 15/B) with a slope of 48.02 ± 8.35 M^{-1}. This value is similar to the value

obtained for the Stern-Volmer constant of free ε-ATP (49.2 M^{-1}) in the case of G-actin alone.

The longer component was 30.4 ns in line with actin alone (34.1 ns), and did not change significantly when the concentration of acrylamide was increased to a final concentration of 0.3 M. These results imply that the binding of cofilin to actin does not modify the lifetime of ε-ATP located in the nucleotide binding cleft and it can be also concluded that it is quenched through the static quenching mechanism.

In the case of the profilin-actin complex the fluorescence lifetimes of 20 μM ε-ATP labelled G-actin was quenched in the presence of 20 μM yeast profilin. The dissociation constant of yeast profilin to α-skeletal G-actin is 2.9 μM, therefore in the lifetime quenching measurements 70 % of actin was in complex with profilin. Because significant amount of monomer (~30 %) was not in complex with profilin in the assays, it was expected that three distinct lifetime components could be identified if profilin altered the lifetime of the actin-bound ε-ATP. However this was not the case, since just two discrete lifetime components were obtained from the measurements suggesting that profilin cannot change the lifetime of the actin-bound ε-ATP. The shorter lifetime

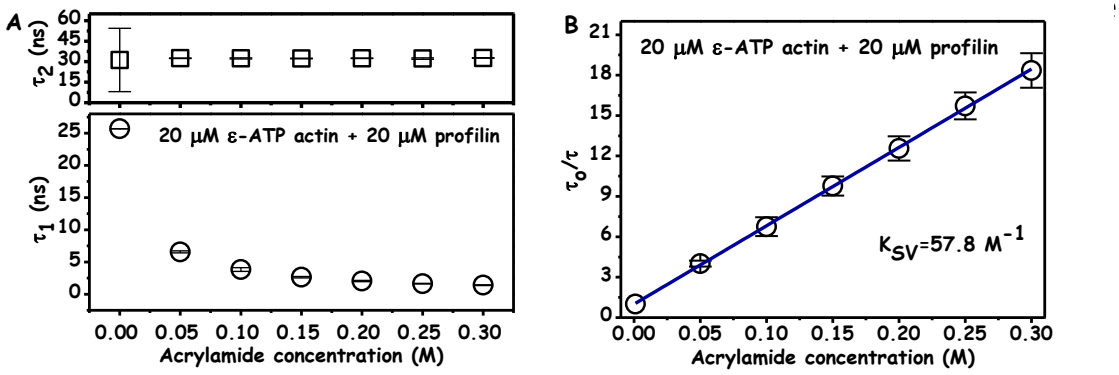

Figure 16.) Time-resolved fluorescence quenching of 20 μM ε-ATP labelled G-actin in the presence of 20 μM yeast profilin. A.) The upper and the lower panel show the change in the lifetime of the longer (τ_2) and shorter (τ_1) lifetime components as a function of the quencher concentration, respectively. B.) Classical Stern-Volmer plot of the fluorescence lifetime of shorter component as a function of the quencher concentration. The black open circles show the values obtained from the experimental data. Error bars represent standard deviation (n=3). Straight line (blue) was obtained by fitting Equation 2. to the plotted values.

The Stern-Volmer plot of the shorter lifetime values (Figure 16/B) showed a linear tendency and the calculated Stern-Volmer constant was 57.8 ± 4.5 M^{-1}. The

longer lifetime component was 31.07 ns close to the value obtained for actin alone (34.1 ± 4.5 ns), and remained the same for all applied quencher concentration. Based on this observation it can be concluded that in the case of the profilin-actin complex the fluorescence of bound ε-ATP is quenched solely in a static quenching process.

IV.1.2.6 Determining the Stern-Volmer constant of ε-ATP bound to actin

To sum up the results of the time-resolved measurements it can be claimed that the free and the actin-bound ε-ATP are quenched solely through dynamic and static quenching processes, respectively. Considering these findings, data obtained from steady-state quenching experiments with 5 µM ε-ATP labelled G-actin were analysed by using a modified form of the Stern-Volmer equation (Equation 4). In the equation the dynamic component ($K_{SV\_D\_free\ \varepsilon\text{-}ATP}$) and the static component ($K_{SV\_S\_free\ \varepsilon\text{-}ATP}$) of the free ε-ATP was fixed to 54.05 M^{-1} and 0 M^{-1}, respectively. The actin-bound ε-ATP was quenched via static quenching process, thus the dynamic component of the bound ε-ATP ($K_{SV\_D\_bound\ \varepsilon\text{-}ATP}$) was considered to be 0 M^{-1}. The fraction ($\alpha_{free\ \varepsilon\text{-}ATP}$) of the free ε-ATP varied between 60-75 % in three independent ε-ATP labelled actin preparations

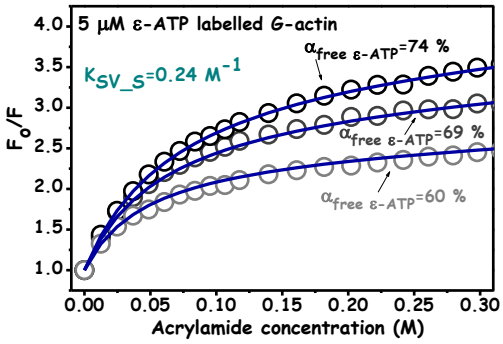

Term	Value	Obtained from
$K_{SV\_D\_free\ \varepsilon\text{-}ATP}$	54.05 M^{-1}	Steady-state quenching of free ε-ATP
$K_{SV\_S\_free\ \varepsilon\text{-}ATP}$	0 M^{-1}	Time-resolved quenching of free ε-ATP
$K_{SV\_D\_bound\ \varepsilon\text{-}ATP}$	0 M^{-1}	Time-resolved quenching of free ε-ATP
$K_{SV\_S\_bound\ \varepsilon\text{-}ATP}$	variable	Steady-state quenching of free ε-ATP
$\alpha_{free\ \varepsilon\text{-}ATP}$	variable	Steady-state quenching of free ε-ATP

Figure 17.) Classical Stern-Volmer plots of the quenching of 5 µM ε-ATP labelled G-actin. Open circles show the ratio of the fluorescence intensity of ε-ATP in the absence (F_0) and presence (F) of the quencher as a function of the quencher concentration at different fractions of free ε-ATP (black circle 74 %, dark grey circle 69 %, grey circle 60 %). Blue lines were obtained by fitting the modified Stern-Volmer equation (Equation 4.) to the three experimental data in a global fashion. B.) Variable and fixed components used in the fitting of the modified Stern-Volmer equation to the experimental data.

The reason why the fraction of the free ε-ATP varies in different preparations is the effectiveness of the application of the ion exchange resin treatment before the measurements. In spite of ensuring the same condition for the treatment it removes

more or less free ε-ATP from the solution in different preparation. The results of three independent measurements were fitted globally resulting in a static quenching component ($K_{SV\_S\_bound\ \varepsilon\text{-}ATP}$) of 0.24 ± 0.05 M^{-1} for the ε-ATP located in the nucleotide-binding cleft of actin (Figure 17/A). This value is two orders of magnitude smaller than the K_{SV} of the free ε-ATP (54.05 M^{-1}). This finding is in good agreement with the consideration of theoretical studies suggesting a decrease with 2 orders of magnitude in the accessibility of fluorophores when they are bound to a protein surface [123].

IV.1.2.7 Determining the Stern-Volmer constant of ε-ATP bound to actin in the presence of actin-binding proteins

Steady-state fluorescence quenching assays were carried out with 5 μM ε-ATP labelled G-actin in the presence of 15 μM cofilin in order to explore the conformational state of the nucleotide binding cleft of actin in complex with cofilin. Considering that cofilin has an affinity of 0.59 μM for ATP G-actin 94 % of the actin monomers were saturated with cofilin in all measurements [124]. The results of the quenching experiments were evaluated in the same way as in the case of actin alone. The fraction of free ε-ATP ($\alpha_{free\ \varepsilon\text{-}ATP}$) was between 28-82 % in three independent preparations. The global fitting of the modified Stern-Volmer equation to the three independent experimental data yielded a static quenching component ($K_{SV\_S\_bound\ \varepsilon\text{-}ATP}$) of

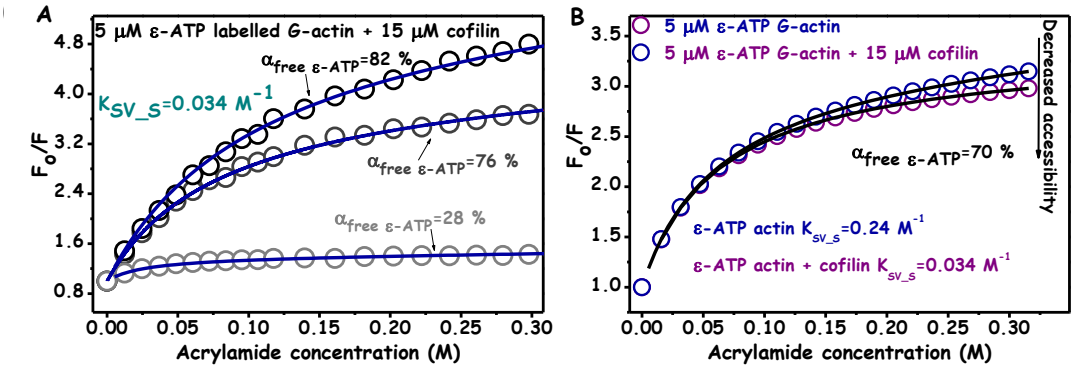

Figure 18.) Classical Stern-Volmer plot of the quenching of 5 μM ε-ATP labelled G-actin in the presence of 15 μM yeast cofilin. A.) Open circles show the ratio of the fluorescence intensity of ε-ATP in the absence (F_0) and presence (F) of the quencher as a function of the quencher concentration at different fractions of free ε-ATP (black circle 82 %, dark grey circle 76 %, grey circle 28 %). Blue lines were obtained by fitting the modified Stern-Volmer equation (Equation 4.) to the three experimental data in a global fashion. B.) Simulated experimental curves for actin alone (blue circles) and in complex with cofilin (purple circles) by using the following values: $K_{SV\_D\_free\ \varepsilon\text{-}ATP}$=0 M^{-1}, $K_{SV\_S\_free\ \varepsilon\text{-}ATP}$= 54.05 M^{-1}, $K_{SV\_D\_bound\ \varepsilon\text{-}ATP}$=0 M^{-1}, $\alpha_{free\ \varepsilon\text{-}ATP}$=70 %, $K_{SV\_S\_bound\ \varepsilon\text{-}ATP}$=0.24 M^{-1} and $K_{SV\_S\_bound\ \varepsilon\text{-}ATP}$=0.034 M^{-1}, in the case of actin and cofilin-actin complex, respectively.

This value is one order of magnitude smaller than the value revealed for actin alone (0.24 M^{-1}) suggesting a less accessible environment around the fluorophore in the cofilin-actin complex (Figure 18/A).

To highlight the effect of the static quenching component ($K_{SV\_S\_bound\ \varepsilon\text{-}ATP}$) on the downward tendency of the classical Stern-Volmer plot, experimental curves were simulated with the values obtained for actin alone and in complex with cofilin assuming that 70 % of the ε-ATP is free ($\alpha_{free\ \varepsilon\text{-}ATP}$). As it was expected the downward curvature was more pronounced for the cofilin-actin complex than for actin alone (Figure 18/B).

In the case of the profilin 5μM ε-ATP labelled actin was quenched in the presence of 20 μM profilin. Taking into account that the yeast profilin has an affinity of 2.9 μM to α-skeletal actin around 85 % of actin was in complex with profilin [125]. The modified Stern-Volmer equation was applied in a global fashion on the results of three independent measurements (Figure 19/A). The fitting revealed that the fraction of the free ε-ATP ($\alpha_{free\ \varepsilon\text{-}ATP}$) varied between 50-79 % in the three independent preparations. The static quenching component ($K_{SV\_S\_bound\ \varepsilon\text{-}ATP}$) of the ε-ATP located in the nucleotide binding cleft was 3.5 ± 1.5 M^{-1} in the presence of profilin. This value is one order of magnitude greater than the value calculated for actin alone (0.24 M^{-1}) indicating a more accessible protein matrix around the fluorophore in the profilin-actin complex.

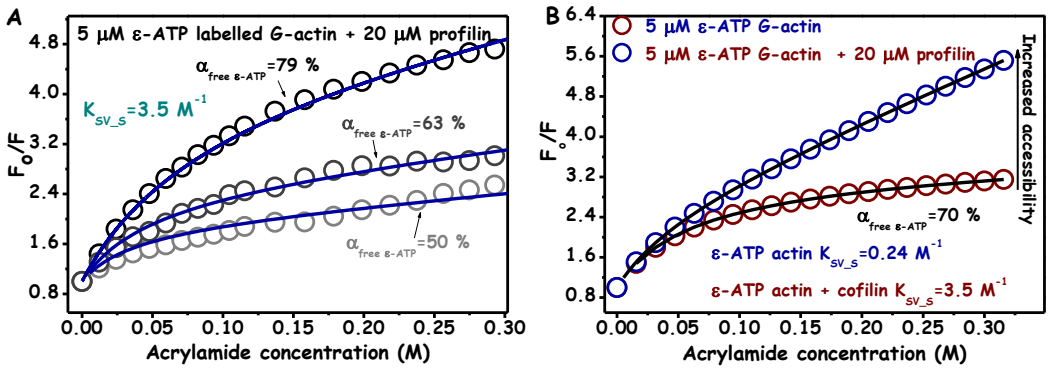

Figure 19.) Classical Stern-Volmer plot of the quenching of 5 μM ε-ATP labelled G-actin in the presence of 20 μM yeast profilin. A.) Open circles show the ratio of the fluorescence intensity of ε-ATP in the absence (F_0) and presence (F) of the quencher in the function of the quencher concentration at different fraction of free ε-ATP (black circle 79 %, dark grey circle 63 %, grey circle 50 %). Blue lines were obtained by fitting the modified Stern-Volmer equation (Equation 4.) to the three experimental data in a global fashion. B.) Simulated experimental curves for actin alone (blue circles) and in complex with profilin (red circles) by using the following values: $K_{SV\_S\_free\ \varepsilon\text{-}ATP}$=0 M^{-1}, $K_{SV\_D\_free\ \varepsilon\text{-}ATP}$= 54.05 M^{-1}, $K_{SV\_D\_bound\ \varepsilon\text{-}ATP}$=0 M^{-1}, $\alpha_{free\ \varepsilon\text{-}ATP}$=70 %, $K_{SV\_S\_bound\ \varepsilon\text{-}ATP}$=0.24 M^{-1} and $K_{SV\_S\_bound\ \varepsilon\text{-}ATP}$=3.5 M^{-1}, in the case of actin and profilin-actin complex, respectively.

The effect of the static quenching component ($K_{SV\_S\_bound\ \varepsilon\text{-}ATP}$) on the downward tendency of the classical Stern-Volmer plot was also compared in the case of actin alone and in complex with profilin. In the simulation the fraction of the free ε-ATP ($\alpha_{free\ \varepsilon\text{-}ATP}$) was fixed at 70 %. As it was expected for the profilin-actin complex the deviation from the straight line was less emphasised than for actin alone (Figure 19/B).

Conclusions:

1.) The fluorescence signal of the free and the actin-bound ε-ATP are quenched solely in dynamic and static process, respectively.

2.) The ε-ATP located in the nucleotide-binding cleft of actin is strongly shielded by the main domains of actin, because the Stern-Volmer constant characterising the accessibility of the actin-bound ε-ATP is two orders of magnitude smaller than the accessibility of the free ε-ATP.

3.) Neither cofilin nor profilin change the local environment of the nucleotide because the fluorescence lifetime of ε-ATP is not altered due to the presence of these actin-binding proteins.

4.) Cofilin closes the nucleotide-binding cleft of actin, because the accessibility of ε-ATP located in the cleft reduced in the presence of it.

5.) Profilin opens up the nucleotide-binding cleft of actin, because the accessibility of the ε-ATP located in the cleft increased dramatically in the presence of it.

IV.2 Conformation and dynamics of the small domain of actin

Comparing the atomic structures of α-actin-DNase I, α-actin-gelsolin-S1, and β-actin-profilin complex in the open and closed state it was suggested that the subdomain 2 of actin could rotate autonomously around the central strand (Val35-Arg37) of the β-sheet located at the boundary between subdomain 1 and 2 [28]. This independent motion of the subdomain 2 was suggested by other authors as well [126]. According to this scenario during the opening and closing of the nucleotide binding cleft the small domain of actin does not behave as an integrated unit [28]. In order to clarify whether cofilin- and profilin-caused changes in the conformation of the nucleotide binding cleft of actin are the consequences of the separate motion of subdomain 2 with respect to subdomain 1 or the integrated rotation of the small domain relative to the large domain, fluorescence resonance energy transfer assays were employed. The FRET assays were carried out at different temperature that enables one to explore the intrinsic dynamics of a protein segment between the fluorescently labelled positions. Prior to the fluorescence resonance energy transfer experiments the binding ability of cofilin and profilin to the labelled-actin was tested in steady-state fluorescence anisotropy measurements and local conformational changes were explored around the labelled positions by using fluorescence quenching and anisotropy decay methods.

IV.2.1 Binding of cofilin and profilin to IAEDANS-labelled actin

In the fluorescence resonance energy transfer experiments the donor fluorophore (IAEDANS) was attached to the penultimate cysteine (C374) of the actin monomer that is thought to be a part of the cofilin and profilin-binding region of the actin monomer [58, 79]. To elucidate how the labelling of actin molecule could interfere with the binding of cofilin or profilin, fluorescence anisotropy measurements were carried out on the donor labelled actin monomer in the presence of actin-binding proteins. The concentration of actin monomers was kept at 2 μM and the amount of cofilin (up to 20 μM) and profilin (up to 64 μM) were varied in the samples. The fluorescence anisotropy of IAEDANS-labelled actin was 0.093 ± 0.0048 that is similar to the value (0.097) measured by others under similar conditions [127]. Elevating the concentration

of cofilin to 20 μM in the sample resulted in an increase in the anisotropy value from 0.093 ± 0.005 to 1.12 ± 0.004 (Figure 20/A). The change in the fluorescence anisotropy followed a hyperbolic function and the fitting of Equation 7. to the experimental data revealed a dissociation equilibrium constant (K_D) of 0.68 μM^{-1} for the cofilin-actin complex.

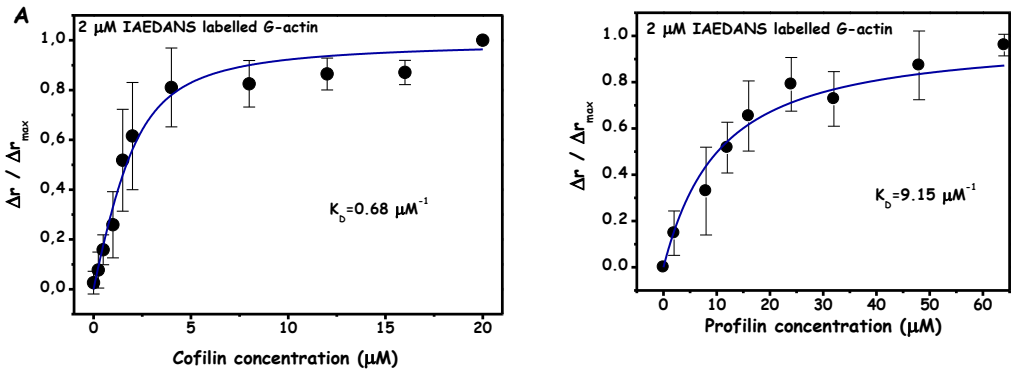

Figure 20.) Normalized steady-state anisotropy of IAEDANS-labelled G-actin in the presence of actin-binding proteins. A.) Normalized fluorescence anisotropy of 2 μM IAEDANS-labelled G-actin as the function of yeast cofilin concentration. B.) Normalized fluorescence anisotropy of 2 μM IAEDANS-labelled G-actin as the function of yeast profilin concentration. The dissociation constant (K_D) was obtained by fitting (blue line) Equation 7. to the experimental data. Error bars represent the standard deviation of the results of three independent measurements.

This value is in good agreement with the K_D (0.59 μM^{-1}) determined for the NBD-labelled actin-cofilin complex [128]. The titration of the donor-labelled actin monomer with profilin up to 64 μM elevated the anisotropy value from 0.093 ± 0.005 to 0.108 ± 0.002. Similarly to cofilin, the binding of profilin followed a hyperbolic function and fitting Equation 7. to the experimental curve resulted in a dissociation equilibrium constant of 9.15 μM^{-1} (Figure 20/B). This value is around 3 times higher than the K_D obtained for the unmodified α-actin-profilin complex [129].

IV.2.2 Fluorescence quenching at Cys374 and Lys61

Fluorescence quenching experiments were employed in order to test whether cofilin and profilin can cause local changes in the conformation of the C-terminus (Cys374) and the acceptor-labelled (Lys61) region of the actin molecule. The

fluorescence intensity of 2 μM labelled-actin (donor or acceptor) saturated with cofilin (10 μM) or profilin (25 μM) was quenched with acrylamide. The concentration of the quencher was raised from 0 to 0.5 M in six steps. In all cases the classical Stern-Volmer plot showed a linear relationship between the quencher concentration (Q) and the ratio of the fluorescence intensity in the absence and presence of the quencher (F_0/F). The Stern-Volmer constant was determined from the slope of the straight line of the experimental data by using Equation 1.

The Stern-Volmer constant of the IAEDANS-labelled actin in the absence of actin-binding proteins was 4.67 M^{-1}. This value is in good agreement with the value reported in an earlier study [130]. Both cofilin and profilin decreased the accessibility of IAEDANS for the quencher molecule. The derived Stern-Volmer constant for the cofilin- and profilin-actin complex was 3.53 M^{-1} and 3.21 M^{-1}, respectively (Figure 21/A). The

The Stern-Volmer constant for the FITC-labelled actin was 0.439 M^{-1} that is one order of magnitude smaller than for the IAEDANS-labelled actin. Upon the addition of the appropriate amount of cofilin and profilin the Stern-Volmer constant changed to 0.388 M^{-1} and 0.517 M^{-1}, respectively (Figure 21/B). The slight decrease and increase in the Stern-Volmer constant maybe the result of the closing and opening of the nucleotide binding cleft of actin in the presence of cofilin or profilin, respectively.

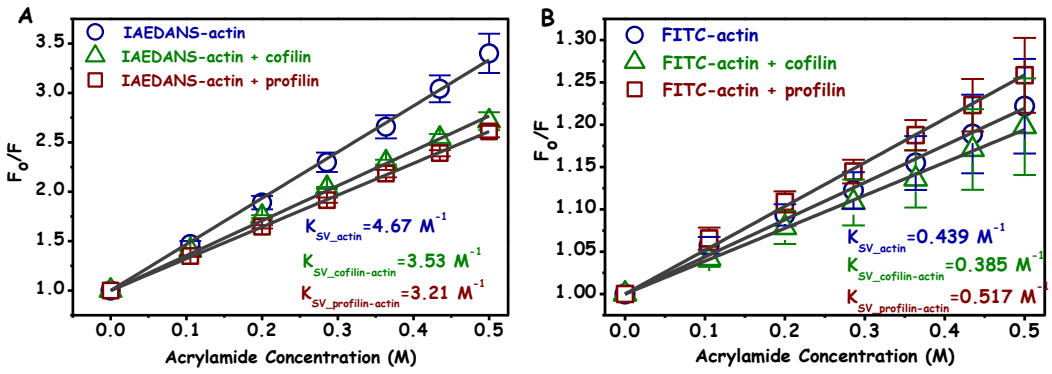

Figure 21.) Fluorescence quenching of the donor and acceptor fluorophores in the absence and presence of actin-binding proteins. A.) The Classical Stern-Volmer plot of the quenching of 2 μM IAEDANS-labelled actin in the absence (blue circles) and presence of 10 μM cofilin (green triangle) or 25 μM profilin (red square). B.) The Classical Stern-Volmer plot of the quenching of 2 μM FITC-labelled actin in the absence (blue circles) and presence of 10 μM cofilin (green triangle) or 25 μM profilin (red square). Grey lines were obtained by fitting Equation 1. to the experimental data. Error bars represent standard deviation of three independent measurements.

IV.2.3 Fluorescence resonance energy transfer between Cys374 and Lys61

Fluorescence resonance energy transfer method was applied to explore the conformational state and intrinsic dynamics of the small domain of actin in the presence of cofilin or profilin. The donor and the acceptor fluorophores were attached to the Cys374 (located in subdomain 1) and Lys61 (located in subdomain 2), respectively (Figure 22). The energy transfer efficiency between the reporter molecules was determined in the temperature range between 5 °C and 35 °C in the steps of 5 °C. The intrinsic dynamics of the protein matrix between the labelled positions was characterised through the change in the flexibility parameter (f') as a function of the temperature. So far this approach has been successfully applied to reveal differences in the conformational dynamics of actin under different circumstances and in the presence of different actin-binding proteins [101, 131-136].

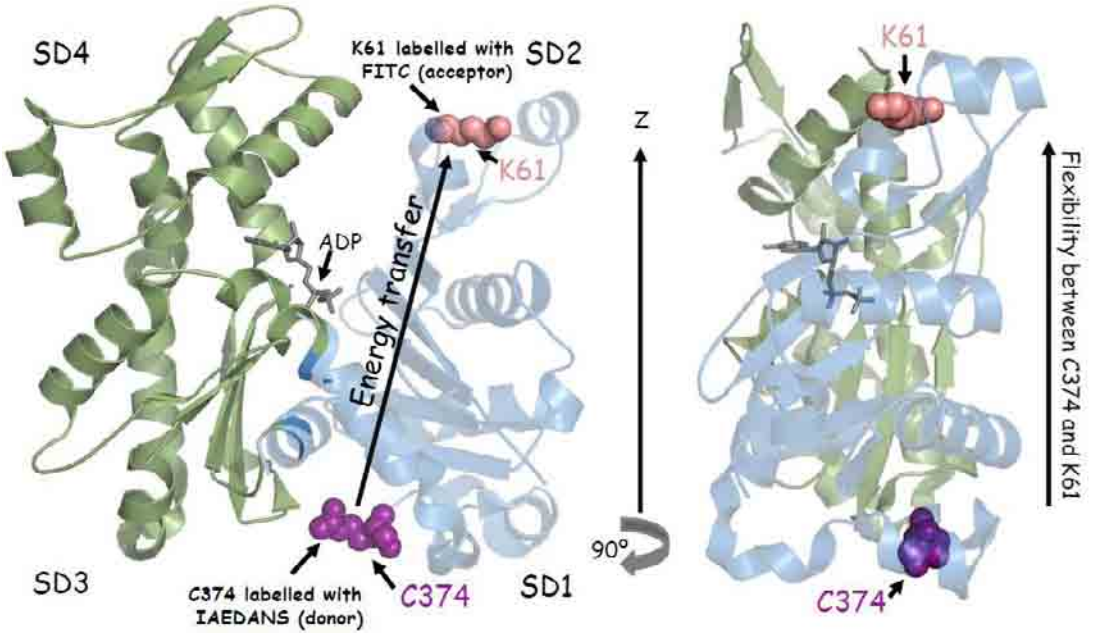

Figure 22.) A.) Front view of the ADP bound actin monomer in cartoon representation (PDB code: 1J6Z). The large and small domains of actin can be seen in green and blue, respectively. The donor and the acceptor fluorophores were attached to cysteine 374 (purple spheres) and lysine 61 (red spheres), respectively. The subdomains are numbered and the ADP is represented as grey stick. B.) Side view of the ATP-bound actin monomer in surface representation.

Comparing the fluorescence spectrum of IAEDANS- and IAEDANS-FITC-labelled actin a large decrease was observed in the intensity of the donor (IAEDANS) fluorophore in the case of the double-labelled actin species (Figure 23). This dramatic drop in the intensity of donor indicates a large energy transfer between the two reporter molecules. The energy transfer efficiency was calculated from the area under the emission spectrum of the donor between 400 and 475 nm. In this wavelength range the fluorescence emission of the acceptor molecule is negligible. The decrease in the intensity of donor in the presence of the acceptor corresponded to 66.7 ± 6.7 % energy transfer efficiency between the labelled positions at 20 °C. This value is in a good agreement with the values obtained by others using the same FRET fluorophore pair on actin [95, 101]. Upon the addition of 10 µM cofilin to the double-labelled actin the fluorescence intensity of the donor in the presence of the acceptor slightly decreased (Figure 23/A). This observation indicates that the cofilin has just a moderate effect on the distance between Cys374 and Lys61 of actin. This result is consistent with an earlier observation suggesting just a slight modification in the orientation of subdomain 1 and 2 upon the binding of cofilin to actin [137]. Similarly to the cofilin-actin complex, the donor intensity of the double-labelled-actin remained the same as 25 µM profilin was added to the solution (Figure 23/B). This result implies that the binding of profilin to actin does not change the distance between the donor and the acceptor fluorophores.

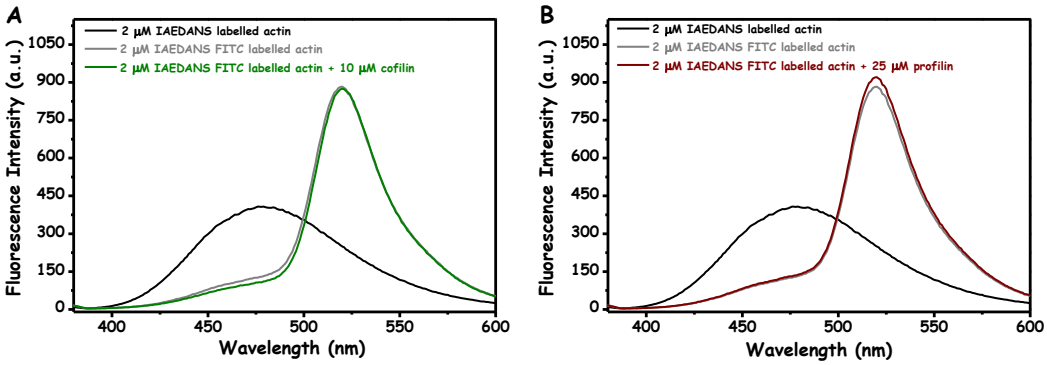

Figure 23.) A.) Emission spectrum of 2 µM actin monomer labelled with the donor (black line) and with both the donor (IAEDANS) and the acceptor (FITC) fluorophore in the presence (green line) and absence (grey line) of 10 µM cofilin. B.) Emission spectrum of 2 µM actin monomer labelled with the donor (black line) and with both the donor (IAEDANS) and the acceptor (FITC) fluorophore in the presence (red line) and absence (grey line) of 25 µM profilin.

Although the energy transfer between the labelled positions of actin did not change significantly upon the binding of cofilin or profilin, the tendency of the flexibility parameter in the function of the temperature was changed by both actin-binding proteins compared to actin alone. The flexibility parameter was determined at each temperature level in the presence of 2 or 10 μM cofilin. The steepness of the change in the flexibility parameter as a function of the temperature was higher for actin alone than in complex with cofilin (Figure 24/A). This result suggests that the binding of cofilin to actin decreases the flexibility of the small domain of actin between the labelled positions. As it was expected at higher cofilin concentration the stabilising effect of cofilin on the small domain of actin was more pronounced.

In the case of the profilin-actin complex flexibility parameter changed less steeply in the function of the temperature than in the case of actin alone (Figure 24/B). The decrease in the steepness was more dramatic when 25 μM profilin was introduced into the solution than at 2 μM. In the former case a break was observed in the tendency of the flexibility parameter between 30 °C and 35 °C. This change in the tendency of the flexibility parameter can be the result of a conformational change induced by profilin above 30 °C [100].

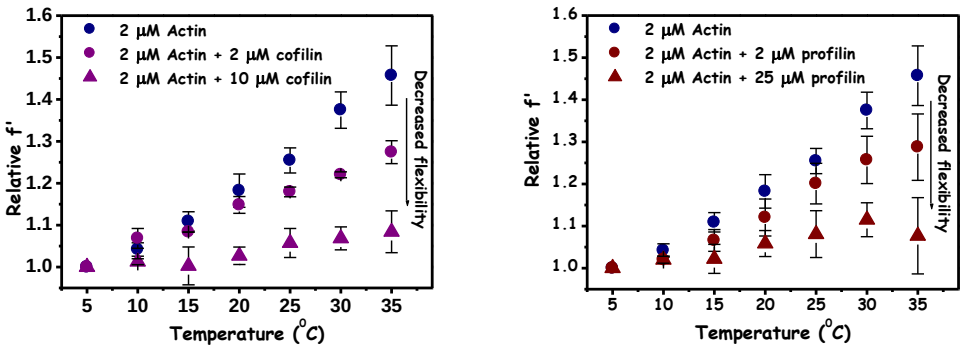

Figure 24.) Relative change in the flexibility parameter (f') as a function of the temperature. A.) The temperature was changed between 5 and 35 °C in the absence (blue circles) and presence of 2 (purple circles) and 10 μM (purple triangle) cofilin. The flexibility parameter (f') was calculated according to the Equation 11. B.) Relative change in the flexibility parameter (f') as the function of the temperature. The temperature was changed between 5 and 35 °C in the absence (blue circles) and presence of 2 (red circles) or 25 μM (red triangle) profilin.

The observed reduction in the flexibility of the small domain between the labelled position in the presence of either cofilin or profilin can arise from the limited

motion of the SD2 relative to the SD1 and/or the reduced dynamics of the reporter molecules respect to the protein surface.

IV.2.4 Local dynamics of actin monomer in the vicinity of the fluorescently labelled positions

In order to decide whether there is a change in the local dynamics of the fluorescent reporter molecules in the presence of cofilin or profilin that can contribute to the observed decline in the flexibility of the small domain of actin, fluorescence anisotropy decay measurements were implemented. This technique can be used to evaluate the hydrodynamic volume of macromolecules and the dynamics and degree of spatial confinement of the movement of a fluorophore molecule attached to the molecule surface.

The anisotropy decay of IAEDANS-labelled actin monomer in the absence and presence of actin-binding proteins were recorded from 5 °C to 35 °C. Two rotational correlation times were resolved explicitly from the anisotropy decay curves. One of that was a slow (θ_1) and the other one was a fast (θ_2) rotational correlation time, which were attributed to the global tumbling of the actin monomer and to the local wobbling of the attached fluorophore, respectively (Appendix Table 3-5) . The slow rotational time is characteristic for the shape and the size of the investigated entity while the fast rotational time is sensitive for the local dynamics of the labelled position of the protein.

In the absence of actin-binding proteins the slow rotational correlation time decreased from 49.29 ± 0.26 ns to 20.0 ± 0.64 ns as the temperature was increased from 5 °C to 35 °C (Figure 25/A). This result is in good agreement with the findings of earlier reports [101, 138]. The decreasing tendency in the rotational correlation time characterising the tumbling of the actin monomer seems to be plausible because the rotational correlation time is inversely proportional to the absolute temperature [139]. The change in the value of θ_1 showed the same tendency in the function of the temperature when actin was in complex with cofilin or profilin. In the case of cofilin-actin complex the θ_1 changed from 59.04 ± 0.77 ns to 28.87 ± 3.42 ns on the applied temperature range (Figure 25/A). When profilin was in complex with actin the θ_1 decreased from 51.79 ± 1.16 ns to 25.51 ± 1.56 ns as the temperature was elevated from 5 °C to 35 °C (Figure 25/A). The fact that the slow rotational correlation time was longer at each temperature level when cofilin or profilin was present in the solution,

indicates the complex formation between actin and actin-binding proteins on the applied temperature range. Therefore this result in line with the steady-state anisotropy measurements carried out at 20 °C further confirms that even though the actin molecule was labelled at the cofilin- and profilin-binding sites these actin-binding proteins were able to associate with the actin monomer.

The fast correlation time in the absence of actin-binding proteins was reduced from 4.83 ± 0.96 ns to 2.06 ± 0.07 ns as a function of the temperature denoting an increased dynamics of the C-terminus of actin at higher temperature levels (Figure 25/A). In the presence of actin-binding proteins the fast rotational correlation time changed correspondingly to actin alone in the function of the temperature. The θ_2 changed from 4.03 ± 1.63 ns to 1.92 ± 0.73 ns and from 3.22 ± 0.29 ns to 2.17 ± 0.43 ns in the presence of cofilin and profilin, respectively (Figure 25/A).

Based on these results the dynamics of the fluorophore attached to the C-terminus of actin is not affected by the presence of cofilin and profilin on the applied temperature range although both actin-binding proteins form an intimate contact with the C-terminus of the actin molecule. Subsequently it can be ruled out that the increased rigidity of the small domain of actin in the presence of cofilin and profilin is the consequence of the decreased dynamics of the C-terminus of actin.

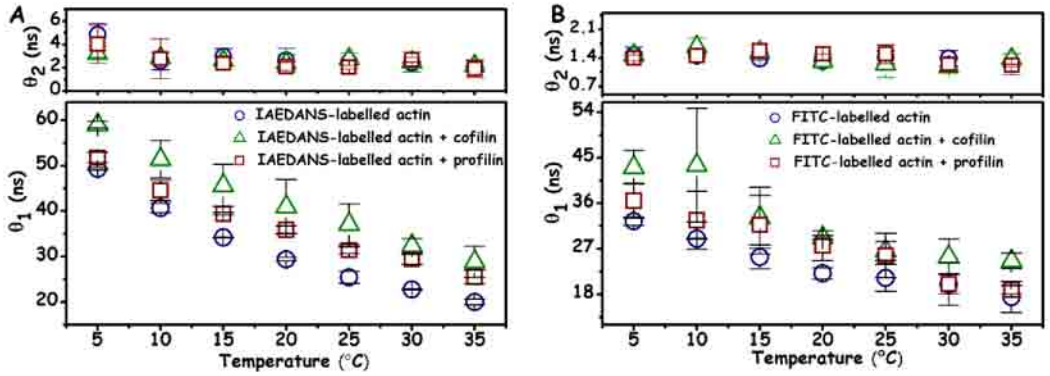

Figure 25.) Rotational correlation times resolved from the anisotropy decay curves. A.) The rotational correlation times of 20 μM IAEDANS-labelled actin in the absence (blue circle) and presence of 25 μM cofilin (green triangle) or 35 μM profilin (red square) as a function of temperature. The upper and lower panels show the slow (θ_1) and fast (θ_2) rotational correlation times, respectively. B.) The rotational correlation times of 2 μM FITC-labelled actin in the absence (blue circle) and presence of 10 μM cofilin (green triangle) or 25 μM profilin (red square). The upper and lower panels show the slow (θ_1) and fast (θ_2) rotational correlation times, respectively. The rotational correlation times were obtained by fitting Equation 8. and 9. to the parallel and perpendicular intensity decay curves simultaneously. Error bars represent standard deviation (n=2).

When actin was labelled on Lys61 with FITC, like in the case of the IAEDANS-labelled actin two rotational correlation times were recovered from the anisotropy decay curves.The slow one (θ_1) was attributed to the overall rotation of the labelled actin molecule, while the fast one (θ_2) was ascribed to the local motion of the fluorophore (Appendix Table 6-8).

The slow rotational time in the absence of actin-binding proteins changed from 32.45 ± 0.81 ns to 17.49 ± 3.08 ns as the temperature was elevated from 5 °C to 35 °C (Figure 25/B). In the case of cofilin-actin complex the slow rotational time declined from 43.12 ± 3.37 ns to 24.61 ± 1.53 ns, while for the profilin-actin complex it changed from 36.5 ± 3.43 ns to 18.91 ± 6.83 ns on the applied temperature range (Figure 25/B). As in the case of the IAEDANS-labelled actin the slow rotational time for the cofilin- and profilin-actin complex was higher than for actin alone at all temperature levels. This observation clearly demonstrates the complex formation between actin and the applied actin-binding proteins. On the other hand the obtained slow rotational time characterising the overall motion of actin was smaller when it was labelled with FITC than in the case of the IAEDANS-labelled actin species. This discrepancy can be resolved by taking into account the lifetimes of the reporter molecules. The IAEDANS has an average lifetime that is in the range of the slow rotational correlation time of the actin monomer while the FITC has an average lifetime (4 ns at 20º) that is much shorter than the rotational correlation time of the actin monomer. It was demonstrated earlier that the rotational correlation time can be resolved accurately when the rotational correlation time is within the range of $0.1\ \tau < \theta < 10\ \tau$ where τ is the average lifetime of the fluorophore [140]. In the light of this consideration the short lifetime of FITC can result in an uncertainty in the estimation of rotational time belonging to the protein tumbling. This explanation seems to be reasonable because as the temperature is increased and consequently the apparent rotational correlation time is decreased the difference between the rotational correlation times obtained for the IAEDANS- and FITC-labelled actin is reduced.

In the absence of actin-binding proteins the fast rotational correlation time decreased from 1.48 ± 0.19 ns to 1.24 ± 0.26 ns as the temperature was raised from 5 °C to 35 °C (Figure 25/B). In the case of cofilin-actin complex the fast correlation time decreased from 1.47 ± 0.05 ns to 1.38 ± 0.13 ns while for the profilin-actin complex this value changed from 1.4 ± 0.67 ns to 1.22 ± 0.03 ns (Figure 25/B). In the presence

of both actin-binding proteins the fast correlation time changed similarly to the case when actin was alone. Therefore it can be deduced that the dynamics of the labelled-position is not influenced by the presence of actin-binding proteins. This consideration excludes that the observed decrease in the flexibility of the small domain of actin in the presence of cofilin or profilin is the consequence of the less dynamic protein structure of actin in the vicinity of Lys61.

In addition to the dynamics of the labelled segments the anisotropy decay measurements can provide information about the protein structure surrounding the reporter molecule as well. In contrast to the free rotation in solution the motional freedom of the fluorophores attached to a protein surface is limited by the steric hindrance of the surrounding protein matrix. To assess this spatial restriction of the rotational diffusion of the reporter molecules the "wobbling in cone" model was applied. Originally this approach was used to characterise the spatial restriction of the rotational motion of fluorophores embedded in highly ordered structures such as membranes [99, 141] and later it was extended to describe also the rotational diffusion of a fluorophore attached to the surface of a macromolecule [142]. The degree of spatial confinement can be expressed with the semiangle θ_o that can define the static cone within the fluorophore performs its rotational diffusion (see materials and methods). The half-cone angle of the wobbling of the fluorophore is related to the fractional amplitude of the fast and slow components resolved from the anisotropy decay curves. A higher contribution of the fast local motion to the depolarisation of the system implies on a smaller spatial restriction for the rotational diffusion of fluorophore with respect to the protein surface.

The half-cone angle for the rotational diffusion of IAEDANS attached to the Cys374 of actin in the absence of actin-binding proteins increased from $14.52 \pm 0.68^{\circ}$ to $32.02 \pm 1.76^{\circ}$ as the temperature was raised from 5 $^{\circ}$C to 35 $^{\circ}$C (Figure 26/A). This change is consistent with the findings of an earlier report obtained in frequency domain time-resolved measurements [101]. The temperature induced increase in the half-cone angle of the wobbling of IAEDANS suggests that the protein structure around the C-terminus of actin becomes less compact upon heat induction which leads to a larger angular freedom for the rotational diffusion of the reporter molecule. The change in the half-cone angle of the fluorophore's wobbling was not influenced significantly by the presence of actin-binding proteins. In the case of the cofilin-actin complex the θ_o

changed from 15.87 ± 1.03° to 33.65 ± 1.56° while in the presence of profilin the θ_o increased from 14.83 ± 1.58° to 28.3 ± 0.93° on the applied temperature range (Figure 26/A). According to these results neither cofilin nor profilin affect the angular freedom of IAEDANS attached to the C-terminus of actin on the applied temperature range. The semiangle of the rotational diffusion of FITC located on Lys61 of actin in the absence of cofilin and profilin increased from 28.59 ± 1.16° to 34.43 ± 1.28° as the temperature was raised from 5 °C to 35 °C (Figure 26/B). Based on this result the degree of orientational constrain of the wobbling of FITC decreases in the function of temperature that implies the development of a less compact structure around the Lys-61 as the temperature is elevated. The change in the half-cone angle when actin was in complex with either cofilin or profilin was very similar to the case when actin was alone. On the applied temperature range the half-cone angle increased from 26.73±2.66° to 32.06±1.99° and from 27.69±1.94° to 32.68±1.4° in the presence of cofilin and profilin, respectively (Figure 26/B).

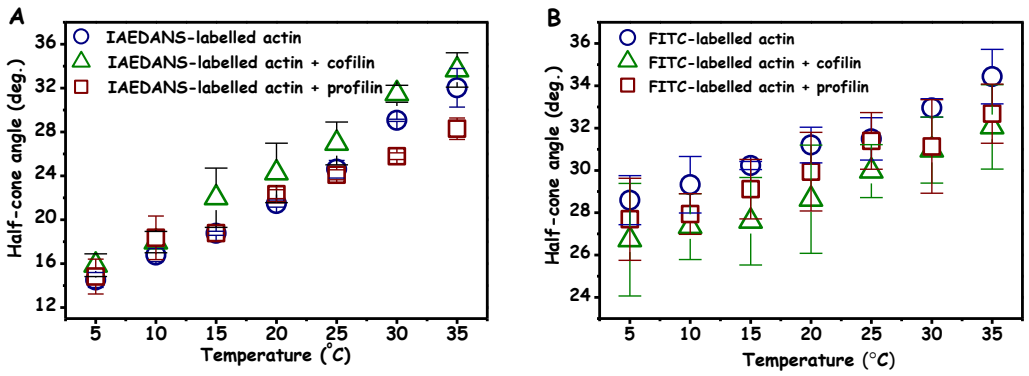

Figure 26.) Half-cone angles (θ_o) characterizing the spatial confinement of the motion of the attached fluorophores with respect to the protein surface in the function of temperature. A.) The change in the half-cone angle of 20 μM IAEDANS-labelled actin in the absence (blue circle) and presence of 25 μM cofilin (green triangle) or 35 μM profilin (red square) as a function of the temperature. B.) The change in the half-cone angle of 2 μM FITC-labelled actin in the absence (blue circle) and presence of 10 μM cofilin (green triangle) or 25 μM profilin (red square) as a function of the temperature. The half-cone angles were calculated according to Equation 10. Error bars represent standard deviation (n=2).

Based on these results neither cofilin nor profilin have impact on the angular freedom of the wobbling of the fluorophore attached to Lys61 at any investigated temperature level. According to the anisotropy decay measurements none of the actin-binding proteins have influence on the dynamics and angular freedom of the reporter molecules applied in the FRET assays. The energy transfer and consequently the

flexibility parameter between the donor and the acceptor molecule strongly depend on the orientation of the dipole momentum of the donor and acceptor with respect to each other. The relative orientation of the reporter molecules can be expressed by the orientation factor κ^2 that is considered to be 2/3 if the orientation of the donor and the acceptor is randomised during the lifetime of the donor fluorophore. This randomisation occurs through the segmental motion of the reporter molecules with respect to the protein surface. The anisotropy decay assays revealed that the segmental motion of both the donor and the acceptor molecule occur within few ns. Taking into account that the donor fluorophore has an average lifetime of 16 ns at the temperature of 20 $^{\circ}$C the dynamic averaging of the orientation of the dipole moment of the reporter molecules are satisfied. The fact that cofilin and profilin cannot change the rotational correlation time of the reporter molecules suggests that the observed decrease in the flexibility of the small domain of actin in the presence of actin-binding proteins is not the consequence of the decreased dynamics of the donor and acceptor fluorophores.

Conclusions:

1.) The opening and closing of the nucleotide-binding cleft occur through the integrated motion of the main domains, because neither cofilin nor profilin can change the orientation of the SD1 and SD2 relative to each other.

2.) The autonomous motion of the SD2 relative to SD1 is restricted in the presence of both actin-binding proteins, because the flexibility of the small domain is drastically reduced in the presence of either cofilin or profilin.

3.) The local dynamics of the reporter molecules do not contribute to the observed decrease in the flexibility of the small domain in the presence of actin-binding proteins, because neither cofilin nor profilin can change the dynamics and spatial degree of the fluorophores' motion.

IV.3 Heat stability of actin monomer

It was proposed earlier that the heat stability of the actin molecule was strongly influenced by the conformation state of the nucleotide-binding cleft and the subdomain 2 of actin [143, 144]. Differential scanning calorimetry method was applied to gain further information about the conformation of nucleotide binding cleft and the small domain of actin in the presence of cofilin and profilin.

In the differential scanning calorimetry assays the samples were heated up from 0 °C to 100 °C twice to check the irreversibility of the heat denaturation process. The heat stability of the proteins was characterised by the melting temperature (T_m) that corresponds to the temperature level where the half of the proteins is denatured. Additionally, the enthalpy change (ΔH) following the heat denaturation process and the full width at half maximum (FWHM) were also calculated. Latter component provides information about the cooperativity of the denaturation process.

The heat denaturation of 23 μM G-actin was irreversible according to the differential scanning calorimetric measurements. The melting temperature of actin monomer was determined from the first heating trace by fitting a single Gaussian to the heat-flow curve (Figure 27/A). The fitting revealed a melting temperature (T_m) of 55.5 °C that is significantly lower than the values obtained in other studies [145-147]. This discrepancy can be resolved by taking into account that the scanning rate was higher in the mentioned studies which can shift the melting point of the proteins toward the higher temperature level [148]. Beside that in these experiments lower Ca^{2+} ion concentration was applied than in the previous reports that can also influence the melting temperature of actin. The enthalpy change (ΔH) following the heat denaturation of actin was calculated based on the area under the heat transition curve. The value obtained for the enthalpy change was 344.5 kJ/mol. The full width at half maximum (FWHM) was 5.9 °C.

The heat denaturation of 23 μM cofilin was also irreversible as in the case of actin. The first melting trace of 23 μM cofilin showed a single heat transition with a melting temperature of 48.2 °C and with the full width at half maximum (FWHM) of 4.7 °C (Figure 27/A). This melting temperature similarly to actin is lower than the melting point of cofilin obtained in other reports. This contradiction can also be

interpreted by the difference in the scanning rate of the measurements. The enthalpy change following the heat denaturation of cofilin was 102 kJ/mol.

When 23 μM G-actin was mixed with 23 μM cofilin one asymmetric peak appeared in the heat transition curve (Figure27/B). Considering that beside the cofilin-actin complex some free actin and unbound cofilin can also be present in the sample the heath transition curve was analysed by fitting multiple Gaussians on that. The best fit was achieved when the heat transition curve was decomposed into two Gaussians. The peak with the smaller area could be characterized with a melting temperature of 55.5 °C. It was reasonable to conclude that this peak belonged to the free actin in the sample, because the melting temperature was identical with the melting temperature of actin measured in the absence of cofilin (55.5 °C). The amount of free actin was around 4 μM based on the comparison with the area under the heat transition curve of 23 μM actin measured alone. The peak with larger area emerged at 59.2 °C that can be associated with the actin-cofilin complex. The shift from 55.5 °C to 59.2 °C in the melting point of actin in the presence of cofilin suggested an increased resistance of the actin molecule against heat denaturation in agreement with the results of other calorimetric studies [145, 147].

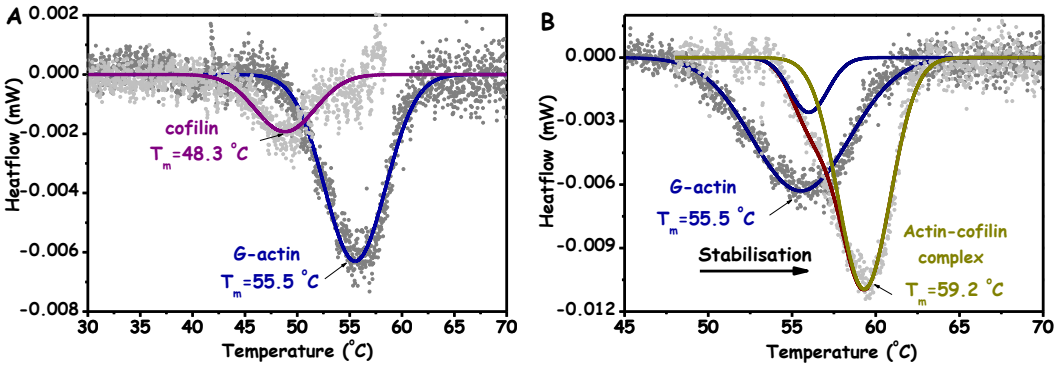

Figure 27.) Heat denaturation profile of actin in the absence and presence of cofilin. A.) Heat denaturation curve of 23 μM ATP-G-actin (grey dots) and 23 μM yeast cofilin (light grey dots). The blue and purple lines represent the Gaussian fit to the heat denaturation curve of actin and cofilin, respectively. B.) Heat denaturation curve of 23 μM ATP-G-actin alone (grey dots) and in complex with 23 μM yeast cofilin (light grey dots). The blue and red lines represent the Gaussian fit to the heat denaturation curve of actin alone and in complex with cofilin, respectively. Heat denaturation curve of actin-cofilin complex was decomposed into two Gaussians; blue and yellow lines represent G-actin alone and actin-cofilin complex, respectively.

It was proposed earlier that cofilin in high concentration can initiate the nucleation of actin, therefore the samples containing cofilin and actin as well were

centrifuged to exclude the presence of filamentous actin that can be also responsible for the observed shift in the melting temperature [43]. The sedimentation assays could clearly demonstrate that the polymerisation did not contribute to the change in the melting temperature of actin in the presence of cofilin (data not shown). The full width at half maximum was 3.3 °C for the cofilin-actin complex that is smaller than the value obtained for actin alone (5.9 °C).

It turned out from the differential scanning calorimetric measurements that the heat denaturation process of profilin was irreversible as well. The Gaussian fit on the heat transition curve of 23 μM profilin resulted in a melting temperature of 53 °C and a full width at half maximum of 1.5 °C (Figure 28/A). The calculated enthalpy change following the heat denaturation of the profilin sample was 246.5 kJ/mol.

When 23 μM profilin was added to 23 μM actin only one prominent peak was detected with a T_m value of 47.6 °C (Figure 28/B). By fitting Gaussians on the heat transition curve it could not be decomposed convincingly to get relevant information about the unbound actin and profilin present in the sample beside the actin-profilin complex. Contrary to cofilin, profilin lowered the melting temperature of actin from 53.6 °C to 47 °C indicating a less resistant structure of actin against the heat denaturation.

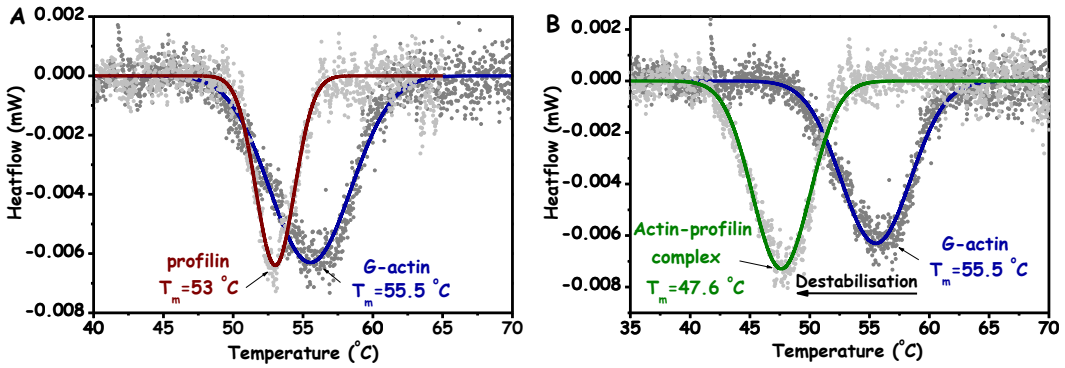

Figure 28.) Heat denaturation profile of actin in the absence and presence of profilin. A.) Heat denaturation curve of 23 μM ATP-G-actin (grey dots) and 23 μM yeast profilin (light grey dots). The blue and red lines represent the Gaussian fit to the heat denaturation curve of actin and cofilin, respectively. B.) Heat denaturation curve of 23 μM ATP-G-actin alone (grey dots) and in complex with 23 μM yeast cofilin (light grey dots). The blue and green lines represent the Gaussian fit on the heat denaturation curve of actin alone and in complex with profilin, respectively.

Similar destabilisation effect of profilin was observed earlier by using DNase I inhibition assay [149]. The full width at half maximum was 4.7 °C for the actin-profilin

complex that is between the values obtained for actin alone (5.9 °C) and in complex with cofilin (3.3 °C)

Conclusions:

1.) The applied actin-binding proteins have opposite effect on the heat stability of the actin monomer; cofilin increases, while profilin decreases that.

2.) The heat stability of the actin monomer strongly depends on the conformation of the nucleotide-binding cleft, wider the nucleotide-binding cleft less resistant the actin monomer against the heat denaturation.

V. Discussion

In this thesis the conformational state and dynamics of actin monomer was investigated in the presence of actin-binding proteins from functional point of view. According to the results of the nucleotide exchange experiments yeast cofilin and profilin can modify the kinetics of the nucleotide exchange on α-actin in opposite direction. The observed rate constant of the nucleotide exchange process decreased by around one order of magnitude (from 0.012 s^{-1} to 0.002 s^{-1}) when 3 μM cofilin was present beside 1 μM actin. In contrast to cofilin, when 1 μM profilin was in complex with 1 μM actin the observed rate constant was around 60-times (from 0.012 s^{-1} to 0.75 s^{-1}) higher than in the case of actin alone. These results are in good agreement with earlier observations made on other orthologues of cofilin and profilin [48, 68].

To explore the connection between the kinetics of the nucleotide exchange and the conformational state of the nucleotide binding cleft of actin, fluorescence quenching assays were completed in the presence of cofilin or profilin. The fluorescence quenching experiments revealed that the ε-ATP located in the nucleotide binding cleft of actin can be quenched through a static quenching process. The Stern-Volmer constant characterising the accessibility of the actin bound ε-ATP was 0.24 M^{-1} that is two orders of magnitude smaller than the Stern-Volmer constant of the free ε-ATP (54.05 M^{-1}). This result indicates that the nucleotide is strongly shielded by the two main domains of actin within the actin molecule. In the presence of cofilin the Stern-Volmer constant of the quenching process further decreased to 0.034 M^{-1} suggesting a less accessible protein matrix around the actin-bound ε-ATP compared to the case when actin monomer was alone. As it was reported earlier cofilin can cause similar shielding of the fluorescent nucleotide analogue bound to the nucleotide binding cleft of the actin filament [150]. It suggests that the cofilin induced conformational change in the nucleotide binding cleft of actin is the same irrespective of the state of the actin molecule (G- or F-actin). Contrary to cofilin, profilin increased the Stern-Volmer constant to 3.5 M^{-1} revealing a more accessible environment around the ε-ATP bound to the nucleotide binding cleft of actin. These findings suggest a strong coupling between the conformation of the nucleotide binding cleft of actin and the kinetics of the nucleotide exchange process. The cofilin locks the nucleotide binding cleft in a closed conformation that can lead to the impaired nucleotide exchange process on the actin

monomer. In contrast profilin opens up the nucleotide binding cleft, that can explain the facilitated nucleotide exchange process observed on actin in the presence of profilin. By using molecular dynamic simulation it was pointed out that the removing of profilin from the profilin-actin structure was accompanied with the closure of the nucleotide binding cleft within 200 ps [151]. This result implies that the open conformation of the nucleotide binding cleft of actin is thermodynamically unstable and only in the presence of profilin can be observed in the actin molecule.

The possible molecular mechanism behind the altered conformational state of the nucleotide binding cleft is the motion of the main domains and/or subdomains of actin relative to each other. This concept is based on the comparison of the atomic structure of profilin-β-actin complex in the tight and open state [78]. The tight to open state transition can be achieved by an overall 9.6° rotation of the two main domains relative to each other. It was suggested that this is principally the result of the 14.7° rotation of the highly flexible subdomain 2 regarding the rest of the molecule. In this term during the opening and closing of the nucleotide binding cleft the subdomain 2 of actin can move independently from the subdomain 1 resulting in the disintegration of the unity of the small domain of actin.

Recently the open and closed atomic structure of profilin-β-actin complex was reinvestigated [80]. Superimposing these structures onto each other through the large domain of actin it was revealed that the closed structure can be transformed into the open by rotating the whole small domain with 9° relative to the large domain. In respect of this scenario the subdomain 1 and 2 move as an integrated unit during the closed to open state transition.

To resolve this discrepancy regarding the motions of domains and/or subdomains of actin, the conformation and intrinsic dynamics of the small domain of actin was investigated in the presence of cofilin and profilin by using fluorescence resonance energy transfer assays. In the FRET experiments the donor fluorophore was attached close to the C-terminus of actin that is involved in cofilin and profilin binding [57, 78-80]. To assess how the labelling interferes with the binding of cofilin or profilin to the actin molecule fluorescence anisotropy measurements were completed. The dissociation equilibrium constant determined for the cofilin-actin complex was 0.68 μM that was around 3-fold greater than the value reported for the unmodified actin-cofilin complex [152]. The K_D determined for the profilin-actin complex was 9.15 μM that

was around 3 times higher than the value reported for the unmodified actin-profilin complex. These results suggest that the labelling of the actin monomer at the C-terminus causes a steric conflict with the binding of cofilin and profilin.

The fluorescence quenching of the donor fluorophore attached to Cys374 of actin revealed that both proteins decreased the accessibility of the fluorescence reporter molecule for the neutral quencher. The Stern-Volmer constant obtained for actin alone was 4.67 M^{-1} that dropped to 3.53 M^{-1} and 3.21 M^{-1} in the presence of cofilin and profilin, respectively. The decrease in the accessibility of the donor fluorophore can be explained well with the protection of the fluorophore due to the binding of cofilin and profilin to the vicinity of the C-terminus.

The fluorescence quenching of the acceptor fluorophore attached to Lys61 of actin showed opposite tendency for the accessibility of the fluorophore in the cofilin- or profilin-actin complexes. The Stern-Volmer constant determined for actin alone was 0.44 M^{-1} that is around one order of magnitude smaller than obtained for the quenching of the donor fluorophore attached to Cys374. This result seems to be reasonable, because the Lys61 is the part of the nucleotide binding cleft that is less exposed to the solvent than the C-terminus of actin. The cofilin decreased moderately the accessibility of the acceptor molecule resulting in a K_{SV} value of 0.39 M^{-1}. Profilin increased the accessibility of the acceptor resulting in a K_{SV} value of 0.52 M^{-1}. The tendency of change in the accessibility of FITC attached to Lys61 resembles the change in the accessibility of ε-ATP due to the binding of cofilin and profilin to actin. However it is difficult to interpret these slight modifications in the K_{SV} value. The possible explanation may be that the Lys61 residue located on the outer part of the nucleotide binding cleft therefore the solvent exposure of the label attached to it changes just slightly during the closing and opening of the nucleotide biding cleft. In the light of this consideration the modified accessibility of the fluorophore bound to Lys61 may reflect the change in the conformation of the nucleotide binding cleft but in a lesser extent than the alteration in the accessibility of ε-ATP located deeply in the nucleotide binding pocket.

The FRET experiments revealed that the distance between Cys374 (subdomain 1) and Lys61 (subdomain 2) labelled positions did not change significantly upon the binding of cofilin or profilin. This finding suggests that the orientation of the subdomain 1 and 2 does not change relative to each other upon cofilin or profilin

binding. Although conformational change was not detected in the small domain of actin in the presence of cofilin or profilin the flexibility of the segment of the small domain between the labelled positions decreased dramatically.

Wealth body of evidence supports that the subdomain 2 of actin can exist in multiple conformations due to the inherent flexible nature of this subdomain. In respect of this fact the large reduction in the flexibility observed in the presence of cofilin or profilin can be the consequence of the reduced motion of the highly mobile subdomain 2 of actin between the possible conformational sub-states.

These results reinforce that the small domain of actin behaves as a rigid unit during the closing and opening of the nucleotide binding cleft in the presence of cofilin or profilin, respectively. Additionally, the overall stabilization of the small domain of actin confirms the allosteric coupling between the subdomain 1 and 2 of actin because the binding of both proteins is restricted only to the subdomain 1 of the actin molecule.

It is worth to mention that a similar integrated domain motion occurs during the G- to F-actin transformation. Based on the X-ray fibre diffraction pattern of actin filaments it was revealed that the main conformational change accompanying the monomer-filament transition is the average 20° propeller-like rotation of the main domains of actin with respect to each other [26]. This domain motion results in the flattening of the actin subunits within the actin filament and the complete closure of the nucleotide binding cleft of actin protomers. This closed conformation of the nucleotide binding cleft can explain well the extremely slow nucleotide exchange process observed in actin filaments [153, 154].

It is long-time established that cofilin can enhance the formation of actin filaments in bulk polymerisation assays however the mechanism underlying this action of cofilin is still the subject of debate [38, 48]. One of the explanation can be the stabilisation of actin dimers by cofilin in the nucleation step of the actin polymerisation. Although this scenario seems plausible based on the binding fashion of cofilin between two adjacent actin subunits within the filament so far all the efforts to demonstrate the existence of the ternary complex of two actin monomers and one cofilin was failed. The other explanation can be that cofilin induces a conformational change in the actin monomer that resembles the conformational state of the actin protomers within the filament. In respect of this scenario the energetic barrier of the nucleation step of the actin polymerisation would be reduced due to the presence of actin monomers mimicking the

conformational state of the actin subunits within the filament. Several studies revealed the existence of this "F-actin like" conformation state of the actin monomers [155, 156]. For instance in a molecular dynamic simulation study the existence of a so called "superclosed" state of the actin monomer was pointed out that was thought to be the polymerization competent form of G-actin [156].

In contrast to cofilin, profilin slows down the nucleation phase of the actin polymerisation. On the top of that the elongation of the actin filaments at the barbed end in the presence of profilin is around 30 % slower than in the absence of that [157] and the incorporation of the profilin-actin complex into the filament is immediately accompanied by the dissociation of profilin from the filament end. These observations imply that the conformation of actin monomer in complex with profilin is severely diverse from the conformation state of the actin subunits within the filament. The profilin similarly to the cofilin does not change the intramolecular distance between the labelled position of subdomain 1 and 2 of actin, but cause the same reduction in the flexibility of the small domain. In the light of this consideration the different behaviour of the actin in complex with cofilin or profilin in the polymerisation process is presumably not due to the different state of the small domain of actin. It can be rather the consequence of the conformational state of the nucleotide binding cleft that is widely open in profilin-actin complex compared to the cleft seize of the cofilin-actin complex or the actin subunit within the filament. This open conformation can be an unfavourable state of the actin monomer in the polymerisation process that can explain well the slower kinetics for the formation of actin nuclei and the incorporation of actin monomers into the filament in the presence of profilin.

The differential scanning calorimetry assays confirmed the altered conformational state of the nucleotide binding cleft of actin in the presence of cofilin or profilin. The melting temperature of actin alone was 55.5 $^{\circ}$C that was shifted to 59.2 $^{\circ}$C and 47.6 $^{\circ}$C in the presence of cofilin and profilin, respectively. These findings suggest that the cofilin can stabilise, while profilin can destabilise the actin monomer. These stabilisation and destabilisation effects are probably the consequence of the different conformational states of the nucleotide-binding cleft. It was proposed earlier that there was a strong link between the conformation of the nucleotide-binding cleft of actin and the heat stability of the actin monomer. In this term the cofilin stabilises the actin monomer against the heat denaturation through rendering the two main domains of

actin in a compact arrangement. In contrast to cofilin the profilin keeps the actin domains far away from each other resulting in a less compact actin structure that is less resistant against the heat denaturation.

According to earlier reports the heat denaturation of actin occurs through the melting of the two main domains in a separate way. These findings did not confirm this mechanism for the denaturation process of actin, because the increased rigidity of the small domain of actin in the presence of cofilin and profilin did not appear in the heat denaturation profiles. It seems that the thermodynamic stability of the actin monomer dominantly depends on the conformational state of the nucleotide binding cleft and not on the stability of the individual domains.

VI. References

1. Anderson, C.M., R.E. Stenkamp, and T.A. Steitz, *Sequencing a protein by x-ray crystallography. II. Refinement of yeast hexokinase B co-ordinates and sequence at 2.1 A resolution.* J Mol Biol, 1978. **123**(1): p. 15-33.
2. Flaherty, K.M., C. DeLuca-Flaherty, and D.B. McKay, *Three-dimensional structure of the ATPase fragment of a 70K heat-shock cognate protein.* Nature, 1990. **346**(6285): p. 623-8.
3. Flaherty, K.M., et al., *Similarity of the three-dimensional structures of actin and the ATPase fragment of a 70-kDa heat shock cognate protein.* Proc Natl Acad Sci U S A, 1991. **88**(11): p. 5041-5.
4. Bork, P., C. Sander, and A. Valencia, *An ATPase domain common to prokaryotic cell cycle proteins, sugar kinases, actin, and hsp70 heat shock proteins.* Proc Natl Acad Sci U S A, 1992. **89**(16): p. 7290-4.
5. Kabsch, W., et al., *Atomic structure of the actin:DNase I complex.* Nature, 1990. **347**(6288): p. 37-44.
6. Dominguez, R., *Actin-binding proteins--a unifying hypothesis.* Trends Biochem Sci, 2004. **29**(11): p. 572-8.
7. Wegner, A., *Head to tail polymerization of actin.* J Mol Biol, 1976. **108**(1): p. 139-50.
8. Moore, P.B., H.E. Huxley, and D.J. DeRosier, *Three-dimensional reconstruction of F-actin, thin filaments and decorated thin filaments.* J Mol Biol, 1970. **50**(2): p. 279-95.
9. Feuer G, et al., *Studies on the composition and polymerisation of actin.* Hung Acta Physiol, 1948. **1**: p. 150-163.
10. Sept, D. and J.A. McCammon, *Thermodynamics and kinetics of actin filament nucleation.* Biophys J, 2001. **81**(2): p. 667-74.
11. Pollard, T.D., *Rate constants for the reactions of ATP- and ADP-actin with the ends of actin filaments.* J Cell Biol, 1986. **103**(6 Pt 2): p. 2747-54.
12. Kuhn, J.R. and T.D. Pollard, *Real-time measurements of actin filament polymerization by total internal reflection fluorescence microscopy.* Biophys J, 2005. **88**(2): p. 1387-402.
13. Kasai, M., S. Asakura, and F. Oosawa, *The cooperative nature of G-F transformation of actin.* Biochim Biophys Acta, 1962. **57**: p. 22-31.
14. Kasai, M., S. Asakura, and F. Oosawa, *The G-F equilibrium in actin solutions under various conditions.* Biochim Biophys Acta, 1962. **57**: p. 13-21.
15. Wegner, A., *Treadmilling of actin at physiological salt concentrations. An analysis of the critical concentrations of actin filaments.* J Mol Biol, 1982. **161**(4): p. 607-15.
16. Fujiwara, I., et al., *Microscopic analysis of polymerization dynamics with individual actin filaments.* Nat Cell Biol, 2002. **4**(9): p. 666-73.
17. Narita, A., T. Oda, and Y. Maeda, *Structural basis for the slow dynamics of the actin filament pointed end.* EMBO J, 2011. **30**(7): p. 1230-7.
18. Straub, F.B. and G. Feuer, *[Adenosine triphosphate, the functional group of actin].* Kiserl Orvostud, 1950. **2**(2): p. 141-51.
19. Wegner, A. and G. Isenberg, *12-fold difference between the critical monomer concentrations of the two ends of actin filaments in physiological salt conditions.* Proc Natl Acad Sci U S A, 1983. **80**(16): p. 4922-5.
20. Neuhaus, J.M., et al., *Treadmilling of actin.* J Muscle Res Cell Motil, 1983. **4**(5): p. 507-27.

21. Neidl, C. and J. Engel, *Exchange of ADP, ATP and 1: N6-ethenoadenosine 5'-triphosphate at G-actin. Equilibrium and kinetics.* Eur J Biochem, 1979. **101**(1): p. 163-9.
22. Selve, N. and A. Wegner, *Rate of treadmilling of actin filaments in vitro.* J Mol Biol, 1986. **187**(4): p. 627-31.
23. Wang, Y.L., *Exchange of actin subunits at the leading edge of living fibroblasts: possible role of treadmilling.* J Cell Biol, 1985. **101**(2): p. 597-602.
24. Okabe, S. and N. Hirokawa, *Incorporation and turnover of biotin-labeled actin microinjected into fibroblastic cells: an immunoelectron microscopic study.* J Cell Biol, 1989. **109**(4 Pt 1): p. 1581-95.
25. Oda, T. and Y. Maeda, *Multiple Conformations of F-actin.* Structure, 2010. **18**(7): p. 761-7.
26. Oda, T., et al., *The nature of the globular- to fibrous-actin transition.* Nature, 2009. **457**(7228): p. 441-5.
27. Galkin, V.E., et al., *A new internal mode in F-actin helps explain the remarkable evolutionary conservation of actin's sequence and structure.* Curr Biol, 2002. **12**(7): p. 570-5.
28. Page, R., U. Lindberg, and C.E. Schutt, *Domain motions in actin.* J Mol Biol, 1998. **280**(3): p. 463-74.
29. Sablin, E.P., et al., *How does ATP hydrolysis control actin's associations?* Proc Natl Acad Sci U S A, 2002. **99**(17): p. 10945-7.
30. Fujiwara, S., et al., *Internal motions of actin characterized by quasielastic neutron scattering.* Eur Biophys J, 2011. **40**(5): p. 661-71.
31. Stokasimov, E. and P.A. Rubenstein, *Actin isoform-specific conformational differences observed with hydrogen/deuterium exchange and mass spectrometry.* J Biol Chem, 2009. **284**(37): p. 25421-30.
32. McKane, M., et al., *Effect of the substitution of muscle actin-specific subdomain 1 and 2 residues in yeast actin on actin function.* J Biol Chem, 2006. **281**(40): p. 29916-28.
33. Bamburg, J.R., H.E. Harris, and A.G. Weeds, *Partial purification and characterization of an actin depolymerizing factor from brain.* FEBS Lett, 1980. **121**(1): p. 178-82.
34. Trinick, J., et al., *Cryo-electron microscopy and three-dimensional reconstruction of actin filaments.* J Microsc, 1986. **141**(Pt 3): p. 349-60.
35. Kim, S.R., Y. Kim, and G. An, *Molecular cloning and characterization of anther-preferential cDNA encoding a putative actin-depolymerizing factor.* Plant Mol Biol, 1993. **21**(1): p. 39-45.
36. Schuler, H., A.K. Mueller, and K. Matuschewski, *A Plasmodium actin-depolymerizing factor that binds exclusively to actin monomers.* Mol Biol Cell, 2005. **16**(9): p. 4013-23.
37. Nishida, E., S. Maekawa, and H. Sakai, *Cofilin, a protein in porcine brain that binds to actin filaments and inhibits their interactions with myosin and tropomyosin.* Biochemistry, 1984. **23**(22): p. 5307-13.
38. Carlier, M.F., et al., *Actin depolymerizing factor (ADF/cofilin) enhances the rate of filament turnover: implication in actin-based motility.* J Cell Biol, 1997. **136**(6): p. 1307-22.
39. Carlier, M.F., F. Ressad, and D. Pantaloni, *Control of actin dynamics in cell motility. Role of ADF/cofilin.* J Biol Chem, 1999. **274**(48): p. 33827-30.
40. Ichetovkin, I., et al., *Actin filaments are severed by both native and recombinant dictyostelium cofilin but to different extents.* Cell Motil Cytoskeleton, 2000. **45**(4): p. 293-306.
41. Maciver, S.K., et al., *The effect of two actin depolymerizing factors (ADF/cofilins) on actin filament turnover: pH sensitivity of F-actin binding by human ADF, but not of Acanthamoeba actophorin.* Eur J Biochem, 1998. **256**(2): p. 388-97.

42. Pavlov, D., et al., *Actin filament severing by cofilin.* J Mol Biol, 2007. **365**(5): p. 1350-8.
43. Andrianantoandro, E. and T.D. Pollard, *Mechanism of actin filament turnover by severing and nucleation at different concentrations of ADF/cofilin.* Mol Cell, 2006. **24**(1): p. 13-23.
44. Maciver, S.K., H.G. Zot, and T.D. Pollard, *Characterization of actin filament severing by actophorin from Acanthamoeba castellanii.* J Cell Biol, 1991. **115**(6): p. 1611-20.
45. Blanchoin, L. and T.D. Pollard, *Mechanism of interaction of Acanthamoeba actophorin (ADF/Cofilin) with actin filaments.* J Biol Chem, 1999. **274**(22): p. 15538-46.
46. Kudryashov, D.S., et al., *Cofilin cross-bridges adjacent actin protomers and replaces part of the longitudinal F-actin interface.* J Mol Biol, 2006. **358**(3): p. 785-97.
47. Yeoh, S., et al., *Determining the differences in actin binding by human ADF and cofilin.* J Mol Biol, 2002. **315**(4): p. 911-25.
48. Blanchoin, L. and T.D. Pollard, *Interaction of actin monomers with Acanthamoeba actophorin (ADF/cofilin) and profilin.* J Biol Chem, 1998. **273**(39): p. 25106-11.
49. Ressad, F., et al., *Kinetic analysis of the interaction of actin-depolymerizing factor (ADF)/cofilin with G- and F-actins. Comparison of plant and human ADFs and effect of phosphorylation.* J Biol Chem, 1998. **273**(33): p. 20894-902.
50. Reymann, A.C., et al., *Turnover of branched actin filament networks by stochastic fragmentation with ADF/cofilin.* Mol Biol Cell, 2011. **22**(14): p. 2541-50.
51. Suarez, C., et al., *Cofilin tunes the nucleotide state of actin filaments and severs at bare and decorated segment boundaries.* Curr Biol, 2011. **21**(10): p. 862-8.
52. Galkin, V.E., et al., *Remodeling of actin filaments by ADF/cofilin proteins.* Proc Natl Acad Sci U S A, 2011. **108**(51): p. 20568-72.
53. McGough, A., et al., *Cofilin changes the twist of F-actin: implications for actin filament dynamics and cellular function.* J Cell Biol, 1997. **138**(4): p. 771-81.
54. Mannherz, H.G., et al., *Mapping the ADF/cofilin binding site on monomeric actin by competitive cross-linking and peptide array: evidence for a second binding site on monomeric actin.* J Mol Biol, 2007. **366**(3): p. 745-55.
55. Wriggers, W., et al., *Cofilin and gelsolin segment-1: molecular dynamics simulation and biochemical analysis predict a similar actin binding mode.* J Mol Biol, 1998. **282**(5): p. 921-32.
56. Kamal, J.K., et al., *Three-dimensional structure of cofilin bound to monomeric actin derived by structural mass spectrometry data.* Proc Natl Acad Sci U S A, 2007. **104**(19): p. 7910-5.
57. Grintsevich, E.E., et al., *Mapping the cofilin binding site on yeast G-actin by chemical cross-linking.* J Mol Biol, 2008. **377**(2): p. 395-409.
58. Paavilainen, V.O., et al., *Structure of the actin-depolymerizing factor homology domain in complex with actin.* J Cell Biol, 2008. **182**(1): p. 51-9.
59. Scott, R.W. and M.F. Olson, *LIM kinases: function, regulation and association with human disease.* J Mol Med (Berl), 2007. **85**(6): p. 555-68.
60. Toshima, J., et al., *Cofilin phosphorylation by protein kinase testicular protein kinase 1 and its role in integrin-mediated actin reorganization and focal adhesion formation.* Mol Biol Cell, 2001. **12**(4): p. 1131-45.
61. Toshima, J., et al., *Cofilin phosphorylation and actin reorganization activities of testicular protein kinase 2 and its predominant expression in testicular Sertoli cells.* J Biol Chem, 2001. **276**(33): p. 31449-58.
62. Huang, T.Y., C. DerMardirossian, and G.M. Bokoch, *Cofilin phosphatases and regulation of actin dynamics.* Curr Opin Cell Biol, 2006. **18**(1): p. 26-31.
63. Gorbatyuk, V.Y., et al., *Mapping the phosphoinositide-binding site on chick cofilin explains how PIP2 regulates the cofilin-actin interaction.* Mol Cell, 2006. **24**(4): p. 511-22.

64. Moriyama, K., et al., *Destrin, a mammalian actin-depolymerizing protein, is closely related to cofilin. Cloning and expression of porcine brain destrin cDNA.* J Biol Chem, 1990. **265**(10): p. 5768-73.
65. Ojala, P.J., V. Paavilainen, and P. Lappalainen, *Identification of yeast cofilin residues specific for actin monomer and PIP2 binding.* Biochemistry, 2001. **40**(51): p. 15562-9.
66. Carlsson, L., et al., *Crystallization of a non-muscle actin.* J Mol Biol, 1976. **105**(3): p. 353-66.
67. Buss, F., et al., *Distribution of profilin in fibroblasts correlates with the presence of highly dynamic actin filaments.* Cell Motil Cytoskeleton, 1992. **22**(1): p. 51-61.
68. Vinson, V.K., et al., *Interactions of Acanthamoeba profilin with actin and nucleotides bound to actin.* Biochemistry, 1998. **37**(31): p. 10871-80.
69. Mockrin, S.C. and E.D. Korn, *Acanthamoeba profilin interacts with G-actin to increase the rate of exchange of actin-bound adenosine 5'-triphosphate.* Biochemistry, 1980. **19**(23): p. 5359-62.
70. Pollard, T.D. and J.A. Cooper, *Quantitative analysis of the effect of Acanthamoeba profilin on actin filament nucleation and elongation.* Biochemistry, 1984. **23**(26): p. 6631-41.
71. Kinosian, H.J., et al., *Actin filament barbed end elongation with nonmuscle MgATP-actin and MgADP-actin in the presence of profilin.* Biochemistry, 2002. **41**(21): p. 6734-43.
72. Carlier, M.F., et al., *Structure, function, and evolution of the beta-thymosin/WH2 (WASP-Homology2) actin-binding module.* Ann N Y Acad Sci, 2007. **1112**: p. 67-75.
73. Ampe, C., et al., *The primary structure of human platelet profilin: reinvestigation of the calf spleen profilin sequence.* FEBS Lett, 1988. **228**(1): p. 17-21.
74. DiNubile, M.J. and F.S. Southwick, *Effects of macrophage profilin on actin in the presence and absence of acumentin and gelsolin.* J Biol Chem, 1985. **260**(12): p. 7402-9.
75. Perelroizen, I., M.F. Carlier, and D. Pantaloni, *Binding of divalent cation and nucleotide to G-actin in the presence of profilin.* J Biol Chem, 1995. **270**(4): p. 1501-8.
76. Yarmola, E.G. and M.R. Bubb, *Effects of profilin and thymosin beta4 on the critical concentration of actin demonstrated in vitro and in cell extracts with a novel direct assay.* J Biol Chem, 2004. **279**(32): p. 33519-27.
77. Pantaloni, D. and M.F. Carlier, *How profilin promotes actin filament assembly in the presence of thymosin beta 4.* Cell, 1993. **75**(5): p. 1007-14.
78. Chik, J.K., U. Lindberg, and C.E. Schutt, *The structure of an open state of beta-actin at 2.65 A resolution.* J Mol Biol, 1996. **263**(4): p. 607-23.
79. Schutt, C.E., et al., *The structure of crystalline profilin-beta-actin.* Nature, 1993. **365**(6449): p. 810-6.
80. Porta, J.C. and G.E. Borgstahl, *Structural basis for profilin-mediated actin nucleotide exchange.* J Mol Biol, 2012. **418**(1-2): p. 103-16.
81. Chereau, D. and R. Dominguez, *Understanding the role of the G-actin-binding domain of Ena/VASP in actin assembly.* J Struct Biol, 2006. **155**(2): p. 195-201.
82. Ferron, F., et al., *Structural basis for the recruitment of profilin-actin complexes during filament elongation by Ena/VASP.* EMBO J, 2007. **26**(21): p. 4597-606.
83. Goldschmidt-Clermont, P.J., et al., *The actin-binding protein profilin binds to PIP2 and inhibits its hydrolysis by phospholipase C.* Science, 1990. **247**(4950): p. 1575-8.
84. Machesky, L.M., P.J. Goldschmidt-Clermont, and T.D. Pollard, *The affinities of human platelet and Acanthamoeba profilin isoforms for polyphosphoinositides account for their relative abilities to inhibit phospholipase C.* Cell Regul, 1990. **1**(12): p. 937-50.

85. Skare, P. and R. Karlsson, *Evidence for two interaction regions for phosphatidylinositol(4,5)-bisphosphate on mammalian profilin I.* FEBS Lett, 2002. **522**(1-3): p. 119-24.
86. Lambrechts, A., et al., *Mutational analysis of human profilin I reveals a second PI(4,5)-P2 binding site neighbouring the poly(L-proline) binding site.* BMC Biochem, 2002. **3**: p. 12.
87. Ezezika, O.C., et al., *Incompatibility with formin Cdc12p prevents human profilin from substituting for fission yeast profilin: insights from crystal structures of fission yeast profilin.* J Biol Chem, 2009. **284**(4): p. 2088-97.
88. Geese, M., et al., *Accumulation of profilin II at the surface of Listeria is concomitant with the onset of motility and correlates with bacterial speed.* J Cell Sci, 2000. **113 (Pt 8)**: p. 1415-26.
89. Grenklo, S., et al., *A crucial role for profilin-actin in the intracellular motility of Listeria monocytogenes.* EMBO Rep, 2003. **4**(5): p. 523-9.
90. Feuer, G., F. Molnar, and et al., *Studies on the composition and polymerization of actin.* Hung Acta Physiol, 1948. **1**(4-5): p. 150-63.
91. Mossakowska, M., J. Belagyi, and H. Strzelecka-Golaszewska, *An EPR study of the rotational dynamics of actins from striated and smooth muscle and their complexes with heavy meromyosin.* Eur J Biochem, 1988. **175**(3): p. 557-64.
92. Spudich, J.A. and S. Watt, *The regulation of rabbit skeletal muscle contraction. I. Biochemical studies of the interaction of the tropomyosin-troponin complex with actin and the proteolytic fragments of myosin.* J Biol Chem, 1971. **246**(15): p. 4866-71.
93. Houk, T.W., Jr. and K. Ue, *The measurement of actin concentration in solution: a comparison of methods.* Anal Biochem, 1974. **62**(1): p. 66-74.
94. Elzinga, M., et al., *Complete amino-acid sequence of actin of rabbit skeletal muscle.* Proc Natl Acad Sci U S A, 1973. **70**(9): p. 2687-91.
95. Miki, M., C.G. dos Remedios, and J.A. Barden, *Spatial relationship between the nucleotide-binding site, Lys-61 and Cys-374 in actin and a conformational change induced by myosin subfragment-1 binding.* Eur J Biochem, 1987. **168**(2): p. 339-45.
96. Hudson, E.N. and G. Weber, *Synthesis and characterization of two fluorescent sulfhydryl reagents.* Biochemistry, 1973. **12**(21): p. 4154-61.
97. Bradford, M.M., *A rapid and sensitive method for the quantitation of microgram quantities of protein utilizing the principle of protein-dye binding.* Anal Biochem, 1976. **72**: p. 248-54.
98. Bernhardt, R., et al., *Modification of cytochrome P-450 with fluorescein isothiocyanate.* Biochim Biophys Acta, 1983. **745**(2): p. 140-8.
99. Kinosita, K., Jr., S. Kawato, and A. Ikegami, *A theory of fluorescence polarization decay in membranes.* Biophys J, 1977. **20**(3): p. 289-305.
100. Somogyi, B., et al., *Forster-type energy transfer as a probe for changes in local fluctuations of the protein matrix.* Biochemistry, 1984. **23**(15): p. 3403-11.
101. Nyitrai, M., et al., *Effect of Ca2+-Mg2+ exchange on the flexibility and/or conformation of the small domain in monomeric actin.* Biophys J, 1998. **74**(5): p. 2474-81.
102. Gershman, L.C., et al., *Preparation and polymerization properties of monomeric ADP-actin.* Biochim Biophys Acta, 1989. **995**(2): p. 109-15.
103. Goldschmidt-Clermont, P.J., et al., *The control of actin nucleotide exchange by thymosin beta 4 and profilin. A potential regulatory mechanism for actin polymerization in cells.* Mol Biol Cell, 1992. **3**(9): p. 1015-24.
104. Ojala, P.J., et al., *The two ADF-H domains of twinfilin play functionally distinct roles in interactions with actin monomers.* Mol Biol Cell, 2002. **13**(11): p. 3811-21.
105. Palmgren, S., M. Vartiainen, and P. Lappalainen, *Twinfilin, a molecular mailman for actin monomers.* J Cell Sci, 2002. **115**(Pt 5): p. 881-6.

106. Perelroizen, I., et al., *Role of nucleotide exchange and hydrolysis in the function of profilin in action assembly.* J Biol Chem, 1996. **271**(21): p. 12302-9.
107. Hayden, S.M., et al., *Analysis of the interactions of actin depolymerizing factor with G- and F-actin.* Biochemistry, 1993. **32**(38): p. 9994-10004.
108. Nishida, E., *Opposite effects of cofilin and profilin from porcine brain on rate of exchange of actin-bound adenosine 5'-triphosphate.* Biochemistry, 1985. **24**(5): p. 1160-4.
109. Singh, B.K., et al., *Crystal structures explain functional differences in the two actin depolymerization factors of the malaria parasite.* J Biol Chem. **286**(32): p. 28256-64.
110. Wang, Y.L. and D.L. Taylor, *Exchange of 1,N6-etheno-ATP with actin-bound nucleotides as a tool for studying the steady-state exchange of subunits in F-actin solutions.* Proc Natl Acad Sci U S A, 1981. **78**(9): p. 5503-7.
111. Han, L., et al., *Direct stimulation of receptor-controlled phospholipase D1 by phospho-cofilin.* EMBO J, 2007. **26**(19): p. 4189-202.
112. Kudryashov, D.S. and E. Reisler, *Solution properties of tetramethylrhodamine-modified G-actin.* Biophys J, 2003. **85**(4): p. 2466-75.
113. Selden, L.A., et al., *Impact of profilin on actin-bound nucleotide exchange and actin polymerization dynamics.* Biochemistry, 1999. **38**(9): p. 2769-78.
114. Lu, J. and T.D. Pollard, *Profilin binding to poly-L-proline and actin monomers along with ability to catalyze actin nucleotide exchange is required for viability of fission yeast.* Mol Biol Cell, 2001. **12**(4): p. 1161-75.
115. Yarmola, E.G., S. Parikh, and M.R. Bubb, *Formation and implications of a ternary complex of profilin, thymosin beta 4, and actin.* J Biol Chem, 2001. **276**(49): p. 45555-63.
116. Korenbaum, E., et al., *The role of profilin in actin polymerization and nucleotide exchange.* Biochemistry, 1998. **37**(26): p. 9274-83.
117. Hawkins, M., et al., *Human actin depolymerizing factor mediates a pH-sensitive destruction of actin filaments.* Biochemistry, 1993. **32**(38): p. 9985-93.
118. Vartiainen, M., et al., *Mouse A6/twinfilin is an actin monomer-binding protein that localizes to the regions of rapid actin dynamics.* Mol Cell Biol, 2000. **20**(5): p. 1772-83.
119. Baek, K., et al., *Modulation of actin structure and function by phosphorylation of Tyr-53 and profilin binding.* Proc Natl Acad Sci U S A, 2008. **105**(33): p. 11748-53.
120. Kinosian, H.J., et al., *Interdependence of profilin, cation, and nucleotide binding to vertebrate non-muscle actin.* Biochemistry, 2000. **39**(43): p. 13176-88.
121. Ando, T., et al., *Spectroscopic isolation of ES complexes of myosin subfragment-1 ATPase by fluorescence quenching.* Biochem Biophys Res Commun, 1982. **109**(1): p. 1-6.
122. Harvey, S.C. and H.C. Cheung, *Fluorescence studies of 1,N6-ethenoadenosine triphosphate bound to G-actin: the nucleotide base is inaccessible to water.* Biochem Biophys Res Commun, 1976. **73**(4): p. 865-8.
123. Johnson, D.A. and J. Yguerabide, *Solute accessibility to N epsilon-fluorescein isothiocyanate-lysine-23 cobra alpha-toxin bound to the acetylcholine receptor. A consideration of the effect of rotational diffusion and orientation constraints on fluorescence quenching.* Biophys J, 1985. **48**(6): p. 949-55.
124. Lappalainen, P., et al., *Essential functions and actin-binding surfaces of yeast cofilin revealed by systematic mutagenesis.* EMBO J, 1997. **16**(18): p. 5520-30.
125. Eads, J.C., et al., *Structure determination and characterization of Saccharomyces cerevisiae profilin.* Biochemistry, 1998. **37**(32): p. 11171-81.
126. Graceffa, P. and R. Dominguez, *Crystal structure of monomeric actin in the ATP state. Structural basis of nucleotide-dependent actin dynamics.* J Biol Chem, 2003. **278**(36): p. 34172-80.

127. Bosch, M., et al., *Analysis of the function of Spire in actin assembly and its synergy with formin and profilin.* Mol Cell, 2007. **28**(4): p. 555-68.
128. Vartiainen, M.K., et al., *The three mouse actin-depolymerizing factor/cofilins evolved to fulfill cell-type-specific requirements for actin dynamics.* Mol Biol Cell, 2002. **13**(1): p. 183-94.
129. Wen, K.K., et al., *Control of the ability of profilin to bind and facilitate nucleotide exchange from G-actin.* J Biol Chem, 2008. **283**(14): p. 9444-53.
130. Tao, T. and J. Cho, *Fluorescence lifetime quenching studies on the accessibilities of actin sulfhydryl sites.* Biochemistry, 1979. **18**(13): p. 2759-65.
131. Ujfalusi, Z., et al., *Effect of tropomyosin on formin-bound actin filaments.* Biophys J, 2009. **96**(1): p. 162-8.
132. Bugyi, B., et al., *Formins regulate actin filament flexibility through long range allosteric interactions.* J Biol Chem, 2006. **281**(16): p. 10727-36.
133. Hild, G., M. Nyitrai, and B. Somogyi, *Intermonomer flexibility of Ca- and Mg-actin filaments at different pH values.* Eur J Biochem, 2002. **269**(3): p. 842-9.
134. Nyitrai, M., et al., *Conformational and dynamic differences between actin filaments polymerized from ATP- or ADP-actin monomers.* J Biol Chem, 2000. **275**(52): p. 41143-9.
135. Nyitrai, M., et al., *The flexibility of actin filaments as revealed by fluorescence resonance energy transfer. The influence of divalent cations.* J Biol Chem, 1999. **274**(19): p. 12996-3001.
136. Hild, G., et al., *The influence of divalent cations on the dynamic properties of actin filaments: a spectroscopic study.* Biophys J, 1998. **75**(6): p. 3015-22.
137. Blondin, L., et al., *The second ADF/cofilin actin-binding site exists in F-actin, the cofilin-G-actin complex, but not in G-actin.* Eur J Biochem, 2001. **268**(24): p. 6426-34.
138. Ikkai, T., P. Wahl, and J.C. Auchet, *Anisotropy decay of labelled actin. Evidence of the flexibility of the peptide chain in F-actin molecules.* Eur J Biochem, 1979. **93**(2): p. 397-408.
139. Ph., W., *New Techniques in Biophysics and Cell Biology*, ed. R.S. Pain, B.1975, Chichester U.K.: Wiley. 223-285.
140. Wahl, P., *Analysis of fluorescence anisotropy decays by a least square method.* Biophys Chem, 1979. **10**(1): p. 91-104.
141. Kawato, S., K. Kinosita, Jr., and A. Ikegami, *Dynamic structure of lipid bilayers studied by nanosecond fluorescence techniques.* Biochemistry, 1977. **16**(11): p. 2319-24.
142. Lipari, G. and A. Szabo, *Effect of librational motion on fluorescence depolarization and nuclear magnetic resonance relaxation in macromolecules and membranes.* Biophys J, 1980. **30**(3): p. 489-506.
143. Pivovarova, A.V., S.Y. Khaitlina, and D.I. Levitsky, *Specific cleavage of the DNase-I binding loop dramatically decreases the thermal stability of actin.* FEBS J, 2010. **277**(18): p. 3812-22.
144. Levitsky, D.I., et al., *Thermal unfolding and aggregation of actin.* FEBS J, 2008. **275**(17): p. 4280-95.
145. Dedova, I.V., et al., *Two opposite effects of cofilin on the thermal unfolding of F-actin: a differential scanning calorimetric study.* Biophys Chem, 2004. **110**(1-2): p. 119-28.
146. Bertazzon, A., et al., *Enthalpic and entropic contributions to actin stability: calorimetry, circular dichroism, and fluorescence study and effects of calcium.* Biochemistry, 1990. **29**(1): p. 291-8.
147. Bobkov, A.A., et al., *Cooperative effects of cofilin (ADF) on actin structure suggest allosteric mechanism of cofilin function.* J Mol Biol, 2006. **356**(2): p. 325-34.

148. Perieteanu, A.A., B. Sweeting, and J.F. Dawson, *The real-time monitoring of the thermal unfolding of tetramethylrhodamine-labeled actin.* Biochemistry, 2008. **47**(36): p. 9688-96.
149. Schuler, H., et al., *Thermal unfolding of G-actin monitored with the DNase I-inhibition assay stabilities of actin isoforms.* Eur J Biochem, 2000. **267**(2): p. 476-86.
150. Muhlrad, A., et al., *Antagonistic effects of cofilin, beryllium fluoride complex, and phalloidin on subdomain 2 and nucleotide-binding cleft in F-actin.* Biophys J, 2006. **91**(12): p. 4490-9.
151. Minehardt, T.J., et al., *The open nucleotide pocket of the profilin/actin x-ray structure is unstable and closes in the absence of profilin.* Biophys J, 2006. **90**(7): p. 2445-9.
152. Guan, J.Q., et al., *Mapping the G-actin binding surface of cofilin using synchrotron protein footprinting.* Biochemistry, 2002. **41**(18): p. 5765-75.
153. Pollard, T.D., I. Goldberg, and W.H. Schwarz, *Nucleotide exchange, structure, and mechanical properties of filaments assembled from ATP-actin and ADP-actin.* J Biol Chem, 1992. **267**(28): p. 20339-45.
154. Newman, J., et al., *Nucleotide exchange and rheometric studies with F-actin prepared from ATP- or ADP-monomeric actin.* Biophys J, 1993. **64**(5): p. 1559-66.
155. Morimatsu, M., et al., *Spontaneous structural changes in actin regulate g-f transformation.* PLoS One, 2012. **7**(11): p. e45864.
156. Splettstoesser, T., et al., *Nucleotide-dependence of G-actin conformation from multiple molecular dynamics simulations and observation of a putatively polymerization-competent superclosed state.* Proteins, 2009. **76**(2): p. 353-64.
157. Gutsche-Perelroizen, I., et al., *Filament assembly from profilin-actin.* J Biol Chem, 1999. **274**(10): p. 6234-43.

VII. List of Abbreviations

*ADF***:** actin depolymerising factor

*ADP***:** adenosine diphosphate

*Arp2/3 complex***:** actin related protein 2/3 complex

*ATP***:** adenosine triphosphate

DSC: differential scanning calorimetry

*ε-ATP***:** 1, N^6- Ethenoadenosine- 5'- O- triphosphate

FITC: fluorescein isothiocyanate

FRET: fluorescence resonance energy transfer

IAEDANS: 5-[2-[(2-Iodo-1-oxoethyl)amino]ethylamino]-1-naphthalenesulfonic acid

K_D: dissociation equilibrium constant

MOPS: 3-(N-morpholino) propanesulfonic acid

P_i: inorganic phosphate

PIP_2: phosphatidylinositol 4,5-bisphosphate

PIP_3: phosphatidylinositol (3,4,5)-triphosphate

TRIS: tris(hydroxymethyl)aminomethane

VASP: vasodilatator-stimulated phosphoprotein

VIII. Appendix

Cofilin conc. (μM)	k_{obs} (s^{-1})	Profilin conc. (μM)	k_{obs} (s^{-1})	
			slower	faster
0	**0.012**	**0**	**0.012**	**-**
0.5	**0.009**	**0.25**	**0.018**	**0.147**
2	**0.005**	**0.5**	**0.021**	**0.021**
3	**0.002**	**1**	**0.026**	**0.026**

Table 1.) The observed rate constants of the nucleotide exchange experiments in the presence of different concentration of actin-binding proteins.

Acrylamide conc. (M)	Lifetime of free ε-ATP (ns)			Lifetime of bound ε-ATP (ns)		
	actin	cofilin-actin complex	profilin-actin complex	actin	cofilin-actin complex	profilin-actin complex
0	25.4±0.1	25.8±0.85	25.7±0.01	34.1±4.5	30.1±30.4	31.2±23.2
0.05	7.05±0.15	6.6±0.1	6.55±0.15	30.5±1.1	31.5±0.9	32.5±0.15
0.1	4.05±0.07	3.9±0.15	3.85±0.3	31.1±0.2	32.9±1.3	32.4±0.4
0.15	2.85±0.06	2.75±0.03	2.65±0.1	30.8±0.6	32.7±1.2	32.3±0.2
0.2	2.15±0.09	2.1±0.05	2.05±0.1	31.1±0.3	32.5±1	32.4±0.2
0.25	1.85±0.01	1.7±0.1	1.63±0.05	31.1±0.3	33±1.5	32.3±0.5
0.3	1.55±0.05	1.5±0.08	1.4±0.05	31.3±0.6	33.2±1.5	32.7±0.15

Table 2.) Results obtained for the fluorescence lifetime of ε-ATP labelled actin samples at different quencher concentrations. The pre-exponential factor associated with each decay time is not involved in the table because the ratio of the free and actin-bound ε-ATP were not the same in all measurements (short ion-exchange resin treatment before the measurement left 20-60 μM free ε-ATP in the solution)

Table 3-8: Results of the anisotropy decay experiments. The values were obtained by fitting Equation 7. and 8. simultaneously on the fluorescence decay curves recorded in parallel and perpendicular polarisation setup.

θ_1*:* rotational correlation time characterising the motion of actin or its complex with actin-binding proteins (ABP)

β_1: fractional amplitude of the motion of actin or its complex with ABPs

θ_2*:* rotational correlation time characterising the motion of the reporter molecule respect to the protein surface

β_2*:* fractional amplitude of the motion of reporter molecule

r_o: time zero anisotropy value

r_{ss}: steady-state anisotropy

θ_o*:* half-cone angle characterising the spatial confinement of the reporter molecules' motion. The half-cone angle was calculated according to Equation 10.

The fluorescence lifetimes which were also recovered from the fluorescence decay curves were not involved in the tables, because they were irrelevant to the aim of the measurements.

Temperature (°C)	θ_1 (ns)	β_1	θ_2 (ns)	β_2	r_o	r_{ss}	θ_o (deg.)
5	49.3	0.17	4.83	0.017	0.187	0.117	14.5
10	40.6	0.169	2.57	0.023	0.192	0.111	16.7
15	34.2	0.16	2.95	0.028	0.188	0.100	18.7
20	29.4	0.151	2.65	0.036	0.187	0.092	21.4
25	25.4	0.138	2.49	0.045	0.184	0.082	24.6
30	22.7	0.124	2.4	0.061	0.185	0.075	29.0
35	19.9	0.112	2.06	0.071	0.184	0.067	32.0

Table 3.) Results of anisotropy decay measurements of IAEDANS-labelled actin in the absence of actin-binding proteins.

Temperature (°C)	θ_1 (ns)	β_1	θ_2 (ns)	β_2	r_o	r_{ss}	θ_o (deg.)
5	59.0	0.175	3.21	0.021	0.197	0.130	15.8
10	51.4	0.170	2.86	0.027	0.197	0.123	17.9
15	45.6	0.159	2.63	0.041	0.200	0.114	22.0
20	40.9	0.152	2.38	0.048	0.201	0.107	24.2
25	37.1	0.136	2.75	0.056	0.193	0.097	26.9
30	32.3	0.121	2.49	0.073	0.195	0.087	31.4
35	28.8	0.110	2.17	0.079	0.190	0.078	33.6

Table 4.) Results of anisotropy decay measurements of IAEDANS-labelled actin in the presence of cofilin.

Temperature (°C)	θ_1 (ns)	β_1	θ_2 (ns)	β_2	r_o	r_{ss}	θ_o (deg.)
5	51.7	0.170	4.03	0.018	0.188	0.119	14.8
10	44.5	0.167	2.78	0.028	0.196	0.113	18.3
15	39.4	0.164	2.39	0.029	0.194	0.108	18.7
20	35.9	0.156	2.11	0.041	0.197	0.101	22.3
25	31.4	0.150	2.04	0.047	0.197	0.095	24.0
30	29.4	0.139	2.69	0.051	0.190	0.088	25.7
35	25.5	0.135	1.92	0.061	0.197	0.082	28.2

Table 5.) Results of anisotropy decay measurements of IAEDANS-labelled actin in the presence of profilin.

Temperature (°C)	θ_1 (ns)	β_1	θ_2 (ns)	β_2	r_o	r_{ss}	θ_o (deg.)
5	32.4	0.164	1.47	0.077	0.242	0.175	28.5
10	29.0	0.158	1.45	0.079	0.237	0.169	29.3
15	25.3	0.152	1.37	0.082	0.235	0.163	30.2
20	22.1	0.147	1.31	0.086	0.234	0.158	31.2
25	21.2	0.144	1.41	0.086	0.230	0.155	31.4
30	19.9	0.135	1.39	0.092	0.227	0.149	32.9
35	17.4	0.129	1.24	0.099	0.229	0.143	34.4

Table 6.) Results of anisotropy decay measurements of FITC-labelled actin in the absence of actin-binding proteins.

Temperature (°C)	θ_1 (ns)	β_1	θ_2 (ns)	β_2	r_o	r_{ss}	θ_o (deg.)
5	43.1	0.167	1.47	0.067	0.234	0.177	26.7
10	43.5	0.167	1.67	0.070	0.238	0.181	27.3
15	33.1	0.166	1.54	0.071	0.237	0.176	27.5
20	29.2	0.160	1.31	0.075	0.235	0.169	28.6
25	26.5	0.154	1.24	0.081	0.236	0.165	29.9
30	25.4	0.148	1.17	0.085	0.233	0.159	30.9
35	24.6	0.137	1.37	0.086	0.223	0.153	32.0

Table 7.) Results of anisotropy decay measurements of FITC-labelled actin in the presence of cofilin.

Temperature (°C)	θ_1 (ns)	β_1	θ_2 (ns)	β_2	r_o	r_{ss}	θ_o (deg.)
5	36.4	0.168	1.39	0.073	0.241	0.178	27.6
10	32.6	0.164	1.45	0.073	0.237	0.173	27.9
15	31.7	0.153	1.57	0.075	0.228	0.165	29.1
20	27.6	0.148	1.49	0.106	0.226	0.160	29.9
25	25.6	0.139	1.49	0.083	0.222	0.154	31.3
30	20.0	0.139	1.25	0.081	0.221	0.148	31.1
35	18.9	0.130	1.21	0.086	0.216	0.141	32.6

Table 8.) Results of anisotropy decay measurements of FITC-labelled actin in the presence of profilin.

IX. Publications

VIII.1. Publications related to the thesis

The effects of ADF/cofilin and profilin on the conformation of the ATP-binding cleft of monomeric actin. *Roland Kardos, Kinga Pozsonyi, Elisa Nevalainen, Pekka Lappalainen, Miklós Nyitrai, and Gábor Hild,* Biophysical Journal, Volume 96, March 2009, Pages 2335–2343

IF: 4.39

The Effect of ADF/Cofilin and Profilin on the Dynamics of Monomeric Actin
Roland Kardos, Elisa Nevalainen, Miklós Nyitrai, and Gábor Hild, Biochimica et Biophysica Acta (BBA) - Proteins and Proteomics, Volume 1834, Issue 10, October 2013, Pages 2010–2019

IF: 3.73

The other side of the coin: Functional and structural versatility of ADF/cofilins

Gábor Hild, Lajos Kalmár , Roland Kardos, Miklós Nyitrai, Beáta Bugyi, European Journal of Cell Biology, Manuscript has been accepted, 2013

IF: 3.32

VIII.2. Other publications

The effect of jasplakinolide on the thermodynamic properties of ADP.BeF(x) bound actin filaments. *Roland Kardos, Andrea Vig, József Orbán, Gábor Hild, Miklós Nyitrai, and Dénes Lőrinczy Thermochim Acta*. 2007 October 25; 463(1-2): 77–80.

IF: 1.805

Cumulative impact factor: 13.25

VIII.3. Posters related to the thesis

-The effect of actin-binding proteins on the dynamic properties of G-actin *Roland Kardos, Elisa Nevalainen, Pekka Lappalaine, Miklós Nyitrai and Gábor Hild,* Symposium for Graduate Students in Biology, November 2009, Pécs, Hungary.

-The effect of actin-binding proteins on the dynamic properties of monomeric actin *Roland Kardos, Mónika Tóth, Kinga Futó, Elisa Nevalainen, Pekka Lappalainen, Miklós Nyitrai and Gábor Hild,* 23rd Congress of Hungarian Biophysical Society, August 2009, Pécs, Hungary.

-The effect of actin-binding proteins on the dynamic properties of monomeric actin *Roland Kardos, Andrea Vig, Réka Dudás, Tünde Kupi, Elisa Nevalainen, Pekka Lappalainen, Miklós Nyitrai and Gábor Hild,* 23rd European Cytoskeleton Forum, FEBS/ECF Workshop, 2008, Potsdam, Germany.

-Effect of actin binding proteins on the conformation of nucleotide binding cleft of actin *Gábor Hild, Roland Kardos, Kinga Pozsonyi, Andrea Vig, Miklós Nyitrai,* 37th Membrane Transport Conference, May 2007, Sümeg, Hungary.

VIII.4. Posters not related to the thesis

-The effects of mouse twinfilin-1 on the structure and dynamics properties of actin *Veronika Kollár, Pekka Lappalainen, Roland Kardos, Gábor Hild,* 8th of European Biophysics Congress, Budapest, Hungary, August 2011.

-Interaction of WH2 domain of ABBA with monomeric actin *Roland Kardos, Pekka Lappalainen, Gábor Hild,* 8th of European Biophysics Congress, August 2011.

-The effects of mouse twinfilin-1 on the structure and dynamics properties of actin *Veronika Kollár, Pekka Lappalainen, Roland Kardos, Gábor Hild,* 8th of European Biophysics Congress, Satellite Conference on intracellular fluorescence spectroscop y, Pécs, Hungary August 2011.

-Twinfilin-1 hatása az aktin szerkezeti és dinamikai tulajdonságaira *Kokas Ágnes, Tóth Mónika Ágnes, Türmer Katalin, Kollár Veronika, Kardos Roland, Nyitrai Miklós, Hild Gábor,* 41. Membrán-Transzport Konferencia Sümeg 2011 Május.

-Aktin filamentumok termodinamikai viselkedése ADPBeFx jelenlétében *Vig Andrea, Kardos Roland, Orbán József, Nyitrai Miklós, Lőrinczy Dénes és Hild Gábor,* 37. Membrán-Transzport Konferencia Sümeg 2007 Május.

-A tropomiozin stabilizálja a forminok által nukleált aktin filamentumok szerkezetét *Ujfalusi Zoltán, Vig Andrea, Kardos Roland, Hild Gábor és Nyitrai Miklós,* 37. Membrán-Transzport Konferencia Sümeg 2007 Május.

-A Possible Novel Mechanism for the Regulation of the Cytoskeleton by Actin Nucleation Factors *Beáta Bugyi[1], Gábor Papp[1], Dénes Lőrinczy, Andrea Vig, Roland Kardos, Elisa M. Nevalainen, Pekka Lappalainen, Béla Somogyi, Gábor Hild and Miklós Nyitra,* Alpbach Workshop on Molecular Motors, Alpbach, Austria, March 2007.

A possible role of formins in the regulation of the cytoskeleton *Beáta Bugy, Gábor Papp, Dénes Lőrinczy, Andrea Vig, Roland Kardos, Elisa M. Nevalainen, Pekka Lappalainen, Béla Somogyi, Gábor Hild and Miklós Nyitrai*

-The effects of formins on the conformation of actin filaments. *Bugyi, B., Papp, G., L_rinczy, D., Vig, A., Kardos, R., Nevalainen, E. M., Lappalainen, P.,Somogyi, B., Hild, G. and Nyitrai, M.* 51st Annual Meeting of the American Biophysical Society, Baltimore, MD, USA, March 2007.

-The Effect of Jasplakinolide on the Thermodynamic Properties of BeFx Bound Actin Filaments *Roland Kardos, Andrea Vig, József Orbán, Gábor Hild, Miklós Nyitrai and Dénes Lőrinczy* 17. Ulm-Freiberger Kalorimetrietage, März 2007.

VIII.5. Lectures related to the thesis

-Effect of actin-binding proteins on the actin monomer *Roland Kardos, Pekka Lappalainen, Miklós Nyitrai, Gábor Hild,* EBSA Satellite Conference on Intracellular Fluorescence Microscopy August 2011, Pécs, Hungary.

-The effect of actin-binding proteins on the dynamic properties of G-actin *Roland Kardos, Elisa Nevalaine, Pekka Lappalaine, Miklós Nyitrai and Gábor Hild,* Symposium for Graduate Students in Biology, Pécs, Hungary, November 2009.

-Aktinkötő fehérjék hatása az aktin monomer dinamikai tulajdonságaira *Kardos Roland, Tóth Mónika, Futó Kinga, Elisa Nevalainen, Pekka Lappalainen, Nyitrai Miklós és Hild Gábor,* MBFT XXIII. Kongresszusa 2009 Augusztus, Pécs.

-The effect of actin-binding proteins on the dynamic properties of monomeric actin *Roland Kardos, Andrea Vig, Réka Dudás, Tünde Kupi, Elisa Nevalaine, Pekka Lappalaine, Miklós Nyitrai and Gábor Hild,* 23rd European Cytoskeleton Forum, FEBS/ECF Workshop, Potzdam, Germany, 2008.

-Aktinkötő fehérjék hatása az aktin nukleotidkötő zsebének konformációjára *Hild Gábor, Kardos Roland, Pozsonyi Kinga, Vig Andrea, Nyitrai Miklós,* 37. Membrán-Transzport Konferencia Sümeg 2007 Május.